DEVELOPMENT OF NAFION/ PALLADIUM NANOFILLER AS NANOCOMPOSITE MEMBRANE FOR FUEL CELL APPLICATIONS

by

Mokone Constance Selina Mothibi

Submitted in accordance with the requirements for

the degree of

Magister Engineering

In the subject

Engineering: Chemical

At the

University of South Africa

Supervisor: Dr Rudzani Sigwadi

Co-supervisor: Prof. Touhami Mokrani

: Dr Ismael Amer

January 2024

Declaration

I hereby declare that "Development of Palladium/Nafion Nanofiller as Nanocomposite Membrane for Fuel Cell Applications'' is my own work and it has not been previously submitted to any other university for any degree. All sources used or quoted have been indicated or acknowledged by means of complete reference.

Signature: Mathibi   Date: 23/01/2024

Acknowledgments

Abstract

The nanocomposite membranes were fabricated by incorporating palladium nanoparticles into Nafion® matrix to develop suitable membrane to be used as polymer electrolyte membrane (PEM) in Direct Methanol Fuel Cell (DMFC). The effect of palladium loading was studied to explore a suitable membrane for DMFC. The recast method was used to synthesize the nanocomposites membranes. Commercial palladium nanoparticles were used as reference for synthesized palladium nanoparticles and palladium nanocomposite membranes. The synthesized palladium nanoparticles by sol-gel method were characterized by TEM, UV-vis, FTIR and DLS. The morphology and crystalline structure of nanocomposite membranes were characterized by FESEM, XRD, FTIR. The distribution of palladium nanoparticles within Nafion® membrane was confirmed by EDS. The thermal properties were analysed by TGA and DSC. The mechanical properties were also investigated.

To evaluate suitability of palladium nanocomposite membranes as polymer electrolyte membranes (PEMs) in DMFC properties such as water uptake (WU), water contact angle, methanol permeability, ion exchange capacity (IEC), proton conductivity and selectivity were determined.

The palladium nanocomposite membranes indicated the lowest water uptake of 0.37% at 25°C and highest water uptake of 14.8% at 100°C. The results of water uptake indicated hydrophobic behaviour which corresponds to water contact angle. The highest water contact angle of 100.3° and lowest water contact angle of 84°were recorded for nanocomposite membrane.

The mechanical properties of nanocomposite membranes such as tensile strength, elastic modulus (stiffness) and elongation at break were improved for all nanocomposite membranes.

The methanol permeability of nanocomposite membranes was improved with reduced methanol permeability of 3.5×10^{-7} cm^{-1}s^{-1} for commercial PdNps/Nafion®, 3.6×10^{-7} cm^{-1}s^{-1} for PdEG22/Nafion®, 3.8×10^{-7} cm^{-1}s^{-1} for PdEG33/Nafion®, 4.5×10^{-7} cm^{-1}s^{-1} for PdEG11/Nafion® compared to 9.12×10^{-7} cm^{-1}s^{-1} of pristine recast Nafion® membrane at temperature of 80°C. The ion exchange capacity recorded values were 1.28 mm/g for PdEG22/Nafion®, 1.32 mm/g for PdEG33/Nafion®,1.47 mm/g for PdEG11/Nafion®,2.18 mm/g commercialPdNps/Nafion® compared to 0.81mm/g of pristine Nafion®. The proton conductivity of 0.6 Scm^{-1} (PdEG11/Nafion®), 0.41 Scm^{-1} (PdEG22/Nafion®), 0.28 Scm^{-1} (PdEG33/Nafion®), 0.26 Scm^{-1} (commercial PdNps/Nafion®) was achieved comparable to pristine Nafion® with 0.25 Scm^{-1}.The membrane selectivity of palladium nanocomposite membranes showed the membranes are suitable to be used as PEM in DMFC due to their selectivity values recorded as 1.33×10^{6} Sc cm^{-3} for PdEG11/Nafion®, 1.14×10^{6} Sc cm^{-3} for PdEG22/Nafion®, 7.4×10^{5} Sc cm^{-3} for both PdEG33/Nafion® and commercial PdNps/Nafion® compared to pristine Nafion® (2.7×10^{5} Sc cm^{-3}) and their ability to reduce methanol crossover.

Research Output Arising from the Research

Conference Poster Presentation

1. Moroenyane, M.C.S (2017). Nafion® Nano-composite Membranes for Fuel Cell

   Applications. 1st Africa Energy Materials Conference held 28 to 31 March 2017

   at the CSIR International Convention Centre, South Africa.

List of abbreviations

ABPBI-MMT   Poly (2.5-benzimidazole-grafted montmorillonite

AFC   Alkaline Fuel Cell

AlO_3 Aluminum oxide

CBO   Cross Beam Optics

CL   Catalyst layer

CNTs   Carbon nanotubes

CO   Carbon monoxide

CVD   Chemical Vapour Deposition

DLS   Dynamic Light Scattering

DMF   N, N-dimethylformamide

DMFC   Direct Methanol Fuel Cell

DSC   Differential Scanning Calorimeter

EDS   Energy Dispersive Spectrometer

EG   Ethylene Glycol

ESMs   Electro-Spun Membranes

EW   Equivalent Weight

Fe_3O_4 Iron oxide

FE-SEM   Field Emission Electron Microscope

FTIR   Fourier Transform Infrared

GDL   Gas Diffusion Layer

GO	Graphene oxide
H_2PdCl_4	Hydrogen chloropalladate
HRTEM	High Resolution Transmission Electron Microscopy
IEC	Ion Exchange Capacity
MCFC	Molten Carbonate Fuel Cell
MCO	Methanol crossover
MEA	Membrane Electrode Assembly
M MM-CNT	Carbon nanotubes containing montmorillonite
MMT	Montmorillonite
$NaPdCl_4$	Sodium tetrachloropalladate
NiO	Nickel Oxide
Ni-Al	Nickel Aluminium
Ni-Cr	Nickel Chromium
NPs	Nanoparticles
NFs	Nanofibers
ORR	Oxygen Reduction Reaction
PA	Polyamide
PAA	Poly (acrylic acid)
PAFC	Phosphoric Acid Fuel Cell
PAN	Poly(acrylonitril)
PBI	Polybenzimidazole

PCL	Poly(e-caprolactone)
$PdCl_2$	Palladium chloride
PdDI	Synthesized palladium nanoparticles using deionized water
PdEG	Synthesized palladium nanoparticles using ethylene glycol
PdNPs	Palladium nanoparticles
PEG	Poly(ethylene glycol)
PEM	Polymer Electrolyte membrane
PEMFC	Polymer Electrolyte Membrane Fuel Cell
PEO	Polyethylene oxide
PET	Poly (ethylene tere-phthalate)
PFSA	Perfluosulfonic acid
PI	Polyimide
PLA	Poly (lactic acid)
PLCL	Poly(lactide-co-caprolactone)
PLGA	Poly(lactide-co-glycolide)
PTFE	Polytetrafluoroethylene
PVA	Polyvinyl alcohol
PVAc	Poly (vinyl acetate)
PVDF	Poly (vinylidene fluoride)
PVP	Polyvinyl pyrrolidone
PVPE	PVP-Ethanol
PVPE/N	Polyvinyl pyrrolidone -Ethanol/Nafion
PVP/N	Polyvinyl pyrrolidone/Nafion

PU   Polyurethane

SAXS   Small-Angle X-ray Scattering

SiWA   Silicotungstic acid.

SOFC   Solid Oxide Fuel Cell

SPAES   Sulfonated poly (arylene ether sulfone)

SPEEK   Sulfonated poly (ether ether ketone)

SPES   Sulfonated polyether sulfone

SPVdF-HFP Sulfonated poly (vinylidene fluoride-co-hexafluoropropylene)

$sTiO_2$ Sulfonated titanium oxide

TGA   Thermal Gravimetric Analysis

THF   Tetrahydrofuran

TNT   Titanium oxide nanotubes

UV-vis   Ultraviolet Visible Spectrometer

WCA   Surface Contact Angle Measurement

WDS   Wavelength Energy Dispersive

XRD   X-ray Diffraction

XRF   X-Ray Fluorescent

Table of Contents

List of Figures

List of Tables

Chapter 1

Introduction

1.1 Background

Currently, the world is experiencing issues of global warming, depletion of ozone layer and environmental pollution due to the use of fossil fuel which are negatively having impact on the human health and atmosphere [1-2]. Fuel cells have brought attention to various sectors such as companies and governments due to their capability of producing highly efficient power generators. They are also regarded as the best choice due to their good environmental performance. Hence, alternative energy systems such as fuel cells are considered since it is economical and environmentally friendly with low level of pollution, low costs, and high energy conversion [3-5].

Fuel cells are electrochemical devices that change chemical energy to electrical energy via an electro-catalytic process [3-4]. The membrane electrode assembly (MEA) is a main component of fuel cells and is composed of an ion conducting electrolyte, a cathode, and an anode [4]. Portable fuel cells have been considered to be the best choice to replace batteries for portable electronics applications because they have much higher energy density storage, and they are easily rechargeable by replacing the fuel cartridge [6].

Fuel cells are divided into two groups, namely those that operate at low temperatures and those that operate at high temperatures. Examples of fuel cells operating at low temperature (60-220°C) are Alkaline Fuel Cell (AFC), Polymer Electrolyte Membrane

Fuel Cell (PEMFC), the Direct Methanol Fuel Cell (DMFC) and the Phosphoric Acid Fuel Cell (PAFC). There are two various types of fuel cells available; high temperature fuel cells that operate at a temperature range of approximately 600-1000 °C, and these are: Molten Carbonate Fuel Cell (MCFC) and the Solid Oxide Fuel Cell (SOFC) [7].

1.2 Problem Statement and Purpose of the Study

The most used type of fuel cells is the low temperature namely, DMFC and PEMFC.DMFC is derived from PEMFC which composed of polymer electrolyte membrane (PEM), anode electrode and cathode electrode [8]. DMFC uses methanol and PEMFC uses hydrogen as fuel. DMFC is preferred than PEMFC because methanol is cheap and easily available [9].

Nafion® is used as a polymer electrolyte membrane (PEM) in fuel cells which is the main component of a polymer electrolyte membrane fuel cell (PEMFC) and direct methanol fuel cell (DMFC) which divide fuels and oxidants between the anode and cathode side and conduct protons (H^+) via polymer electrolyte membrane [10-12]. This perfluorosulfonic acid (PFSA) membrane is extensively used because it possesses excellent properties (i.e., high proton conductivity, thermal, chemical, and mechanical stability well hydrated state) [13-16].
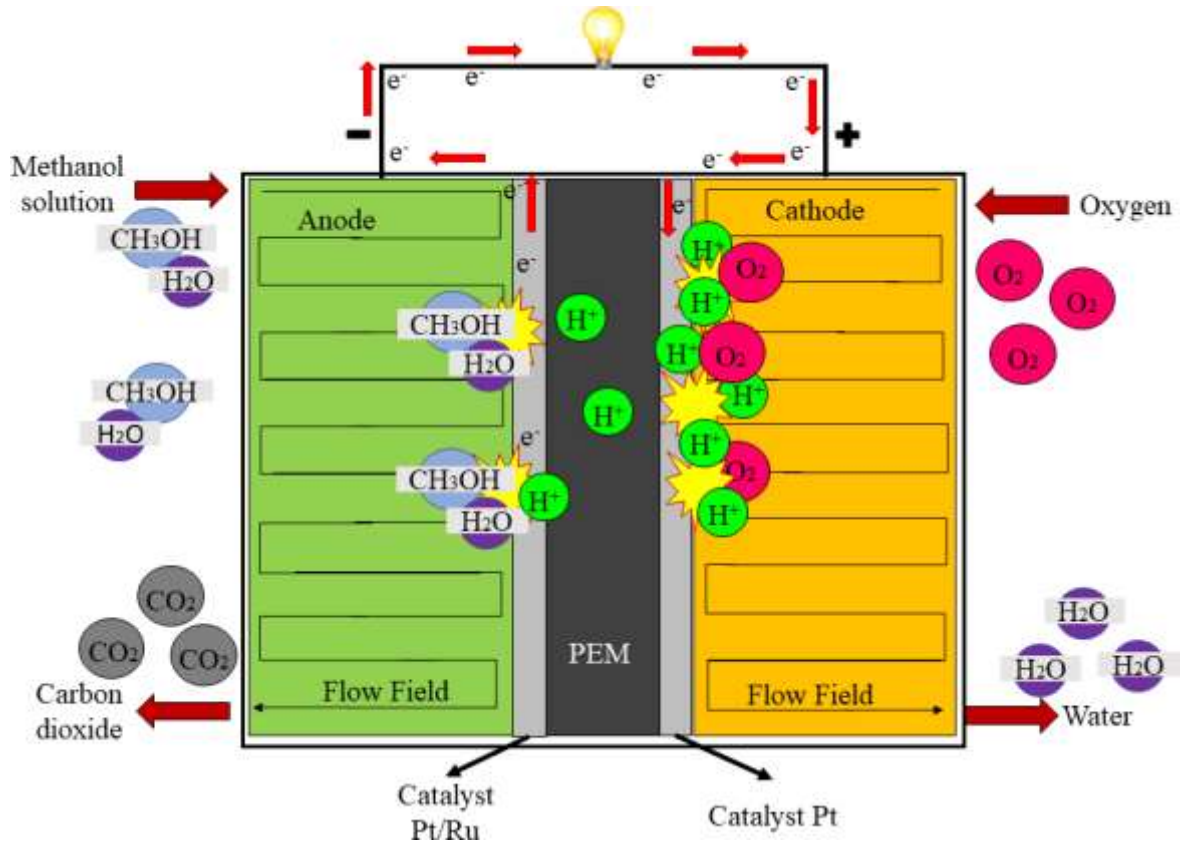
Figure 1.1: Direct Methanol Fuel Cell (DMFC) structure [11].

The following are the reactions tacking place at the cathode and anode in the DMFC:

Anode: $CH_3OH + H_2O \rightarrow CO_2 + 6H^+ + e^-$ (1.1)

Cathode: $\frac{3}{2}O_2 + 6H^+ + 6e^- \rightarrow 3H_2O$ (1.2)

Overall reaction: $CH_3OH + \frac{3}{2}O_2 \rightarrow CO_2 + 2H_2O$ (1.3)
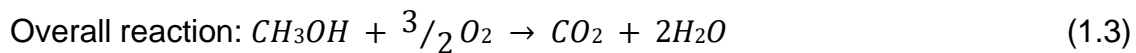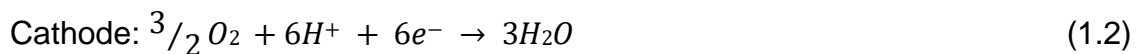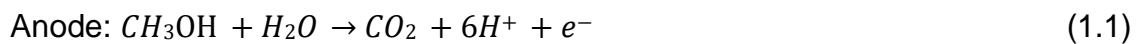
Some of the challenges of polymer electrolyte membrane (PEM) made of Nafion® include high methanol permeability; high cost of the platinum (Pt) electro-catalyst and high cross-potential generated when used in DMFC [13]. In DMFCs high methanol crossover causes membrane selectivity (ratio of proton conductivity and methanol permeability) to be low; increase cross-potential which reduces current and power

outputs [13, 16]. Therefore, the commercial feasibility of DMFC as an alternative energy harnessing device is at risk [13].

Methanol is used as fuel in DMFC, and it is preferable because it has high efficiency, it produces nearly zero pollution, easy handling of fuel and application as low power devices in electronics. There are several problems that have hindered the development of DMFC such as the incomplete electro-oxidation of methanol and sluggish kinetics of methanol oxidation, adsorbed intermediate species that is poisoned on the Pt electrocatalyst, the high methanol crossover across the Nafion[®] membrane, and the price of Pt or Pt-alloy and Nafion[®] polymer membrane that is expensive [17]. According to Yin et al. [18], the agglomeration or detachment of nanoparticles from the support at normal operating conditions causes performance reduction and lifetime depletion of the fuel cells [18-19]. To get membrane electrode assembly (MEA) to be successful commercialized, it must meet 3 main standards namely performance, cost, and durability [18,20]. Therefore, it is important to select support material that will maintain the nanoparticles durability of the catalyst since the lifespan and performance of the catalyst is compromised due to methanol crossover from anodic chamber of DMFC [18,21].

Direct methanol fuel cells are the best choice since the methanol is directly being fed to the cell [22-23]. The DMFCs cannot be commercially utilized because of expensive cathodic materials, poor stability, low efficiency, and high methanol permeability [22, 24-27]. Basically, the low efficiency is caused by low reaction rate at the cathode side due to oxygen reduction reaction (ORR) [22, 28-34]. The efficiency of the fuel cell is limited because of the incapability of discovering a suitable material for oxygen reduction at the cathode side. The palladium is regarded as a suitable material for oxygen reduction.

4

reaction that can substitute Platinum because its cost is lower, and its physicochemical characteristics are close resemblance to Platinum [22,35].

1.3 Research Aim and Objectives

The aim of this project is to develop an inorganic-organic nanocomposite membrane by modifying the traditional Nafion$^{®}$ membrane with palladium to enhance properties such as proton conductivity, water retention/permeability and reduce methanol crossover.

The objectives of this study are to:

1. Synthesize palladium nanoparticles.

2. Incorporate the prepared palladium nanoparticles in Nafion$^{®}$ film using a recasting process.

3. Determine nanocomposite membrane properties.

4. Study the impact of palladium loading on methanol crossover.

5. Determine selectivity (ratio of proton conductivity and methanol permeability) of nanocomposite membranes for optimum palladium loading.

6. Compare proton conductivity and methanol crossover of modified Nafion$^{®}$ and pristine Nafion$^{®}$.

1.4 Dissertation Structure

The dissertation consists of six chapters. First chapter is the introduction with background, problem statement and purpose of study, aims and objectives. Chapter two is the literature review composed of Nafion® membrane and its modification including the history of nanotechnology, fuel cell and its applications.

Chapter three gives information about methodology and characterization used to prepare nanoparticles and nano-composites membranes. Chapter four is the preparation of palladium nanoparticles and their characterization. It also includes discussion of the results. Chapter five is the preparation of nano-composite membranes, their characterization and discussion of the results. Chapter six is the conclusion and recommendations.

1.5 References

1. Na H., Zhang, L., Qiu, H., Wu, T., Chen, M., Yang, N., Li, L.-Z., Xing, F., and Gao, J. (2015). A two step method to synthesize palladium–copper nanoparticles on reduced graphene oxide and their extremely high electrocatalytic activity for the electrooxidation of methanol and ethanol. Journal of Power Sources, 288, pp.160–167.

2. Zakil, F.A., Kamarudin, S.K. and Basri, S. (2016). Modified Nafion membranes for direct alcohol fuel cells: An overview. Renewable and Sustainable Energy Reviews, 65, pp.841–852.

3. Kamarudin, S.K., Achmad, F. and Daud, W.R.W. (2009). Overview on the application of direct methanol fuel cell (DMFC) for portable electronic devices. International Journal of Hydrogen Energy, 34(16), pp.6902–6916.

4. Smith, T.A., Santamaria, A.D., Park J.Y., and Yamazaki, K. (2014). Alloy Selection and Die Design for Stamped Proton Exchange Membrane Fuel Cell (PEMFC) Bipolar Plates. Procedia CIRP, 14, pp.275–280.

5. Narayanamoorthy, B. and Balaji, S. (2015). Physicochemical characterization of amino functionalized synthetic clay/Nafion nanocomposite film with embedded platinum nanoparticles for PEM fuel cells. Applied Clay Science, 104, pp.66–73.

6. Gupta, R., Guin, Saurav.K., and Aggarwal, S.K. (2014). Electrocrystallization of palladium (Pd) nanoparticles on platinum (Pt) electrode and its application for electro-oxidation of formic acid and methanol. Electrochimica Acta, 116, pp.314–320.

7. Carrete L., Friedrich K.A., and Stimming U (2001). Fuel-Fundamentals and Applications. Fuels Cells, 1 (1), pp. 5-39.

8. Prapainainar P., Du, Z., Theampetch A., Prapainainar C., Kongkachuichay P., and Holmes, S.M. (2020). Properties and DMFC performance of Nafion/mordenite composite membrane fabricated by solution-casting method with different solvent ratio. Energy, 190, p.116451.

9. Thiam H.S., Chia M.Y., Cheah Q.R., Koo C.C.H., Lai S.O., and Chong K.C. (2017). Proton Conductivity and Methanol Permeability of Nafion/ SiO2/SiWA Composite Membranes. AIP Conference Proceedings, 1828, p. 020007.

10. Li H.Y, Lee Y.Y, Lai J.Y, Liu Y.L (2014). Composite membranes of Nafion and poly (styrenesulfonicacid)-graftedpoly (vinylidene fluoride) Electrospun nanofiber mats for fuel cells. Journal of Membrane Science, 466, pp. 238–245.

11. Junoh, H., Jaafar, J., Nordin, N., Ismail, A., Othman, M., Rahman, M., Aziz, F. and Yusof, N. (2020). Performance of Polymer Electrolyte Membrane for Direct Methanol Fuel Cell Application: Perspective on Morphological Structure. Membranes, 10(3), p.34.

12. Li, X., Miao, Z., Marten, L. and Blankenau, I. (2021). Experimental measurements of fuel and water crossover in an active DMFC. International Journal of Hydrogen Energy, 46(5), pp.4437–4446.

13. Dutta, K., Das, S., and Patit Paban Kundu (2015). Partially sulfonated polyaniline induced high ion-exchange capacity and selectivity of Nafion membrane for application in direct methanol fuel cells. Journal of Membrane Science, 473, pp.94–101.

14. Sharma D.K., Li, F. and Wu, Y. (2014). Electrospinning of Nafion and polyvinyl alcohol into nanofiber membranes: A facile approach to fabricate functional adsorbent for heavy metals. Colloids and Surfaces A: Physicochem. Eng. Aspects 457, pp.236–243.

15. Takemori R., and Kawakami H. (2010). Electrospun nanofibrious blend membranes for fuel cell electrolytes. Journal of Power Sources, 195, pp. 5957-5961.

16. Dutta, K., Das, S., and Kundu P.P. (2014). Low methanol permeable and highly selective membranes composed of pure and/or partially sulfonated PVdF-co-HFP and polyaniline. Journal of Membrane Science 468, pp.42–51.

17. Mallakpour, S., Zhiani, M., Barati, A. and Rostami, H. (2013). Improving the direct methanol fuel cell performance with poly (vinyl alcohol)/titanium dioxide nanocomposites as a novel electrolyte additive. International Journal of Hydrogen Energy, 38(28), pp.12418–12426.

18. Yin, Z., Lin, L. and Ma, D. (2014). Construction of Pd-based nanocatalysts for fuel cells: opportunities and challenges. Catalysis Science & Technology, 4(12), pp.4116–4128.

19. Zhang, S., Shao, Y., Yin, G. and Lin, Y. (2013). Recent progress in nanostructured electrocatalysts for PEM fuel cells. Journal of Materials Chemistry A, 1(15), pp.4631-4641.

20. Sharma s., and Pollet B. G. (2012). Support materials for PEMFC and DMFC electrocatalysts—A review. Journal of Power Sources, 208, pp. 96-119.

21. Rabis, A., Rodriguez, P. and Schmidt, T.J. (2012). Electrocatalysis for Polymer Electrolyte Fuel Cells: Recent Achievements and Future Challenges. ACS Catalysis, 2(5), pp.864–890.

22. Sanij, F.D., Balakrishnan, P., Leung, P., Shah, A., Su, H. and Xu, Q. (2021). Advanced Pd-based nanomaterials for electro-catalytic oxygen reduction in fuel cells: A review. International Journal of Hydrogen Energy, 46(27), pp.14596–14627.

23. Zhao Y, Mao Y, Zhang W, Tang Y, Wang P (2020). Reviews on the effects of contaminations and research methodologies for PEMFC. International Journal of Hydrogen Energy, 45, pp. 23174-23200.

24. Jamil, R., Sohail, M., Baig, N., Ansari, M.S. and Ahmed, R. (2019). Synthesis of Hollow Pt-Ni Nanoboxes for Highly Efficient Methanol Oxidation. Scientific Reports, 9(1).

25. Mei, R., Xi, J., Ma, L., An, L., Wang, F., Sun, H., Luo, Z. and Wu, Q. (2017). Multi-Scaled Porous Fe-N/C Nanofibrous Catalysts for the Cathode Electrodes of Direct Methanol Fuel Cells. Journal of The Electrochemical Society, 164(14), pp. F1556–F1565.

26. Feng, Y., Ye, F., Liu, H. and Yang, J. (2015). Enhancing the methanol tolerance of platinum nanoparticles for the cathode reaction of direct methanol fuel cells through a geometric design. Scientific Reports, 5(1).

27. Shi, Y., Lyu, Z., Zhao, M., Chen, R., Nguyen, Q.N. and Xia, Y. (2020). Noble-Metal Nanocrystals with Controlled Shapes for Catalytic and Electrocatalytic Applications. Chemical Reviews, 121(2), pp.649–735.

28. Wang K., Wang F., Zhao Y., Zhang W. (2020). Surface-tailored Pt Pd Cu ultrathin nanowires as advanced electrocatalysts for ethanol oxidation and oxygen reduction reaction in direct ethanol fuel cell. Journal of Energy Chemistry, 52, pp. 251-261.

29. Oh, T., Kim, K. and Kim, J. (2019). Controllable active sites and facile synthesis of cobalt nanoparticle embedded in nitrogen and sulfur co-doped carbon nanotubes as efficient bifunctional electrocatalysts for oxygen reduction and evolution reactions. Journal of Energy Chemistry, 38, pp.60–67.

30. Sarkar, S., Patel S., and Sampath, S. (2020). Efficient oxygen reduction activity on layered palladium phosphosulphide and its application in alkaline fuel cells. Journal of Power Sources, 445, pp.227280–227280.

31. Sun, W., Zhang, W., Su, H., Leung, P., Xing, L., Xu, L., Yang, C. and Xu, Q. (2019). Improving cell performance and alleviating performance degradation by constructing a novel structure of membrane electrode assembly (MEA) of DMFCs. International Journal of Hydrogen Energy, 44(60), pp.32231–32239.

32. Fang, Y., Zhang, T., Wang, Y.-H., Chen, Y., Liu, Y., Wu, W. and Zhu, J. (2020). The highly efficient cathode of framework structural Fe_2O_3/Mn_2O_3 in passive direct methanol fuel cells. Applied Energy, 259, pp.114154–114154.

33. Mansor, M., Timmiati, S.N., Lim, K.L., Wong, W.Y., Kamarudin, S.K. and Nazirah Kamarudin, N.H. (2019). Recent progress of anode catalysts and their support materials for methanol electrooxidation reaction. International Journal of Hydrogen Energy, 44(29), pp.14744–14769.

34. Wang, Y.-H., Wang, F., Fang, Y., Zhu, J., Luo, H., Qi, J. and Wu, W. (2019). Self-assembled flower-like MnO_2 grown on Fe-containing urea-formaldehyde resins-based carbon as catalyst for oxygen reduction reaction in alkaline direct methanol fuel cells. Applied Surface Science 496, pp.143566–143566.

35. Arukula R., Vinothkannan M., Kim A.R., Yoo D.J (2019). Cumulative effect of bimetallic alloy, conductive polymer, and graphene toward electrooxidation of methanol: an efficient anode catalyst for direct methanol fuel cells. Journal of Alloys and Compounds, 771, pp.477-488.

Chapter 2

Literature Review

2.1. Introduction

Due to incorporation of nanomaterials, fuel cells have shown increased consistency and lower costs in the past few years. Fuel cells (Figure 2.1) have a higher electrical efficiency than heat engines and may help to reduce poisonous emissions to the atmosphere as well as minimize use of fossil fuels [1] as the use of fossil fuel has a negatively impact on the human health and atmosphere [2]. Recently research has been focused on developing PEMs with excellent properties such as high oxidative stability, high proton conductivity, good mechanical stability, low fuel crossover and with low cost of membrane electrolyte fabrication and assembly [3].
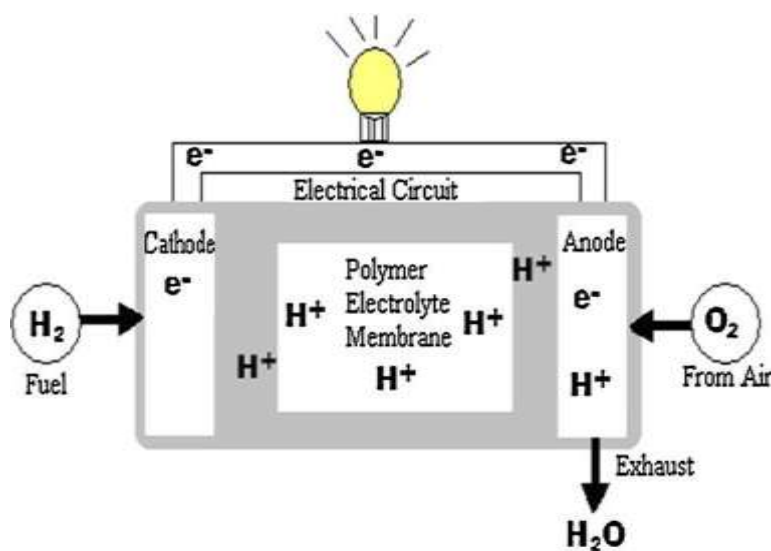
Figure 2.1: Operating principle of a fuel cell [4].

2.2. History of Fuel Cells

The process of using electricity to break water into hydrogen and oxygen was introduced in 1800s by William Nicholson and Anthony Carlisle as shown in figure 2.2. The process is called electrolysis [5-6]:

$$2H_2O_{(l)} \rightarrow 2H_{2\,(g)} + O_{2(g)} \qquad\qquad (2.1)$$
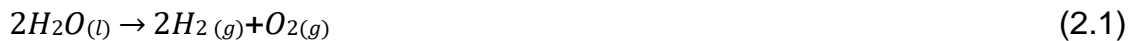
The fundamental laws of electrolysis were established by Michael Faraday in 1832 whereby he described that the quantity of elements separated by passing an electrical current through a dissolved salt was proportional to the quantity of electric charge passed through the circuit [5-6].

William Grove combined these ideas of Nicholson, Carlise and Faraday and developed a fuel cell. The initial fuel cell was implemented by Grove in 1839. William Grove used electrodes in a series circuit to breakdown water to establish gas battery. This fuel cell was called the Grove cell which generated approximately 12A of current at around 1.8V using a platinum electrode immersed in nitric acid and zinc sulfate [5-6].

Ludwig Mond and Carl Langer used a coal -derived gas to perform numerous experiments with gas-powered batteries. The battery generated 6A per square foot (the surface area of electrode) at 0.73V using thin, perforated platinum electrodes. In 1853- 1932, Friedrich Wilhelm Ostwald provided theoretical understanding of how fuel cells work. Through his experimental work, he discovered various roles of fuel cell components: electrolyte, electrodes, anions, and cations, oxidizing and reducing agents [5-6]

13

> 1800 British scientists William Nichols and Anthony Carlisle had described the electrolysis of water

> 1838 William Robert Grove created the "gas battery". The first fuel cell

> 1889 Ludwig Mond and assistant Carl Langer conduce early experiments with fuel cell

> 1893 Friedrich Wilhem Ostwald provided much of the theoretical understanding of how fuel cell operate

> 1930 Emil Baur and H Preis experimented with high temperature solid oxide electrolites

> 1939 Francis Thomas began researching alkaline fuel cell

> 1958 Francis Thomas Bacon worked on an alkaline fuel cell to power a Royal Navy submarine

> 1958 G.H.J. Broers and J.A. Ketelaar began to build a Molten Carbonate fuel cell

> 1959 Research into solid oxide fuel cell began to accelerate at the Central Technical Institute in Netherlands, and General Electric in New York

> 1960 The first PEM fuel cell was developed at General Electric by Thomas Grubb and Leornard Niedrac

> 1961 G.V. Elmore and H.A. Tanner published their experiments on Phosphoric acid fuel cell

> 1965 Pratt and Whitney licenced the Francis Thomas Bacon alkaline fuel cell patents and win a contract to power the Apollo Spacecraft on space mission

> 1990 The direct methanol fuel cell was developed by NASA Jet Propulsion Laboratory and the University of California

> 2007 Honda announced the first mass produce fuel cell powered car called the Honda FCX

Figure 2.2: The history of fuel cells [5-6].

2.3. Fuel Cell Principle

PEMFC consists of polymer electrolyte membrane (PEM) which is sandwich between anode and cathode electrodes connected in an external circuit. The hydrogen fuel will be supplied at anode and oxygen at cathode (Figure 2.3) [7]. The oxidation of

14

hydrogen occurs at the anode and proton will flow through PEM to the cathode. The reaction at cathode yields electrons. The water is formed in the cathode from the reaction of oxygen ions and protons. Only hydrogen ions must penetrate through PEM to cathode side and electrons must flow around the external circuit to cathode side so that convectional current can be produced which flows from cathode to anode [2,8]. The following reaction takes place at anode and cathode [7,9-10].

Anode:

$$H_2 + \frac{1}{2}O_2 \rightarrow H_2O \qquad\qquad (2.2)$$

$$H_2 \rightarrow 2H^+ + 2e^- \qquad\qquad (2.3)$$

Cathode

$$O_2 + 4e^- \rightarrow 2O^{2-} \qquad\qquad (2.4)$$

$$O_2 + 4H^+ \rightarrow H_2O \qquad\qquad (2.5)$$
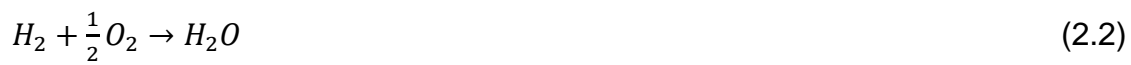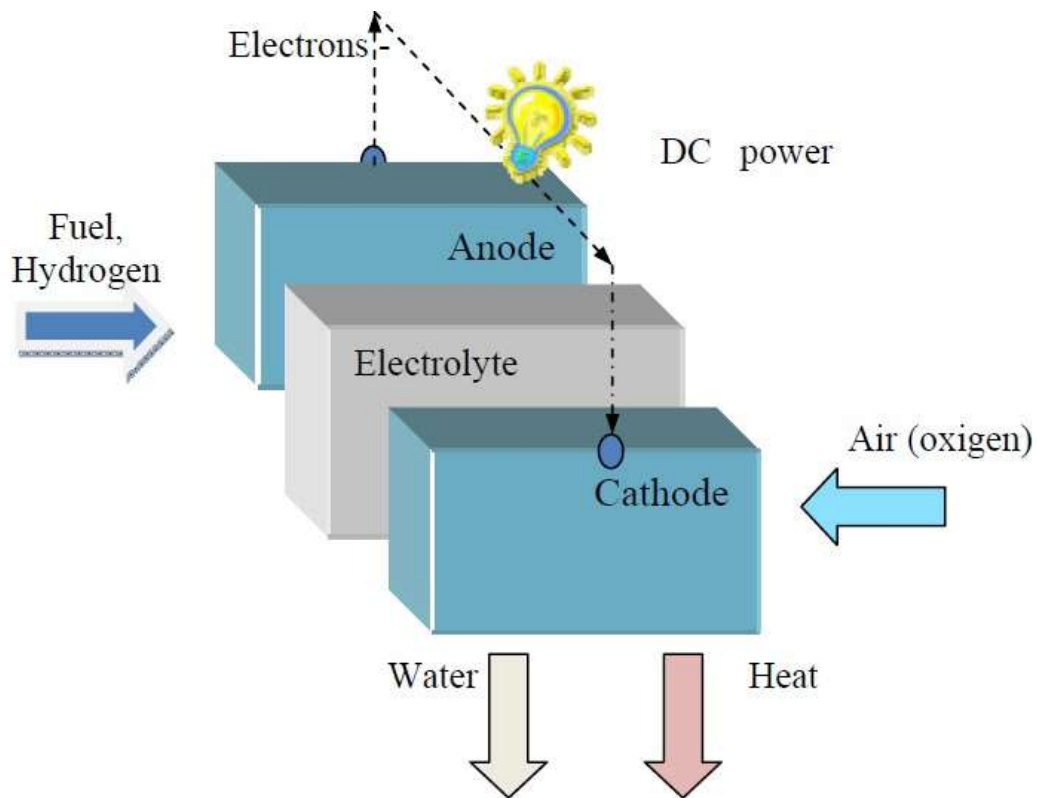
Figure 2.3: Proton Exchange Membrane Fuel Cell (PEMFC) [7].

When a reaction takes place in an anode, hydrogen releases energy. Although energy is released but does not mean the rate of reaction is not restricted. This energy needed to be supported by supplying activation energy to get over the "energy hill", Figure 2.4 [8]. The reaction will proceed slowly if a molecule has low energy apart from fuel cell reactions whereby high temperatures are used.

If there is a slow reaction, the following can be supplied to speed up reaction to get over the "energy hill" Figure 2.4 [8]:

1. Use catalyst.

2. Raise the temperature.

3. Increase area of electrode.

The use of catalysts and raising the temperature can be used for any chemical reaction but increasing the area of electrode is important in fuel cell. For instance, the

16

reaction of hydrogen and hydroxyl ions from the electrodes need activation energy which occurs on the electrode surface. In this case the reaction rate will be equivalent to the area of electrode. The area of electrode plays an important role in terms of fuel cell performance. Therefore, the electrode is made of highly porous material to increase its surface area. Additional to surface area, a catalyst can be added to solve rate of reaction issues [8].

The following can cause voltage drop in the fuel cells [8]:

1. Activation losses that occur which is the resultant of reactions being slow on the electrodes surface.

2. Fuel crossover and internal currents caused by electrons that passes through electrolyte and fuel that diffuses through electrolyte.

3. Ohmic loss which is the result of resistance to electrons flowing in electrodes and resistance to ions flowing via the electrolyte.

4. Mass transport or concentration losses due to changing of reactants concentration at electrode surface.
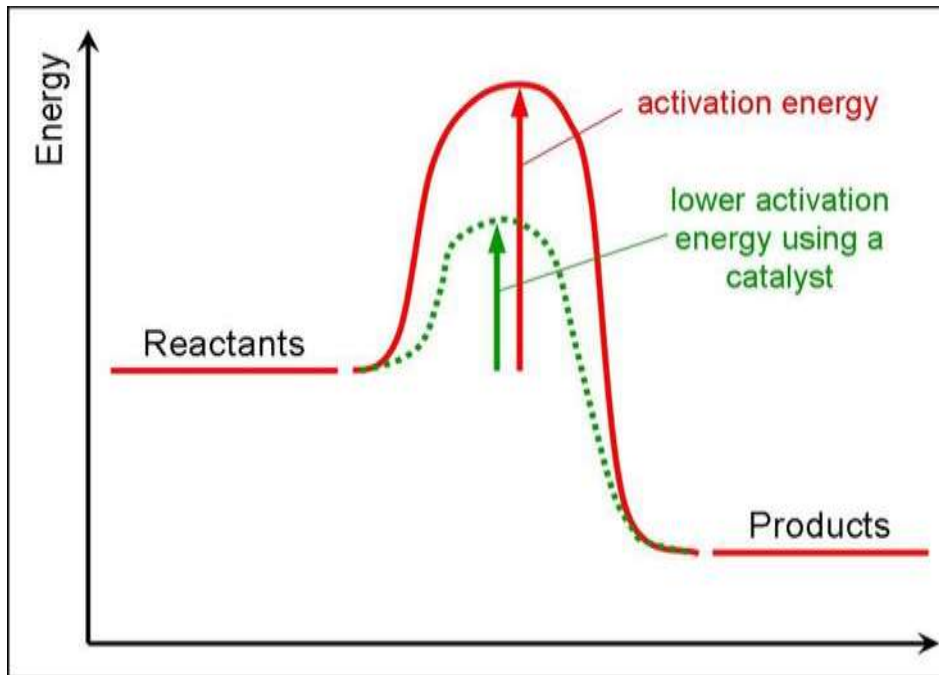
Figure 2.4: Classical energy for a simple exothermic chemical reaction [8].

2.4 Types of Fuel Cells

Fuel cells are classified according to operational parameters such as temperature, fuel type, and oxidizer type or charger carrier. The different types of fuel cells are described below.

•   Proton Exchange Membrane Fuel Cell (PEMFC)

In the PEMFC (Figure 2.5), the production of electrical energy is enhanced by reacting H_2 and O_2 giving H_2O and heat as by products as shown in Figure 2.5. The main components of a PEMFC are Proton Exchange Membrane (PEM), Anode Catalyst Layer, Anode Gas Diffusion Layer, anode plate, Cathode plate, Cathode Catalyst Layer and Cathode Gas Diffusion Layer. Hydrogen gas from the anode side enters through the anode gas diffusion layer (GDL) and reaches the anode catalyst layer (CL). Hydrogen separates

18

from its electron in the presence of catalyst and moves through the PEM on the other side as proton H+ [11].

PEMFCs can work at ambient temperature conditions and have a fast start up. Therefore, they are preferred for transportation and portable power applications [5]. PEMFCs have their drawbacks when it is used in automotive applications, it frequently struggles to start-up and shutdown or nearly continuously power load cycling, causing Nafion® membrane not to perform well because of failure of MEA under insufficient humidifying condition and different interface that reacted between catalyst layer and membrane [12].

The ratio of performance to manufacturing cost of PEMFCs acts as a main barrier to broader PEMFC adoption. The bipolar plate in PEMFC is a component that is a main driver of both performance and manufacturing cost [11].

Stable high proton conductivity of membrane in PEMFCs can be maintained by using hydrated polymer and the flooding can be prevented by removing excess water [13]. Water transport process is being affected by membrane hydration as well as fuel cell operating parameters and inlet gases conditions [13-14]. To achieve optimal performance of the membrane the water balance must be stable. Two processes of water transports affect water balance in a PEMFC namely: electro-osmotic drag and back diffusion, which in turn affect membrane hydration [13].
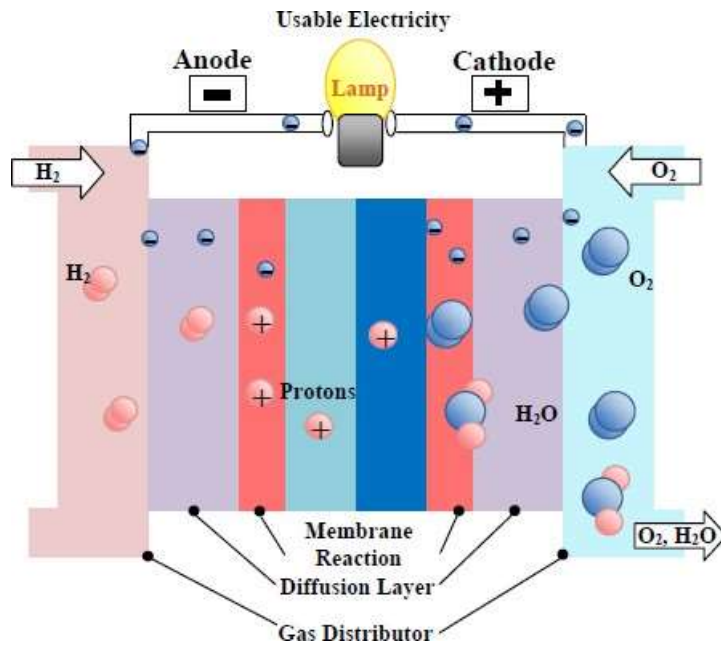
Figure 2.5: Proton Exchange Membrane Fuel Cell [7].

- Direct Alcohol Fuel Cells (DAFCs)

The direct alcohol fuel cells (DAFC's) have good impact on environmental and they are preferred for clean and efficient power generators hence researchers, governments and companies have shown their interests in their design [15]. There are two types of direct alcohol fuel cells (DAFCs) namely direct methanol fuel cells DMFCs and direct ethanol fuel cells (DEFCs) have application in portable electric devices as power sources. DAFCs are preferable to PEMFCs since they use low molecular weight alcohols such as methanol, ethanol, ethylene glycol, 2-propanol, 1-propanol, and glycerol whereas PEMFC uses hydrogen as source of energy. Since methanol is cheap and it is oxidized more than other alcohol fuels, it is considered as the simplest alcohol used as fuel for DAFC application [2]. DAFCs have the highest catalytic activity among anode electro-catalyst for methanol and ethanol oxidation [16].

Direct Methanol Fuel Cell (DMFC)

DMFCs (Figure 2.6) have been successfully used in power backup and applications for electrical appliances [13,17-19]. In DMFCs, methanol is used as a fuel to directly change chemical to electrical energy. DMFCs use a simplified design that does not require a fuel reformer, it is not costly and uses liquid methanol as a fuel which is easily available and can be handled easily and have a high energy density and zero pollution [15,18,20-21]. Since the DMFC has appropriate characteristics for portable devices, it has become priority research for fuel cell applications especially portable devices. DMFC can generate an improved environment for human beings as it represents a potential energy source that is readily used nowadays [19].

Methanol issues such as crossovers, its relative toxicity, high flammability, and low boiling point limit its extensive application in DMFCs. In this case, other alcohols that have higher boiling point and non-toxic can be used as alternatives such as ethanol. The crossover rates through Nafion® membranes were reduced when ethanol was used, and performance of cathode was less affected and slower electro- chemical oxidation kinetics over a Pt/C cathode were experienced when compared to methanol [22].

However, there are several factors affecting the performance of DMFCs such as slow methanol oxidation and oxygen reduction reactions kinetics, high noble metal catalyst loading within membrane electrodes assembly, structure, and fabrication of the MEA [23,17]. Research studies indicate that most researchers have been focused on different approaches for improving required properties for application in DMFCs such as optimization of membrane swelling, water uptake, methanol permeability and mechanical stability [24].

Most of these challenges are caused by methanol crossover (MCO). In DMFCs methanol crossover (MCO) is experienced from the side of anode via MEA to the cathode side [20]. Proton exchange membrane (PEM) in DMFC should indicate good proton conductivity to methanol permeability ratio [25]. Hence, high proton conductivity and low alcohol crossover polymers are needed to improve efficiency and power density of PEM in DMFC [26].
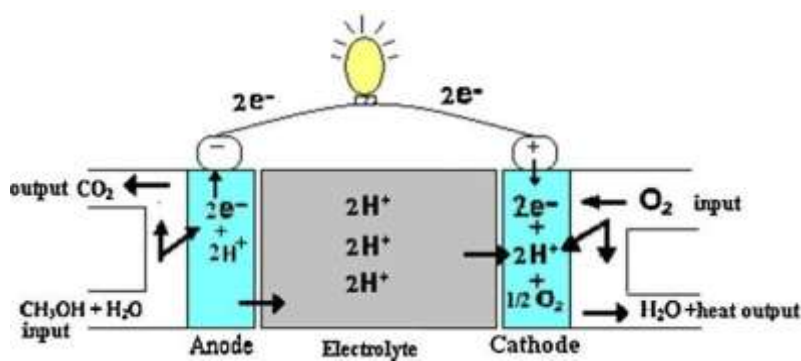
Figure 2.6: Direct Methanol Fuel Cell [4].

- Microbial Fuel Cell (MFC)

MFC (Figure 2.7) converts chemical to electrical energy by using organisms as biocatalyst. This microbial fuel cell device has recently attracted more attention because of its ability to produce electricity from different waste materials. The device comprises of an anode and a cathode, which are divided by a proton exchange membrane. The performance of this type of fuel cell can be affected by factors such as microorganisms, membrane electrode, and cell resistance, ionic strength of the solution, electrode spacing and the distance between electrodes. The membrane contributes more than 38% of the overall capital cost of MFCs therefore, it is considered to be the most important component of MFCs.

It is reported that not much research has been done on the application of nano-composite membranes in MFCs [27].
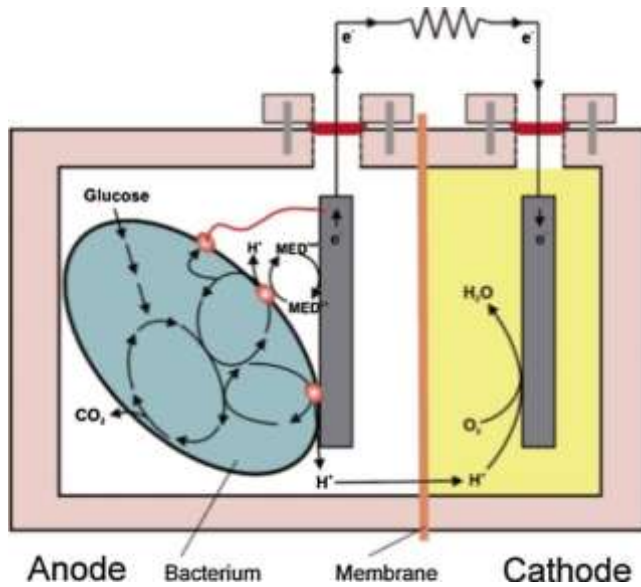
Figure 2.7: Microbial Fuel Cell [28].

• Alkali Fuel Cell (AFC)

AFC (Figure 2.8) operates properly only with very pure gases which makes it not preferable for most applications, but it can generate very high efficiencies compared to other fuel cells. Its anode and cathode are made of Ni based catalyst and it can be occasionally activated with Pt. Pt/C gas diffusion electrodes [2].
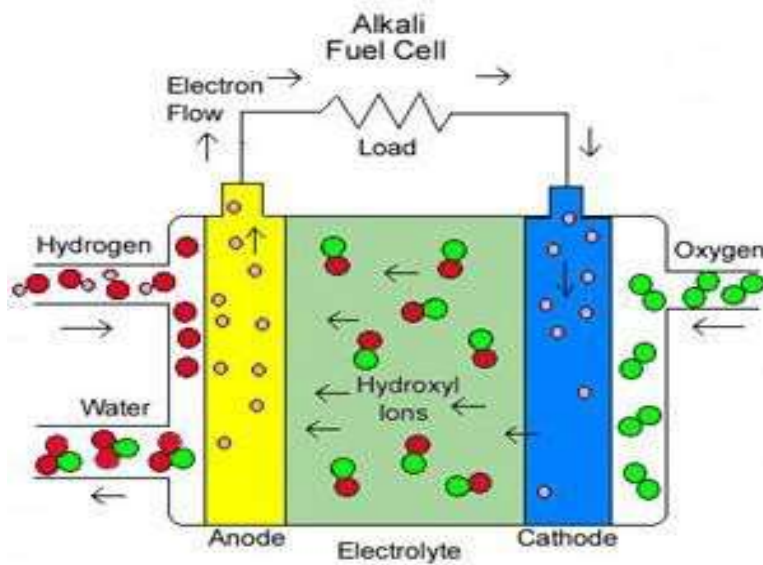
Figure 2.8: Alkali Fuel Cell [29].

•   Phosphoric Acid Fuel Cell (PAFC)

PAFC (Figure 2.9) is regarded as the most advanced system when it comes to commercial development. It uses Pt based catalyst as electrodes [2]. The PAFC can be constructed simple. It is thermally, chemically, electrochemically stable and its electrolyte volatility is low at temperatures between 150-200°C. Due to these factors, this type of fuel was commercialized earlier compared to other fuel cells [1]. It also has cogeneration efficiency of about 85% and can tolerate carbon monoxide of about 1.5% [6].
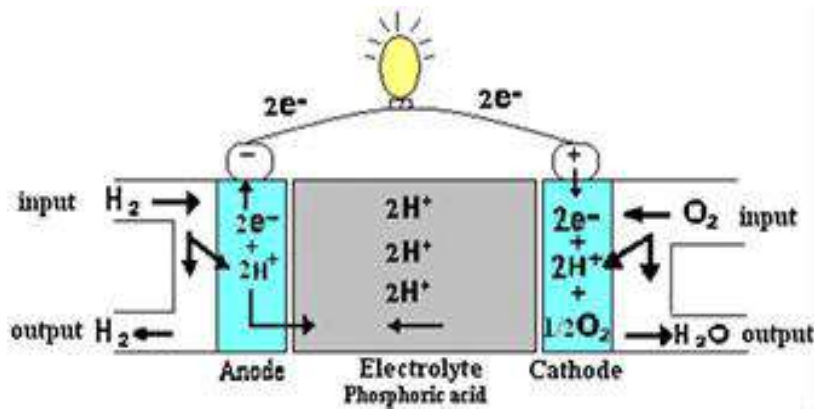
Figure 2.9: Phosphoric Acid Fuel Cell [4].

• Molten Carbon Fuel Cell (MCFC)

MCFCs (Figure 2.10) can use waste heat in combined cycle power plants and the high temperatures to improve the oxygen reduction kinetics intensely reducing the need for very high loadings of metal catalyst. The advantage of MCFCs is the internal reforming because of high operating temperatures (600-700°C). MCFCs cathode is made up of NiO by anodic oxidation of a Ni sinter or by an in-situ oxidation of Ni metal during start-up time of a cell and anode is made of Ni-Al or Ni-Cr metals [2].
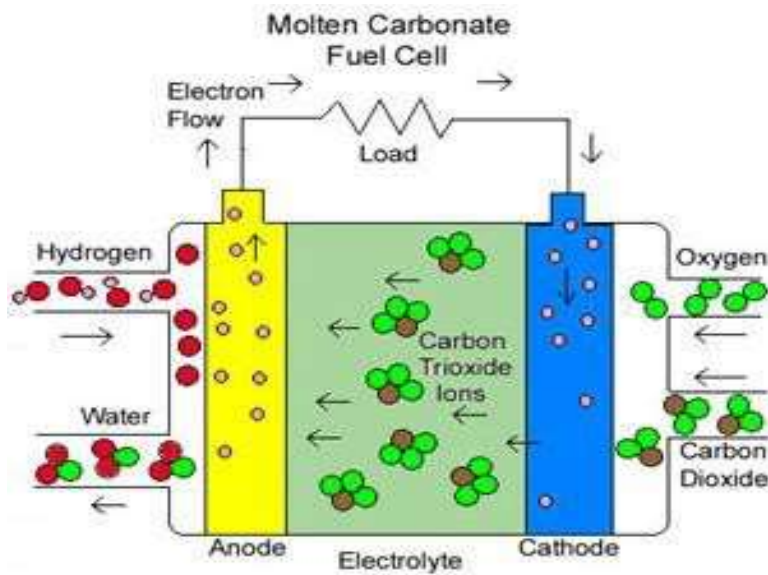
Figure 2.10: Molten Carbon Fuel Cell [29].

• Solid Oxide Fuel Cell (SOFC)

SOFC (Figure 2.11) does not have problems of H2O management, flooding of the catalyst layer or sluggish reduction of O2 kinetics but it is not easy to develop appropriate electrode/electrolyte materials that have suitable properties such as stability and thermal operating at high temperatures [2].
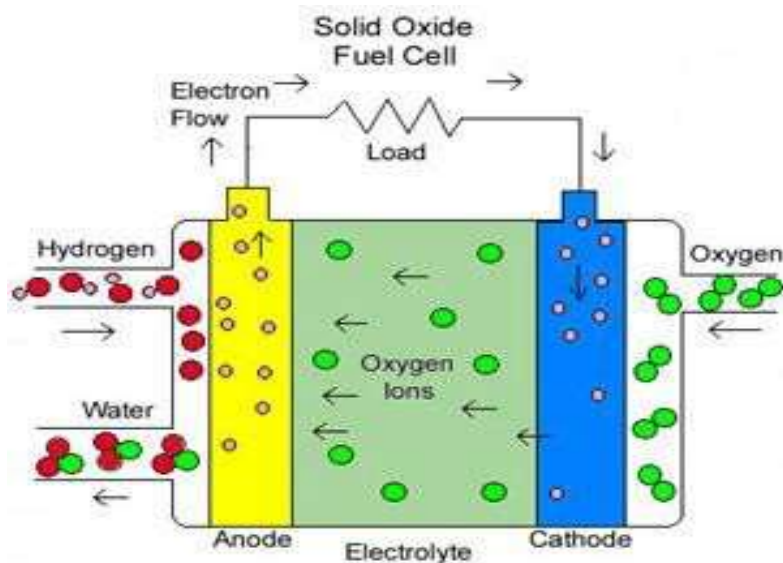
Figure 2.11: Solid Oxide Fuel Cell [30].

2.5 Nafion® membrane

Nafion® is a type of perfluosulfonic acid (PFSA) ionomer membrane used widely in fuel cells [14,27] and it is a generally known as polymer electrolyte membrane for DMFCs due to its good conductivity, excellent mechanical property, chemical stability, and commercial availability [18,24,31-33]. It is made up of a polytetrafluoroethylene (PTFE) backbone, which is attached on fluorodiether side chains with sulfonic acid end groups [12,34].

Three regions of Nafion® structure were proposed by the Yeager Model in which region number is polytetrafluoroethylene (PTFE) backbone that has characteristics of hydrophobic, large chemical and mechanical stability. The second structure is an intermediate region with characteristics of amorphous and hydrophobic, which contains a minimum of water and some radical anions. The third region gives absorbing character to the membrane because ionic coexists where most water molecules are absorbed [35].

Commercially, Nafion® is obtained in various forms such as extruded and solution cast films of different thickness and similar weights, dispersions in water/alcohol solutions and pellets [23].
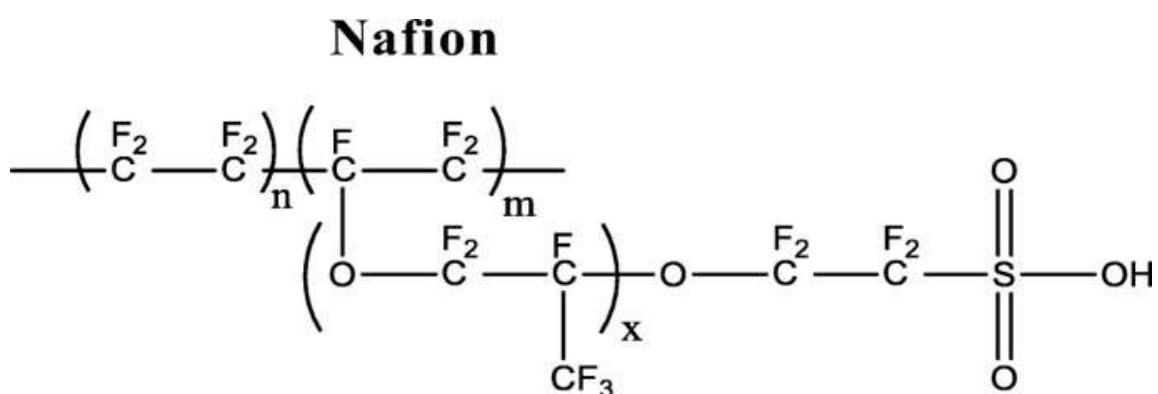
Figure 2.12: Structure of Nafion® Membrane [36].

To achieve an excellent fuel cell performance, PFSA/PTFE membrane containing high proton conductivity and good mechanical property should be achieved [12]. The ionic clusters of Nafion® membrane allow high proton conductivity. This higher performance and higher fuel utilization can be achieved with low methanol crossover. Therefore, to keep high performance membrane high conductivity is needed [37].

2.6 Proton Conductivity Mechanism

Transportation of proton occurs via two principal mechanisms namely "hoping" and "vehicular" in hydrated polymeric matrices. The vehicular mechanism is when the hydrated proton responds to an electrochemical difference by diffusing through either the aqueous medium or other liquid. Water as vehicular site diffuse through medium with protons attached to it thus act as proton carrier. In this case, proton transfer rate is dependent on vehicular diffusion rate and existence of three volumes within polymeric chains, which is responsible for hydrated protons diffusion through the membrane [3]. In fuel cell, electro-osmotic drag occurs because of hydrogen ions movement from anode to the cathode dragging water molecules to the cathode side [8].

Electro-osmotic drag (Figure 2.13) occurs when water molecules are pulled by the protonic current from anode side to cathode side. Cathode will be filled with water and water will diffuse back from cathode to anode [38]. Therefore, water flooding will occur, and it can be controlled by balancing hydration of membrane [39]. These phenomena will lead to reducing performance of fuel cell as well as increasing resistance of membrane. Humified fuel gas may also cause additional water at the anode side.

Therefore, to achieve optimum performance of membrane, different operating parameters should be accurately controlled to manage water in membranes [38]. Hence, it is important to manage water to achieve optimum performance [39].
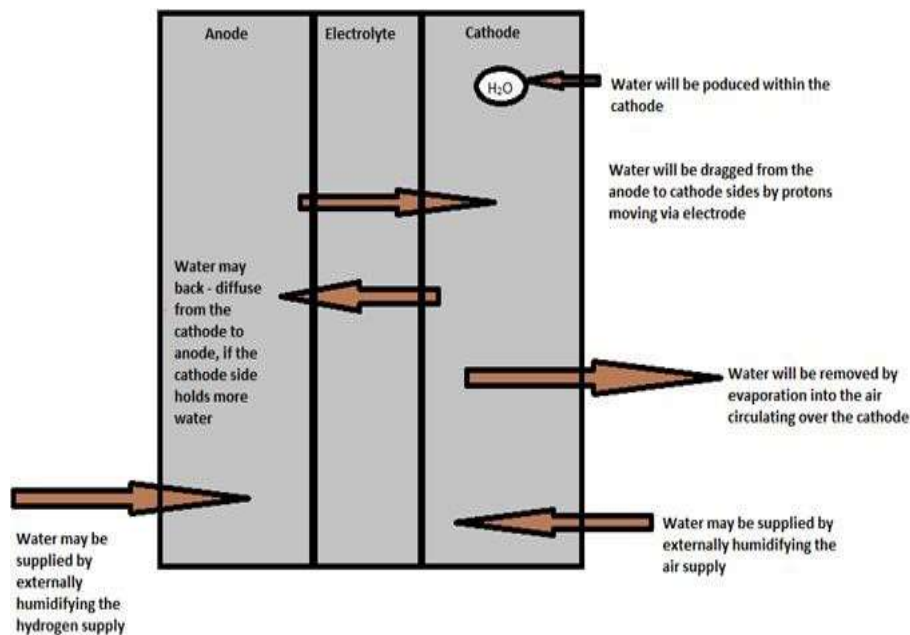
Figure 2.13: Movement of water from different directions via electrolyte of PEMFC [8].

2.7. Limitations of Nafion® membrane

Lower proton conductivity, caused by water loss, is experienced in Nafion® membrane since Nafion® is limited to conditions of well humified operation and must be operated below or at 80°C [40,33]. Proton conductivity is reduced when the membrane is not properly hydrated [20,41]. Usually, determination of Nafion® membrane ion conductivity depends on water content, temperature, and strongly being affected by water content. Applied temperature, the acid concentration, and the type of proton acid donor during pretreatment have impact on the ionic conductivity [42].

2.8. Modification of Nafion® Membranes

According to Wu et al. [12] and Thiam et al. [43], a non-reinforced thin membrane has a less lifetime than when reinforced with porous PTFE membranes, which has considerably more life span due to its higher mechanical strength. The most prevalent type of mechanical failure found in pure Nafion® based MEA is from the edge, where a tear or holes happen near or along a gas diffusion layer (GDL) after a life test. Research indicates that PTFE reinforcement might offer an active barrier to enlargement or crack propagation originated in Nafion® membrane [12].

Nafion® membranes are mostly used as proton exchange membranes (PEM) and as a proton-conducting separator in a fuel cell, which utilizes H_2 as fuel and O_2 as oxidant. Application of Nafion® PEMs in DMFC causes methanol crossover. Research indicates that modification of Nafion® PEM can be done by incorporating low compatible polymers such as sulfonated poly (ether ether ketone) s (SPEEKs),polybezimidazole (PBI), polyaniline (PANI), poly (tetrafluoroethylene) (PTFE) with Nafion® or by introducing nanoparticles to the Nafion® membrane to reduce methanol crossover [44, 24].

PEM acts as electrolyte transferring the protons from anode to cathode and prevents fuel and electrons flowing through the membrane. Good mechanical strength, thermal and chemical stability, high proton conductivity, long lifespan and compatibility with other fuel cell components are the main characteristics needed for PEMs. Different approaches have been used to modify polymers with various materials such as hydrophilic polymers to improve interaction of organic- inorganic phase and thermal properties as well as inorganic materials (compounds) to develop nanocomposite membrane to improve mechanical and thermal stability of the membrane [45].

According to Narayanamoorthy and Balaji [5] alternative composite materials have been developed by introducing additives such as clay mineral (e.g., montmorillonite or inorganic silicate materials). Nafion® has relatively high proton conduction; modification of Nafion®-based membrane could be an active approach to highly get proton-conductive membranes. Other properties of Nafion® like methanol permeability and mechanical strength could be improved by modifying the Nafion® membrane [46].

Nanostructured hybrid or Nafion® nanocomposite membranes can be generated by incorporating organic or inorganic nanoparticles of different materials such as clay, PVA, zirconium phosphate, silica, metal oxides, zeolites and polypyrrole. These membranes often indicate better properties such as chemical, electrical, physical, thermal, and mechanical properties. By modifying Nafion® membranes, less Nafion® solution will be used and Nafion® membrane will be less expensive. Various researchers have indicated that Nafion® composite membranes exhibited high proton conductivity, high water retention performance at high temperatures and low alcohol permeability [22].

For long-term mechanical stability the membrane needs to be strong enough and at the same time be flexible and tough. However, agglomeration and poor dispersion can be experienced if inorganic particles are added after certain loading causing membrane to be brittle. In this case a methanol barrier polymer such as polyvinyl alcohol (PVA), polyvinylidene (PVDF) and polybenzimidazole (PBI) can be blended or cross linked with Nafion® physically, chemically, or ionically [29].

In recent studies it is indicated that Nafion®-oxides composites with a high load of inorganic particles are presented with improved thermo-mechanical properties and lower alcohol permeability with respect to Nafion® membrane [11]. PFSA nanofiber membranes have been fabricated by electrospinning, it was indicated that performance was improved. However, Nafion® dissolves in the most known solvent under mild conditions. At high pressure and elevated temperature, PFSA chains can be soluble in mixtures of special solvents but if room temperature is reduced aggregation of micelles structures will occur. The aggregation causes PFSA solutions to have inadequate polymer chain entanglement, making them not be suitable for electro-spinning [23].

It was discovered that blending Nafion® with other polymers, increased viscosity of solution and solution could be easily spinnable because Nafion® has low viscosity and cannot be spinnable. It is advisable that polymers such as polyvinyl alcohol (PVA), poly (acrylic acid) (PAA), polyvinyl pyrrolidone (PVP) and polyethylene oxide (PEO) can be blended with Nafion® to make spinnable solution [47].

Materials that cause fouling in membranes are hydrophobic in nature. Therefore, fouling can be reduced in membrane by incorporating hydrophilic functional group at membrane surface to improve its performance. Various nanoparticles have been fabricated for water treatment applications such as graphene oxide (GO), carbon nanotubes (CNTs), silver (Ag), titanium (TiO_2), aluminum (AlO_3), silica (SiO_2), Iron (Fe_3O_4), zirconium (ZrO_2), zinc oxide (ZnO), clay nanoparticles and zeolite (NaX). Poor dispersion of nanomaterials less than 100nm diameter causes agglomeration and distribution in the polymer matrix becomes not uniform. Properties such as free surface energy, hydrophilicity, antifouling, pore size, roughness of nanocomposite membrane can be affected due to agglomeration [48].

2.9. Applications of Nafion® membrane

Nafion® is one of widely investigated polymers due to its exception properties such as distinctive thermal and mechanical stability and good conductivity and it also has large application in electrochemical devices, morphing structure, fuel cells, batteries, water electrolysis, drug release, sensor, and super-acid catalysis [26].

2.10. Methanol Crossover

Methanol crossover occurs when molecules of methanol penetrate a membrane and methanol directly oxidizes these molecules on the cathode [19]. Two processes that transport methanol in the fuel cell membrane namely `electrostatic drag and diffusion. The methanol is transported from anode to cathode through membrane and is also pulled along with the hydrated protons caused by a flow of current across the cell. In this case, the methanol carried to cathode badly affects the cell performance [49].

Methanol crossover in the cell is regarded as a critical problem, which decreases cell performance by reducing cell voltage, current density, and fuel utilization. Less than 30% of the total chemical energy found in methanol can be exploited and the rest of it can be changed into heat because of methanol crossover and the irreversibility reactions of electrode mainly on the positive electrode [19].

However, dilution of methanol is necessary so that methanol crossover can be generated even if its energy density approximately can be high about, 1.8 kW/h kg^{-1} or 1.7 kW/L^{-1}. The disadvantage of diluting methanol is that uniform increment of the cell stack dimensions must be applied. To increase dimensions, the following considerations must be made: estimation of the relationship between dimensions and

power requirements as well as the cell that is going to be used in portable applications. The other disadvantage associated with methanol crossover is kinetics of oxygen electro-reduction, which reduces reactions rate. The solution to this problem is to accelerate the rate of reaction by adding more platinum-ruthenium and by selection of proper membranes and methanol tolerant cathode catalyst [19].

The methanol crossover was reduced when oxides of silica, zirconia, titania, organo-montmorillonite are incorporated in Nafion® membrane. Mainly the performance of the membrane-electrode assembly (MEA) was not improved because proton conductivity of composite membranes was low compared to the pristine Nafion® membrane [50].

2.10.1. Factors influencing the methanol Crossover Rate.

2.10.1.1. Thickness of Membrane and Equivalent Weight (EW)

Methanol crossover rate is reduced when membrane thickness is increased. Thick membranes or high EW membranes may be used to decrease the methanol crossover rate, but higher voltage losses will be experienced because of higher specific resistance of thicker or high EW membranes. It is recommended that these membranes be used in applications where amount of power densities and current are low since loss of voltage is not that important and where methanol crossover increases fuel efficiency low [49].

It was discovered that proton conductivity of nanofibers increases when fiber diameter is reduced. Conclusion based on comparison between nanofiber and blended type of membranes on Nafion® and PVA revealed that all types of membranes are capable of lower methanol crossover. However, the nanofiber morphology displayed lower twisted proton conduction pathways and better performance of DMFC when compared

to the blended membranes in which agglomeration and non-homogeneous distribution of PVA occurred [51].

2.10.1.2. Cell Operating Parameters

Normally the feed concentration of methanol used in DMFC is 1M. The concentration above 1M will rapidly increase the methanol crossover which will negatively affect the overall performance of DMFC [49].

2.10.1.3. Cell Temperature

Reducing temperature will result in decreasing methanol crossover rate between temperature of 90-22°C. According to results of experiments conducted, performance of fuel cell is reduced when temperature decreases. Hence, fuel cells should be operated at lower temperatures to obtain higher efficiency [49].

2.10.2. Strategies for Reducing Methanol Crossover in DMFC:

- Lower temperature and methanol concentration.

- Use lean feed method to obtain higher fuel efficiency.

- Use of methanol tolerant cathode catalyst to improve potential of cathode.

- Use of fillers to modify pristine Nafion® membrane to lower methanol crossover and

- Blending of Nafion® membrane with other polymers. It was reported that absence of electroosmotic drag was experienced when Nafion® was blended with polybenzimidazole (PBI) [49].

2.11. Nanotechnology

The interest in nanotechnology started to develop applications in all disciplines after Nobel laureate Richard P. Feynman introduced it. In general, nanotechnology refers to material sizes of 100 nanometer (nm) or no less than one dimension. More interest has developed for the size of material decreasing from 100nm to atomic level (about 0.2 nanometer) since material would have increased surface area and dominance quantum effects over this size range which causes the nanomaterial to reveal different and better properties compared to those of the same material at a micro size [16].

Hence, nanomaterials with high surface area (per unit mass), and high chemical reactivity are most likely to find applications in various fields. In the field of nanotechnology, nanomaterials that are mostly investigated are the nanoparticles (NPs), nanofibers (NFs), nanopowders, nanorods, nanotubes and nanowires [16,38]. Among these types of nanomaterials, NFs are preferable and seem to be promising and efficient because of their characteristics such as large surface area to volume ratio, surface functionalities flexibility, and greater mechanical properties [16].

Conventional inorganic materials are being replaced by nanostructured inorganic materials in application such as fuel cells, solar cells, catalysis, high mechanical strength unit, biosensors, hydrogen storage and batteries due to their unique properties. The advantages of nanomaterials are large surface area, small particle size and quantum size that are suitable for technological applications [52].

2.11.1. Nanofibers

Polymer nanofibers are classified as fiber of less than 100nm. Polymer nanofibers have unique properties due to their large surface area per unit mass and small pore size. Specific properties of polymer nanofibers are important since their features have an effect on adsorption, electrical conductivity, wettability, biocompatibility, and optical properties. Some special application, it will be necessary to modify polymer nanofiber to improve their surface properties [53-54].

Nanofibers are regarded as good material for many applications such as DMFC, hydrogen storage and hydrogen production because of their characteristics such as one-dimensional network structure, large surface area, high porosity, enough solvent uptake, and high mechanical strength [11].

The fabrication of NFs such as drawing, template synthesis, phase separation, self-assembly, solvothermal synthesis, and solution-phase growth based on capping reagent, and electrospinning have been reported. Electro-spinning is the most preferable method because it costs less, it is handy, and it is a high-speed technique to fabricate NFs with diameter ranging from 50 to 100nm or greater. The advantages of NFs produced by electro-spinning are a small diameter, large aspect ratio (ratio of length to diameter), high surface area (surface area to volume ratio), various in composition, exceptional physicochemical properties, and design flexibility for chemical or functionalization of physical surface [16].

2.11.2. Metal Nanoparticles

Properties such as small size and large surface area of metal nanoparticles have recently drawn great attention of researchers as well as their application in heterogeneous applications. Surfactants, polymers as stabilizers and carbon nanotubes have been used successfully to control the size of nanoparticles and to suppress their aggregation. It is advisable that effective metal nanoparticles be loaded on the supporting materials surface which has good conductivity so that catalytic performance of metal catalyst is enhanced [55].

The unique properties of metal nanoparticles (NP's) make them to be preferable for many applications than the bulk. A few reduction methods were used to synthesis metal NP's and mixed metal NP's [56].

Lin and Chang [57] reported that with a humified hydrogen fuel, Nafion® based PEMFC could operate up to maximum temperature of 130°C. In addition, it was reported that addition of inorganic nanoparticles to Nafion® improved the performance of PEMFC when operated at temperature of 90 – 130 °C and methanol permeability was reduced [58]. Research has demonstrated that polymer/ silica nanocomposite can improve physical properties of materials e.g., mechanical, and thermal properties as well as unique properties [51].

Unique physical and chemical properties of nano-sized noble metal particles which are different from bulk have attracted many researchers [59]. Nanomaterial of coinage and transition metals has been extensively studied and they are considered as potential catalysts due to their high surface area to volume ratio [60].

Usually, nanoparticles are not thermodynamically stable in terms of agglomeration. Therefore, they need to be stabilized by using polymers, dendrimers, surfactants, or organic ligands. "Polyol" method is used to stabilize nanoparticles in which metal precursor such as PVP or PVA is dissolved in solvent and reduction is done at high temperature by alcohols such as ethylene glycol [60].

The chemical and physical properties of metal nanoparticles such as large surface area, small sized and their great application in heterogeneous catalysis have drawn the attention of many researchers. The studies revealed the nanoparticle size, and the suppression of aggregation were successfully controlled by adding stabilizers such as surfactants, polymers, and carbon nanotubes. Hence, the catalytic support should have the ability to stabilize and disperse metal nanoparticles [55].

The electrochemical deposition is the most preferred than the chemical or hydrothermal synthesis process because there is no interference of products produced during metal nanoparticle electrodeposition and synthesis of nanoparticles by electrodeposition can be done at room temperature [59].

2.11.3. Composite membranes

Composite- is combination of bulk phase or matrix and a reinforcement phase of two different materials. Composite material has excellent properties due to the combination reinforcement strength and toughness of matrix. The reinforcement gives composite stiffness and strength which carries most of the load while matrix is simply ductile or tough [61].

Polymer matrix composites can be developed by various ways such as blending conductive polymer with other polymer to form conductive composite, adding metal particles to polymer matrix, incorporate enzymes in polymer matrix for application of biosensors, and adding metals on the surface of the polymer matrix to obtain good conductivity and mechanical strength [61].

Nano-sized materials are applied in fuel cells due to lack of performance of membranes in low humidified regions and at high temperatures [62]. Nano-composite membranes as engineered materials had indicated a huge possibility in chemical engineering industry whereby most compounds two or more compounds can be established by synthesis with distinctive properties, and they can be used in different applications [63]. According to Thiam et al. [43], use of nanomaterials has increased in production, purification, and storage of H_2 for use in fuel cells.

The problem of high methanol crossover in DMFC has led to use of nanotechnology in PEM to improve DMFC performance which causes improvement of methanol barriers and transportation of proton, cost effectiveness, acceptable mechanical, thermal, and chemical stability. Incorporation of nanomaterials with Nafion can improve properties such as methanol permeability, water uptake and mechanical properties [12].

According to Thiam et al. [64] nano-composite membranes showed lower permeability and good ionic conductivity when compared to unmodified Nafion® 117. Other research on nanocomposite/nanoparticles have been conducted such as nano-composite based on PVA nanofiber [12], Pd- SiO_2 [64], Titania nanocomposite [16], polybenzimadazole (PBI), and SiO_2 nanoparticles [43].

Both organic and inorganic nano-composite materials have attracted more attention since all the nano-composite materials have the advantages of organic components such as light weight, flexibility, and mold ability, and inorganic component, such as high strength, heat stability, and chemical resistance [16, 26]. Hence, more research of fabrication of composite NFs involving inorganic nanostructured material encapsulated in polymer matrix has been conducted in the past few years [16].

Organic/inorganic materials can be developed by sol-gel method. If fabrication of these materials is at nanoscale, properties such as wettability, thermal stability, chemical resistance, and flexibility could be improved. The results indicated that hydrophobic/hydrophilic properties of micro or nano-structure materials low surface energies were advanced when compared to bulk materials. The research indicated that hydrophobic property of electrospun nanofiber composite was observed after heat treatment [26].

To have a high interface between inorganic and organic components, inorganic solids need to be homogeneously dispersed in the solution. If inorganic solids are not well dispersed in the solution, it will lead to composite membranes not being homogeneous with high inorganic solids agglomerations. Proton conductivity increases when the size of particle is reduced since proton conductivity pathway for inorganic particulates are not through bulk but across the surface. Preparation in situ methods such as ion exchange techniques or sol gel can help to modify polymer microstructure, influence swelling, conductivity, and characteristics of hydrophobic/hydrophilic [49].

Electrospinning is regarded as appropriate technology to fabricate nanomaterial such as fibers, tubes, or belts. The electrospinning is preferable mostly due to its capabilities to allow prepared solution such as sol-gel, particulate suspension, and

polymer solution and melt solution to be electros-pun into fibers when high electric field is applied [26].

Various types of fillers have been added into Nafion® matrix to reduce the methanol crossover in the Nafion® membrane. Palladium has been used as fillers since it has permeability towards protons and lower permeability towards methanol. Proton conductivity can be increased, and alcohol permeability be reduced when fillers are incorporated in the Nafion®. Results indicated that the thermal stability and mechanical stability of organic-inorganic modified membranes were improved hence water swelling and methanol permeability were reduced. Most research has indicated that proton conductivities of modified membranes have been reduced compared to the convectional Nafion® membrane [65].

2.11.3.1. Palladium nanocomposite membranes

Study of palladium nanoparticle has been extensively studied in different applications such as electrochemical, oxidations, hydrogenations, carbon-carbon bond reactions in fuel cell. It can also be used in sensing and hydrogen storage applications [64]. Recent studies indicate that due to the important role exhibited by palladium in chemical sensors, hydrogen storage and catalysis, most researchers have been focused on the synthesis of palladium nanoclusters. Lately preparation of Pd nanoparticle is preferable than that of platinum (Pt) due to its lower cost, its large surface area to volume ratio and its unique function in absorption of hydrogen [59]. The catalytic activity of Pd nanoparticle depends on its shape and size and it has been discovered as an efficient catalyst for various compounds catalytic reactions [66]. Various techniques such as microwave method, hydrogen reduction, refluxing

alcohol reduction, electrochemical deposition, and chemical liquid deposition have been used. Mostly the particles are produced by the reduction of metal ions in the presence of stabilizers [59].

Generally, pre-synthesis of the nanoparticles is done by reducing agents' solution via the reduction of metal ions. Surface tension modification using polymer/ligands or suitable solid matrix is often used to stabilize catalyst particles. It has been reported that the stabilization causes the loss of catalytic activity badly and Pd nanoparticles have poor stability under these conditions [59].

Pd nanoparticles have been used in few methods of coupling reactions but some of these reaction methods suffer due to use of bulky, high cost and commercially unavailable ligands, prolonged reaction times and high boiling solvents [67],

Pd and Pd derivatized catalysts have recently been used in DAFC's due to its extensive properties such as good electrocatalytic activity and excellent anti-CO toxic ability. The main factor affecting the performance of electro- catalytic catalysts is the selection of appropriate support with strong adsorption of metals, good conductivity, and high surface area because the choice of metal has effect on the size and dispersion of the metal nanoparticles [68].

Stable loading sites and dispersion of catalytic metal nanoparticles are done by employing electro-catalyst support that forms the catalyst layer between Polymer electrolyte membrane (PEM) and gas diffusion layer (GDL). It also forms continuous porous pathways for mass transfer and electrons. The catalyst support degrades because of the harsh corrosion supports which damages the loading sites and causes the interaction between support and nanoparticles to be weak thus causing detachment of catalytic metal nanoparticles or agglomeration.

Therefore, the electro-catalyst support should display high electrical conductivity, stable porous structure, and have strong interaction with catalytic metal nanoparticles promoting electrode reactions [69].

Palladium nanoparticles were mixed with silica nanoparticles solution prepared by sol-gel method to be used in electrospinning to create Pd-SiO$_2$ fibre. Pd-SiO$_2$ fibre was incorporated in Nafion$^®$ polymer to develop polymer electrolyte membrane for fuel cell. The results indicated that the reduction in methanol permeability was successfully achieved with no change in proton conductivity of the Nafion$^®$ [65].

Pd nanoparticles were dispersed in polymer matrix of poly block amide (Pebax® MV 3000) to create nanocomposite membrane. The property of Pebax matrix was improved from non-conductive to conductive material due to incorporation of palladium nanoparticles. It is recommended that this type of nanocomposite membrane may be used in sensing applications due to improved electrical conductivity and its ability to store hydrogen [70].

Synthesized palladium nanoparticles were produced by chemical infusion method. Pd nanoparticles were diffused into poly[tetrafluoroethylene-co-(perfluoropropyl) vinyl ether)] [PFA; Cs Hyde] matrix for fabrication of nanocomposite membrane. The results demonstrated that process temperature and polymer matrix structural properties have impact on nucleation and increasing amount of palladium nanoparticles [41].

2.11.3.2. Silica nanocomposite membranes

Silica (SiO$_2$) has been utilized in most research to create polymer electrolyte membranes for fuel cells. It can be incorporated with other fillers to different polymer matrix [65]. The sol-gel reaction was used to prepare silica and sulfonic acid-

functionalized silica (sul- SiO_2) nanoparticles and blended with poly (vinylidene floride) (PDVF) to create composite membranes. Both membranes exhibited promising results thus making them suitable to be used as polymer electrolyte membranes in fuel cell [71].

Other research studies indicate that composite membranes of SiO_2/Nafion[®] were successfully fabricated. Water retention properties and methanol permeability were improved but experienced durability reduction due to strain to failure of membranes being reduced by 50% in comparison with pristine Nafion[®] membrane [72]. The silica nanoparticles incorporated into sulfonated polymers to create nanocomposite membraned yielded improved results in terms of methanol crossover reduction, water retention, thermal stability and increase in proton conductivity [73-75].

Incorporation of silica nanoparticles into blended solution of sulfonated poly (ether ether ketone) (SPEEK) and sulfonated poly (vinylidene fluoride-co-hexafluoropropylene) (SPVdF-HFP) yielded better results of proton conductivity [70-71]. silica has hygroscopic affinity and highwater absorption capacity. Therefore, addition of silica improves hydrophilic property of membrane leading to improvement of water uptake for composites membranes [73].

Silica /silicotungstic acid (SiO_2/SiWA) were blended with Nafion[®] solution. The nanocomposite membrane indicated higher selectivity (proton conductivity to methanol permeability ratio) as compared to recast Nafion[®]. The methanol permeability was reduced with enhanced proton conductivity, but it is reported that nanocomposite membrane encountered leaching of dopant throughout pre-treatment process [76].

2.11.3.3 Titanium oxide nanocomposite membranes

Porous titanium oxide nanotubes (TNT) were synthesized by calcination process. The composite membranes were created by impregnating titanium oxide nanotubes into the Nafion® matrix. The composite membranes exhibited higher water retention which increased proton conductivity under low and high relative humidity conditions. Nafion®- TNT composite membranes also indicated improved mechanical property compared to pure Nafion® membrane [77]. Sulfonated titanium oxide nanoparticles were prepared and blended with sulfonated polyethersulfone (SPES) polymer to create nanocomposite membrane. The membrane exhibited better proton conductivity and lower methanol permeability than pure SPES membrane. Addition of TiO_2 into polymer matrix improved its hydrophilic properties thus resulted in higher water uptake [78].

TiO_2 nanoparticles were prepared and incorporated in poly (2.6-dimrthyl-1,4 phenylene (PPO) and polysulfone (PSF) for fabrication of nanocomposite membranes. The proton conductivity of the membranes was reduced at higher loading, and this can be due to agglomeration of nanoparticles that lead to formation of macroparticles but increase in nanoparticles reduced methanol permeability [79].

Nafion® composite membrane was prepared by incorporating TiO_2 nanoparticles into polymer matrix. The results showed lower water uptake, higher proton conductivity and low methanol permeability than pristine Nafion® membrane. The nanocomposite membrane can be used in temperatures of more than 100ºC [80] and sulfonated titanium oxide ($sTiO_2$) nanoparticles were blended with sulfonated poly (arylene ether sulfone) (SPAES). The nanocomposite membranes proton mobility and proton conductivity were improved by adding $sTiO_2$ nanoparticles [81].

2.11.3.4 Montmorillonite (MMT) nanocomposite membranes

The composite membrane of montmorillonite was fabricated by blending poly (2.5-benzimidazole-grafted montmorillonite (ABPBI-MMT) with sulfonated PVA (SPVA). Higher proton conductivity and water uptake were recorded for the composite membranes [82]. Carbon nanotubes containing montmorillonite (MM-CNT) were prepared by chemical vapour deposition (CVD) and blended with Nafion® to develop nanocomposite membrane. It is reported that the nanocomposite membrane can successfully be used in PEM fuel cell because of its thermal stability properties [83]. Polymide (PI)/Montmorillonite (MMT) composite membranes were developed by doping method. The composite showed higher water uptake as well as proton conductivity and lower methanol uptake [84].

The Nafion®/MMT-CsPW nanocomposite membranes showed higher selectivity. The hydrophilic groups in the polymer membrane were increased by adding MMT-CsPW resulting in higher water uptake and IEC. It also indicated that high proton conductivity and low methanol permeability were recorded when adding CsPW content and reducing amount of MMT [85].

Sulfonated PEEK/MMT nanocomposite membranes were evaluated to be used as PEM in fuel cells. The proton conductivity of membrane was reduced when increasing MMT content, but low methanol crossover was recorded when increasing loading content of MMT. Despite low proton conductivity, the overall results indicate that selectivity of more than 60% was achieved with loading of 1% MMT. Therefore, it was concluded that this nanocomposite membrane may be used in fuel applications [86]. The Nafion®/Montmorillonite nanocomposite membranes showed similar results with low proton conductivity and fuel crossover when increasing MMT content [87-88].

2.12 References

1. Carrete L., Friedrich K.A., and Stimming U (2001). Fuel-Fundamentals and Applications. Fuels Cells, 1 (1), pp. 5-39.

2. Heya Na, Zhang, L., Qiu, H., Wu, T., Chen, M., Yang, N., Li, L.-Z., Xing, F. and Gao, J. (2015). A two-step method to synthesize palladium–copper nanoparticles on reduced graphene oxide and their extremely high electrocatalytic activity for the electrooxidation of methanol and ethanol. Journal of Power Sources, 288, pp.160– 167.

3. Kamarudin, S.K., Achmad, F. and Daud, W.R.W. (2009). Overview on the application of direct methanol fuel cell (DMFC) for portable electronic devices. International Journal of Hydrogen Energy, 34(16), pp.6902–6916.

4. Mekhilef, S., Saidur, R. and Safari, A. (2012). Comparative study of different fuel cell technologies. Renewable and Sustainable Energy Reviews, 16(1), pp.981– 989.

5. Turco M.C., Ausiello, A. and Micoli L. (2016). Treatment of Biogas for Feeding High Temperature Fuel Cells. Springer, Online ISBN -13: 9783319032153.

6. Ortiz-Rivera E. I., Reyes-Hernandez A.L., and Rey A. Febo (2007). Understanding the History of Fuel Cells. Institute of Electrical and Electronics Engineers, pp. 117-122.

7. Giorgi L. and Leccese F. (2013). Fuel Cells: Technologies and Applications. The Open Fuel Cells Journal, 6, pp. 1-20.

8. Larminie J., and Dicks A (2003). Fuel Cell Systems Explained: Second Edition. John Wiley and Sons Ltd. ISBN 0-470-84857X.

9. Yandrasits M. and Hamrock S. (2012). Poly (Perfluorosulfonic Acid) Membranes. Polymer Science: A Comprehensive Reference, 10, pp. 601-619.

10. Maheshwari K., Sharma S., Sharma A., Verma S. (2018). Fuel Cell and Its Applications: A Review. International Journal of Engineering Research & Technology, 7 (6), pp. 6-9.

11. Smith, T.A., Santamaria, A.D., Park J.Y., and Yamazaki, K. (2014). Alloy Selection and Die Design for Stamped Proton Exchange Membrane Fuel Cell (PEMFC) Bipolar Plates. Procedia CIRP 14, pp.275–280.

12. Wu, B., Zhao, M., Shi, W.-Y., Liu, W., Liu, J., Xing, D., Yao, Y., Hou, Z., Ming, P., Gu, J. and Zou, Z. (2014). The degradation study of Nafion/PTFE composite membrane in PEM fuel cell under accelerated stress tests. International Journal of Hydrogen Energy 39(26), pp.14381–14390.

13. Yan Q., Toghiani H., Wu J. (2006). Investigation of water transport through membrane in a PEM fuel cell by water balance experiments. Journal of Power Sources, 158, pp. 316–325.

14. Zawodzinski T.A., Dawy J., Valerio J., and Gottesfeld S. (1995). The water content dependence of electro-osmotic drag in proton-conducting polymer electrolytes. Electrochemica Acta, 40, pp. 297-302.

15. Mondal, S., Soam S., and Kundu P.P. (2015). Reduction of methanol crossover and improved electrical efficiency in direct methanol fuel cell by the formation of a thin layer on Nafion 117 membrane: Effect of dip-coating of a blend of sulphonated PVdF-co- HFP and PBI. Journal of Membrane Science 474, pp.140–147.

16. Mallakpour, S., Zhiani, M., Barati, A. and Rostami, H. (2013). Improving the direct methanol fuel cell performance with poly (vinyl alcohol)/titanium dioxide nanocomposites as a novel electrolyte additive. International Journal of Hydrogen Energy, 38(28), pp.12418–12426.

17. Zainoodin, A.M., Kamarudin, S.K., Masdar, M.S., Daud, W.R.W., Mohamad, A.B.

and Sahari, J. (2014). Investigation of MEA degradation in a passive direct methanol fuel cell under different modes of operation. Applied Energy, 135, pp.364–372.

18. Chen, P., Wu, H., Yuan, T., Zou, Z., Zhang, H., Zheng, J. and Yang, H. (2014). Electronspun nanofiber network anode for a passive direct methanol fuel cell. Journal of Power Sources, 255, pp.70–75.

19. Kim D.Y., Jo M.-W., and Nam S.Y. (2015). A review of polymer–nanocomposite electrolyte membranes for fuel cell application. Journal of Industrial and Engineering Chemistry, 21, pp.36–52.

20. Iwai Y., Ikemoto S., Haramaki K., Hattori R., Yonezawa S. (2014). Influence of ligands of palladium complexes on palladium/Nafion composite membranes for direct methanol fuel cells by supercritical CO_2 impregnation method. Journal of Supercritical Fluids ,94, pp. 48-58.

21. Müller, M., N. Kimiaie and Glüsen, A. (2014). Direct methanol fuel cell systems for backup power – Influence of the standby procedure on the lifetime. International Journal of Hydrogen Energy 39(36), pp.21739–21745.

22. Zakil, F.A., Kamarudin, S.K. and Basri, S. (2016). Modified Nafion membranes for direct alcohol fuel cells: An overview. Renewable and Sustainable Energy Reviews, 65, pp.841–852.

23. Sharma D. K., Li, F. and Wu, Y. (2014). Electrospinning of Nafion and polyvinyl alcohol into nanofiber membranes: A facile approach to fabricate functional adsorbent for heavy metals. Colloids and Surfaces A: Physicochem. Eng. Aspects 457, pp.236–243.

24. Beydaghi H., Javanbakht M., Salarizadeh P., Bagheri A., Amoozadeh A. (2017). Novel proton exchange membrane nanocomposites based on sulfonated tungsten trioxide for application in direct methanol fuel cells. Polymer, 119, pp.

253-262.

25. Dutta, K., Das, S., and Kundu P.P. (2014). Low methanol permeable and highly selective membranes composed of pure and/or partially sulfonated PVdF-co-HFP and polyaniline. Journal of Membrane Science 468, pp.42–51.

26. Yao, Y., Li, J., Lu, H., Gou, J. and Hui, D. (2015). Investigation into hybrid configuration in electrospun Nafion/silica nanofiber. Composites Part B: Engineering, 69, pp.478– 483.

27. Matos, B.R., Isidoro, R.A., Santiago, E.I., and Fonseca, F.C. (2014). Performance enhancement of direct ethanol fuel cell using Nafion composites with high volume fraction of titania. Journal of Power Sources, 268, pp.706–711.

28. Takemori R., and Kawakami H. (2010). Electrospun nanofibrious blend membranes for fuel cell electrolytes. Journal of Power Sources, 195, pp. 5957-5961.

29. Rahimnejad, M., Adhami, A., Darvari, S., Zirepour, A. and Oh, S.-E. (2015). Microbial fuel cell as new technology for bioelectricity generation: A review. Alexandria Engineering Journal, 54(3), pp.745–756.

30. Smithsonian Institution (2017). A Basic Overview of Fuel Cell Technology. [online] Si.edu. Available at: https://americanhistory.si.edu/fuelcells/basics.htm.

31. Cui, Y., Baker, A.P., Xu, X., Xiang, Y., Wang, L., Lavorgna, M. and Wu, J. (2015). Enhancement of Nafion based membranes for direct methanol fuel cell applications through the inclusion of ammonium-X zeolite fillers. Journal of Power Sources, 294, pp.369–376.

32. Wu, X., Wu, N., Shi, C.-Q., Zheng, Z., Qi, H. and Wang, Y. (2016). Proton conductive montmorillonite-Nafion composite membranes for direct ethanol fuel cells. Applied Surface Science, 388, pp.239–244.

33. Dutta, K., Das, S., and Patit Paban Kundu (2015). Partially sulfonated polyaniline

induced high ion-exchange capacity and selectivity of Nafion membrane for application in direct methanol fuel cells. Journal of Membrane Science, 473, pp.94–101.

34. Lee, S.-J., Yu, T. Leon., Lin, H.-L., Liu, W.-H. and Lai, C.-L. (2004). Solution properties of Nafion in methanol/water mixture solvent. Polymer, 45(8), pp.2853–2862.

35. Bautista-Rodríquez C. M., Rosas-Paleta A., Rivera-Marquez J.A., Omar Solorza Feria O.S. (2009). Study of electrical resistance on the surface of Nafion 115 membrane used as electrolyte in PEMFC technology Part I: Statistical inference. International Journal of Electrochemical Science, 4, pp. 43-59.

36. Pyshkina O. A., Novoskoltseva O. A., Zakharova J. A. (2019). Modification of Nafion membrane by polyaniline providing uniform polymer distribution throughout the membrane. Colloid and Polymer Science Membrane, 297, pp. 423–432.

37. Park, Y.-S. and Yamazaki, Y. (2005). Low methanol permeable and high proton-conducting Nafion/calcium phosphate composite membrane for DMFC. Solid State Ionics 176(11-12), pp.1079–1089.

38. Luo, Z., Chang, Z., Zhang, Y., Liu, Z. and Li, J. (2010). Electro-osmotic drag coefficient and proton conductivity in Nafion® membrane for PEMFC. International Journal of Hydrogen Energy, 35(7), pp.3120–3124.

39. Tripathi, B.P. and Shahi, V.K. (2011). Organic–inorganic nanocomposite polymer electrolyte membranes for fuel cell applications. Progress in Polymer Science, 36(7), pp.945–979.

40. Yarrow K.M., De Almeida N.E., Easton E. B. (2015). The impact of pre-swelling on the conductivity and stability of Nafion/sulfonated silica composite membranes. Journal of Thermal Analysis and Calorimetry, 119, pp. 807–814.

41. Zeng, F., Zhang, D. and Spicer, J. (2018). Palladium nanoparticle formation processes in fluoropolymers by thermal decomposition of organometallic precursors. Physical Chemistry Chemical Physics, 20(37), pp.24389–24398.

42. Kuwertz, R., Kirstein, C., Turek, T. and Kunz, U. (2016). Influence of acid pretreatment on ionic conductivity of Nafion® membranes. Journal of Membrane Science, 500, pp.225–235.

43. Thiam, H.S., Daud, W.R.W., Kamarudin, S.K., Mohammad, A.B., Kadhum, A.A.H., Loh, K.S. and Majlan, E.H. (2011). Overview on nanostructured membrane in fuel cell applications. International Journal of Hydrogen Energy, 36(4), pp.3187–3205.

44. Lin, H.-L. and Wang, S.-H. (2014). Nafion/poly (vinyl alcohol) nano-fiber composite and Nafion/poly (vinyl alcohol) blend membranes for direct methanol fuel cells. Journal of Membrane Science, 452, pp.253–262.

45. Lade, H., Kumar, V., Gangasalam Arthanareeswaran and Ahmad Fauzi Ismail (2017). Sulfonated poly (arylene ether sulfone) nanocomposite electrolyte membrane for fuel cell applications: A review. International Journal of Hydrogen Energy, 42(2), pp.1063– 1074.

46. Li H.Y, Lee Y.Y, Lai J.Y, Liu Y.L (2014). Composite membranes of Nafion and poly (styrenesulfonicacid)-graftedpoly (vinylidene fluoride) Electrospun nanofiber mats for fuel cells. Journal of Membrane Science, 466, pp. 238–245.

47. Dong Z., Kennedy S.J., Wu Y. (2011). Electrospining materials for energy related applications and devices. Journal of Power Sources, 196, pp. 4886-4904.

48. Aani A., S., Wright, C.J., Atieh, M.A. and Hilal, N. (2017). Engineering nanocomposite membranes: Addressing current challenges and future opportunities. Desalination, 401, pp.1–15.

49. Vielstich W., Lamm A., and Hubert A. Gasteiger (2003). Handbook of Fuel Cells:

Fundamentals technology and Application. Volume 3 Fuel Cell Technology and Application: Part 1. John Wiley and Sons Ltd. ISBN: 0-471-49926-9.

50. Yen, C.-Y., Lee, C.-H., Lin, Y.-F., Lin, H.-L., Hsiao, Y.-H., Liao, S.-H., Chuang, C.-Y., and Ma, C.-C.M. (2007). Sol–gel derived sulfonated-silica/Nafion® composite membrane for direct methanol fuel cell. Journal of Power Sources, 173(1), pp.36–44.

51. Mollà S., and Compañ V (2015). Nano-composite SPEEK-based membranes for Direct Methanol Fuel Cells at intermediate temperatures. Journal of Membrane Science, 492, pp. 123-136.

52. Wu, N. and Wei, Q. (2012). Inorganic functional nanofibers: processing and applications. Woodhead Publishing Series in Textiles, pp.71–91.

53. Panthi G., Park, M., Kim H.-Y and Park, S.-J. (2015). Electrospun polymeric nanofibers encapsulated with nanostructured materials and their applications: A review. Journal of Industrial and Engineering Chemistry, 24, pp.1–13.

54. Huang F. Q., Wei, Q. and Cai, Y. (2012). Surface functionalization of polymer nanofibers. Woodhead Publishing Series in Textiles, pp.92–118.

55. Liao, F., Wang, Z., Guo, T., Zhang, T. and Wu, Z. (2012). Synthesis of well dispersed palladium nanoparticles-decorated poly(o-phenylenediamine) colloids with excellent performance for hydrazine oxidation. Journal of Electroanalytical Chemistry, 673, pp.38–42.

56. Kumar, K.M., Mandal, B.K., Kumar, K.B., Reddy, S.P. and Sreedhar, B. (2013). Biobased green method to synthesise palladium and iron nanoparticles using Terminalia chebula aqueous extract. Spectrochimica Acta Part A: Molecular and Biomolecular Spectroscopy, 102, pp. 128-1333.

57. Lin, H. and Chang, T. (2008). Preparation of Nafion/PTFE/Zr (HPO4)2 composite membranes by direct impregnation method. Journal of Membrane Science,

325(2), pp.880–886.

58. Kumar, A.P., Kumar, B.P., Kumar, A.B.V.K., Huy, B.T. and Lee, Y.-I. (2013). Preparation of palladium nanoparticles on alumina surface by chemical co- precipitation method and catalytic applications. Applied Surface Science, 265, pp.500–509.

59. Gupta, R., Guin, Saurav.K. and Aggarwal, S.K. (2014). Electrocrystallization of palladium (Pd) nanoparticles on platinum (Pt) electrode and its application for electro- oxidation of formic acid and methanol. Electrochimica Acta, 116, pp.314–320.

60. Cookson J. (2012). The Preparation of Palladium Nanoparticles. Platinum Metals Review, 56, pp. 83–98.

61. Ramakrishna, S., Fujihara, K., Teo, W.-E., Lim, T.-C. and Ma, Z. (2005). An Introduction to Electrospinning and Nanofibers. World Scientific Publishing Co. Pty. Ltd.

62. Chen, L.-J., Liao, J.-D., Lin, S.-J., Chuang, Y.-J. and Fu, Y.-S. (2009). Synthesis and characterization of PVB/silica nanofibers by electrospinning process. Polymer, 50(15), pp.3516–3521.

63. Bai, Z., Zhang, Q., Li, Z., Chao, S., Yang, L. and Qiao, J. (2015). Facile Preparation of Palladium Catalysts Supported on Hollow Polypyrrole Nanospheres for Ethanol Oxidation. Electrochimica Acta, 177, pp.107–112.

64. Thiam, H.S., Daud, W.R.W., Kamarudin, S.K., Mohamad, A.B., Kadhum, A.A.H., Loh, K.S. and Majlan, E.H. (2013). Nafion/Pd–SiO2 nanofiber composite membranes for direct methanol fuel cell applications. International Journal of Hydrogen Energy, 38(22), pp.9474–9483.

65. Thiam, H.S., Daud, W.R.W., Kamarudin, S.K., Mohamad, A.B., Kadhum, A.A.H., Loh, K.S. and Majlan, E.H. (2013). Performance of direct methanol fuel cell with a

palladium–silica nanofibre/Nafion composite membrane. Energy Conversion and Management, 75, pp.718–726.

66. Nguyen V.L., Hirata H., Ohtaki M., Hayakawa T., Nogami M. (2010). Chemical synthesis and characterization of palladim nanoparticles. Advances in Natural Sciences: Nanoscience and Technology, 1, p. 035012 (5pp).

67. Mandali, P.K., and Chand, D.K. (2013). Palladium nanoparticle catalyzed SUZUKI cross-pcoupling reactions in ambient conditions. Catalysis Communications, 31, pp.16-20.

68. Narayanamoorthy, B. and Balaji, S. (2015). Physicochemical characterization of amino functionalized synthetic clay/Nafion nanocomposite film with embedded platinum nanoparticles for PEM fuel cells. Applied Clay Science, 104, pp.66–73.

69. Du, L., Shao, Y., Sun, J., Yin, G., Liu, J. and Wang, Y. (2016). Advanced catalyst supports for PEM fuel cell cathodes. Nano Energy, 29, pp.314–322.

70. Dal Pont, K., Serghei, A. and Espuche, E. (2021). Multifunctional Pd-Based Nanocomposites with Designed Structure from in Situ Growth of Pd Nanoparticles and Polyether Block Amide Copolymer. Polymers, 13(9), p.1477.

71. Tran T.N., Pham T.V.A., Le M.LP., Nguyen T.P.T., and Tran V.M. (2013). Synthesis of amorphous silica and sulfonic acid functionalized silica used as reinforced phase for polymer membrane. Advances in Natural Sciences: Nanoscience and Nanotechnology, 4, pp.045007 (6pp).

72. Tang H.L., and Pan M. (2008). Synthesis and Characterization of a Self – Assembled Nafion/Silica Nanocomposite Membrane for Polymer Electrolyte Membrane Fuel Cells. Journal of Physical Chemistry C, 112, pp.11556–11568.

73. Rodriguez J. I. G, Dicks A. L., Duke M. C., Da Costa J. C. D. (2006). Silica Nafion Modified Composite Membranes for Direct Methanol Fuel Cells. Asia Pacific Journal of Chemical Engineering,14, pp.119-131.

74. Su, Y.-H., Liu, Y.-L., Sun, Y.-M., Lai, J.-Y., Wang, D.-M., Gao, Y., Liu, B. and Guiver, M.D. (2007). Proton exchange membranes modified with sulfonated silica nanoparticles for direct methanol fuel cells. Journal of Membrane Science, 296(1), pp.21–28.

75. Pereira, F., Vallé, K., Belleville, P., Morin, A., Lambert, S. and Sanchez, C. (2008). Advanced Mesostructured Hybrid Silica−Nafion Membranes for High-Performance PEM Fuel Cell. Chemistry of Materials, 20(5), pp.1710–1718.

76. Thiam H.S., Chia M.Y., Cheah Q.R., Koo C.C.H., Lai S.O., and Chong K.C. (2017). Proton Conductivity and Methanol Permeability of Nafion/ SiO2/SiWA Composite Membranes. AIP Conference Proceedings, 1828, p. 020007.

77. Ketpang K., Shanmugam, S., Suwanboon C., Chanunpanich N., and Lee, D. (2015). Efficient water management of composite membranes operated in polymer electrolyte membrane fuel cells under low relative humidity. Journal of Membrane Science, 493, pp.285–298.

78. Elakkiya, S., Arthanareeswaran, G., Ismail, A.F., Das, D.B. and Suganya, R. (2019). Polyaniline coated sulfonated TiO2 nanoparticles for effective application in proton conductive polymer membrane fuel cell. European Polymer Journal, 112, pp.696–703.

79. Msomi, P.F., Nonjola, P.T., Ndungu, P. and Ramontja, J. (2020). Poly (2, 6-dimethyl- 1, 4-phenylene)/polysulfone anion exchange membrane blended with TiO2 with improved water uptake for alkaline fuel cell application. International Journal of Hydrogen Energy 45(53), pp.29465–29476.

80. Cozzi, D., Catia de Bonis, D'Epifanio, A., Mecheri, B., Ana and Licoccia, S.

(2014). Organically functionalized titanium oxide/Nafion composite proton exchange membranes for fuel cells applications. Journal of Power Sources 248, pp.1127–1132.

81. Haragirimana, A., Li, N., Ingabire, P.B., Hu, Z. and Chen, S. (2020). Multi-component organic/inorganic blend proton exchange membranes based on sulfonated poly (arylene ether sulfone) s for fuel cells. Polymer, 210, p.123015.

82. Altaf, F., Batool, R., Gill, R., Rehman, Z.U., Majeed, H., Ahmad, A., Shafiq, M., Dastan, D., Abbas, G. and Jacob, K. (2021). Synthesis and electrochemical investigations of ABPBI grafted montmorillonite-based polymer electrolyte membranes for PEMFC applications. Renewable Energy, 164, pp.709–728.

83. Manikandan, D. Viswanathan M. R., Ávila R. E., Siddheswaran R., Solaiappan A. (2012). Carbon nanotubes rooted montmorillonite (CNT-MMT) reinforced nanocomposite membrane for PEM fuel cells. Materials Science and Engineering B,177, pp. 614–618.

84. Abidin K. S., Kannan, R., Palani P. B., and Rajashabala S. (2017). Role of structural modifications of montmorillonite, electrical properties effect, physical behavior of nanocomposite proton conducting membranes for direct methanol fuel cell applications. Materials Science-Poland, 35(4), pp.707–716.

85. Azimi, M. and Peighambardoust S. H. (2017). Methanol crossover and selectivity of Nafion/heteropolyacid/montmorillonite nanocomposite proton exchange membranes for DMFC applications. Iranian Journal of Chemical Engineering, 14(3), pp.65–81.

86. Hasani-Sadrabadi M.M., Emami, S.H., Ghaffarian R., and Moaddel H. (2008). Nanocomposite Membranes made from Sulfonated Poly (ether ether ketone) and Montmorillonite Clay for Fuel Cell Applications. Energy & Fuels, 22(4), pp.2539–2542.

87. Felice, C., Ye, S. and Qu, D. (2010). Nafion−Montmorillonite Nanocomposite Membrane for the Effective Reduction of Fuel Crossover. Industrial & Engineering Chemistry Research, 49(4), pp.1514–1519.

88. Lee, W., Kim, H., Kim, T. and Chang, H. (2007). Nafion based organic/inorganic composite membrane for air-breathing direct methanol fuel cells. Journal of Membrane Science, 292(1-2), pp.29–34.

Chapter 3

Characterization Techniques and Membrane Testing Methods

3.1. Characterization of Palladium nanoparticles and nanocomposite membranes

3.1.1. Field Emission Scanning Electron Microscope (FE-SEM)

Field Emission Electron Microscope (FE-SEM), model: JSM-7800F (Figure 3.1) with Cathodoluminescence spectrometer, X-ray Energy Dispersive spectrometer (EDS) and Wavelength Energy Dispersive (WDS) was used to analyze morphology of Nafion® recast and nanocomposite membranes. The system is high resolution which can be able to measure a sample at sub nanometer resolution (1,000,000X magnification). In SEM, the e-beam is generated within an electron gun and accelerated by a high voltage. It is then transformed into a fine probe by electromagnetic lenses. The first lens that influences the electron beam is the condenser lens, which causes the e-beam to converge and pass through a focal point that is produced above a condenser aperture. Condenser lens with accelerating voltage is responsible for determining the intensity of e-beam when it scans at a given specimen.

Figure 3.1: Field Emission Electron Microscope (FE-SEM) instrument.

3.1.2. X-ray Diffraction (XRD)

The phase composition and crystallinity of palladium nanoparticles and nanocomposite membranes were analyzed by Rigaku Smartlab X-ray diffraction (Figure 3.2) with Cu K α radiation, λ = 1.54 Å. It measures various samples such as thin films, liquids, nanomaterials, and powders. The system offers a full automated alignment under computer control, optional in-plane diffraction arm for in-plane measurements without reconfiguration, focusing and parallel beam geometries without reconfiguration and Small-angle X-ray scattering (SAXS) capabilities. It incorporates a high resolution θ/θ closed loop goniometer drive system, cross beam optics (CBO), an in-plane scattering arm, and an optional 9.0 kW rotating anode generator.

Figure 3.2: X-ray Diffraction (XRD) instrument.

3.1.3. Fourier Transform Infrared (FTIR)

FTIR is used to determine the functional groups in molecules. The system comprises of a source, an interferometer, a sample compartment, a detector, and a computer. The source emits infrared energy. This beam passes through an aperture which controls the amount of energy presented to the sample, and ultimately to the detector. It can be used to detect an unknown material, the quality of sample and composition of the mixture. Part of infrared radiation in FTIR is absorbed by sample and another portion is transmitted through sample. Three main regions of the infrared spectrum namely: the far infrared (<400 cm^{-1}), mid-infrared (400-4000 cm^{-1}) which is the most used spectra and near infrared (4000 to 13000 cm^{-1}) [1]. The Bruker FTIR instrument (Figure 3.3) was used over the range of 4000-500 cm^{-1} and a resolution of 4 cm^{-1} to analyse Nafion® and its nanocomposite membranes and palladium nanoparticles. A

small amount of material was placed on the diamond coated detector and pressed onto the electrode to get FTIR measurements.

Figure 3.3: FTIR instrument.

3.1.4. X-Ray Fluorescent (XRF)

X-Ray Fluorescent is used to perform elemental analysis in all kinds of samples. It is a powerful system used in food, electronics, petroleum and coal, ceramics, iron and steel, agriculture and food, pulp and paper, environmental and chemical industries. Each element has a specific characteristic X-ray. The accelerated electrons and absorbing X-ray photon emit the X-ray. In this case, the material absorbs an x-ray of a certain wavelength and emits the X-ray with a different wavelength. It provides qualitative or quantitative analysis using higher -order X-rays and mapping. The Shimadzu XRF 1800 (Figure 3.4) was used to perform elementary analysis of commercial palladium samples as well as Nafion® and its nanocomposite membranes. The sample was placed on stainless steel on sample holder and analysed.

Figure 3.4: XRF instrument.

3.1.5. Thermal Gravimetric Analysis TGA

The thermal properties of the Nafion® and nanocomposite membranes were studied by Perkin Elmer thermal gravimetric analysis (Figure 3.5), using a TG under nitrogen flow. Thermal stability of the membranes between 35 °C and 900 °C was evaluated at the heating rate of 10 °C/min. Thermal stability of membranes was studied through thermal dehydration, decomposition, and degradation losses.

Figure 3.5: TGA instrument.

3.1.6. Differential Scanning Calorimeter (DSC)

DSC is a thermal analysis technique in which the heat flow into or out of a material is measured as a function of temperature or time, while the sample is exposed to a controlled temperature program. It is used to measure properties of metals and polymers such as glass transition, phase changes, melting, crystallization, product stability, cure/cure kinetics, oxidative stability, heat capacity and heat of fusion. The Perkin Elmer DSC 400 (Figure 3.6) was used to determine glass transition of Nafion®️ and its nanocomposite membranes from thermograms. The samples were analyzed under nitrogen gas at heating rate of 10°C/min from room temperature to 800°C.
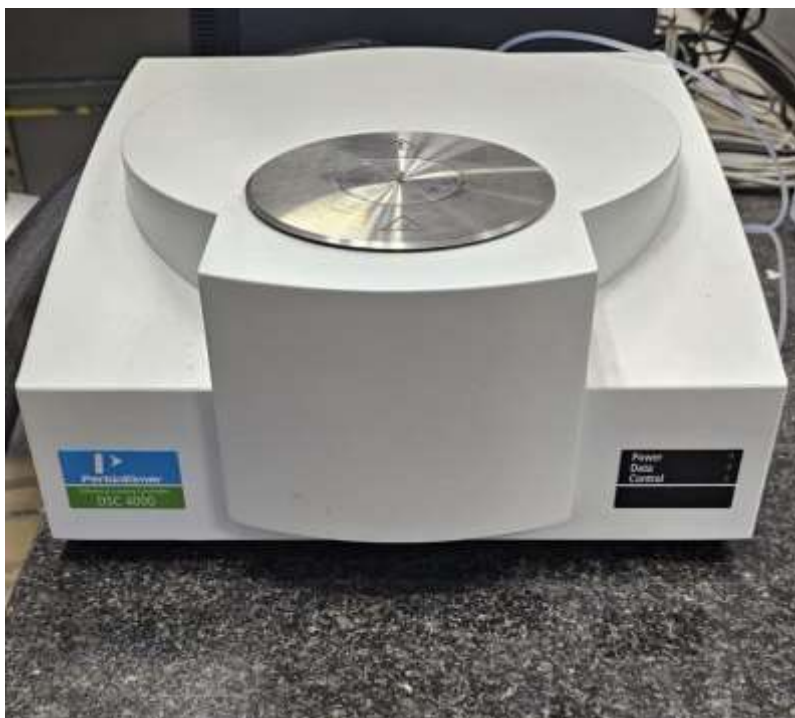
Figure 3.6: DSC instrument.

3.1.7. Surface Contact Angle Measurement (WCA)

The drop shape method is used to measure contact angle of samples using sessile drop or sessile bubble. KRUSS Drop Shape Analyzer (Figure 3.7) was used to perform contact angle of pristine Nafion® and its composite membranes using sessile drop method. Water contact angle equipment is used to measure the surface contact angle of materials. The angle between the droplet and the surface is measured through the image analyzer which analyses a distill water droplet injected from a syringe onto the surface of membrane. If membrane is hydrophobic results will indicate high contact angle (less contact between water droplet and surface) and for hydrophilic it will indicate low contact angle (water spread, all over the surface). Advancing Contact Angle is the most common measurement used [2].

All measurements were carried out at room temperature. The water drop was deposited a few times on membrane surface by needle and water contact angle was recorded for consecutive seconds.

Figure 3.7: KRUSS Drop Shape Analyze for Surface Contact Angle.

3.1.8. High Resolution Transmission electron microscopy (HRTEM)

Transmission electron microscopy (TEM): JEOL-Jem 2100 (Figure 3.8) is a microscopy technique whereby a beam of electrons is transmitted through an ultra-thin specimen, interacting with the specimen as it passes through. The system can provide sample information such as crystal structure, growth of layers, composition, quality, shape, and size. High Resolution Transmission electron microscopy was used to estimate the particle size of palladium and observe the morphology and agglomeration state of Pd nanoparticles. Palladium nanoparticles were placed on carbon -coated copper grid and analysed.

Figure 3.8: HRTEM instrument.

3.1.9. Malvern Zetasizer

Dynamic light scattering (DLS) is the most used technique to measure metal nanoparticles' size. The process of measuring nanoparticles size involves a light scattering projected to nanoparticles solution. The technique analyzes the sample in shorter times [3]. The system is designed to produce high quality data by optimizing components at every stage in the measurement chain from the laser and temperature control, through to the optical design and detector. The particle size distribution of the synthesized Pd nanoparticles and commercial Pd particles was measured by dynamic light scattering (DLS) using a Malvern Zetasizer (Figure 3.9), Nano ZS laser particle size analyzer. DLS measures Brownian motion and relates this to the size of the

particles. The Brownian motion speed depends on the temperature off the particles. Hence it is important to take care of sample temperature to get accurate size measurement. At the end of analysis, the curve is obtained whereby it can be analysed to give the size and the size distribution of the material.

Figure 3.9: Malvern Zetasizer instrument.

3.1.10. Ultraviolet Visible Spectrometer (UV-vis)

A UV-vis spectrometer is used to absorb light of different compounds. Various compounds exhibit different maximum absorbance. The light beam of UV light source split into equal intensity beams by half-mirrored device. Two cuvettes are placed in the cavity, one with the compound to be studied and the second one with reference sample (de-ionized water). The Shimadzu UV-vis spectrometer 1800 (Figure 3.10) in the

range of 200 to 1100nm was used to perform analysis of commercial palladium nanoparticles and synthesized palladium nanoparticles. The system can work in absorbance and transmittance mode. It is an ideal system for understanding the absorption characteristics of a material and to calculate the optical band gap.

Figure 3.10: UV-1800 instrument.

3.2. Fuel Cell Membrane Properties

3.2.1. The water uptake measurements and ion exchange capacity (IEC)

The water uptake of the membrane was measured using Equation (3.1). The membrane was placed in the vacuum at 80°C for 1hour and weighed representing mass of dry membrane. Then, the membrane was immersed in water deionized at 60°C for 1 hour. The membrane surface was dried, and mass was recorded as mass

of hydrated membrane. The following Equation was used to calculate water uptake [4-8]:

$$\text{Water uptake (\%)} = \frac{W_{wet} - W_{dry}}{W_{dry}} \times 100 \qquad (3.1)$$

$W_{wet} and W_{dry}$ are the weight of swollen/hydrated membrane and weight of dry membrane.

The measurement of IEC was performed using Equation (3.2). An acid –based titration was carried out on the membranes. The conversion of sulfonic acid to sodium was performed by immersing the dried membranes in 2 M NaCl solutions. The solution released H$^+$ ions from membrane sample and it was titrated with 0.1 M NaOH. The drops of phenolphthalein indicator were added and volume and pH of NaOH solution was recorded [4-7]:

$$\text{IEC (mmolg}^{-1}) = \frac{C_{NaOH} V_{NaOH}}{W_{dry}} \times 100 \qquad (3.2)$$

3.2.2. Proton Conductivity Measurements

The proton conductivity of palladium nanocomposite membranes was analysed using cell compartment. The compartment has two cells namely cell A filled with 20% HCl solution and cell B filled with deionized water. The membrane was inserted between two cell compartments for the entire experiment without stirring. The pH of acid cells and deionized water cells was taken at 10minutes intervals for duration of 1h:30min [8]. The value of pH was used to determine concentration of acid solution and deionised

water using Equation (3.3). Mass transfer was calculated using Equation (3.4) and its value was used to determine resistance (Equation (3.5)).

Concentration of protons, $H^+ = 10^{-p^H}$ (3.3)

$$m_H = \frac{-V}{zat} \left[\frac{C_{x1} + C_{y1} - 2C_{y2}}{C_{x1} - Cy_2} \right]$$ (3.4)

Where:

m_H is mass transfer coefficient, C_{x1} is initial concentration of HCl, C_{y1} is initial concentration of H_2O, C_{y2} is final concentration of H_2O, v is a volume, z is membrane thickness, a is area of membrane, t is time.

$$R = \frac{1}{m_H}$$ (3.5)

The data was collected, and Figures plotted. The measured R-value was determined from collected data and the following Equation [9-14] was used to calculate ionic conductivity of different membranes.

$$\sigma = L/(AR)$$ (3.6)

where σ is the proton conductivity, A and L are cross-section area and the thickness of the membrane.

3.2.3. Methanol permeability

The methanol permeabilities of palladium nanocomposite membranes were measured at different temperatures of 20°C, 40°C, 60°C and 80°C by flow meter connected to cell compartment. The compartment has two cells namely cell A filled with 5M methanol

solution (90mL) and cell B filled with deionized water (90mL). The membrane was inserted between two cell compartments for the entire experiment. The compartment was immerspoints a circulating water bath where temperature was regulated and kept constant at different set point. The amount of methanol diffused via the membrane was analysed by a flow meter connected to the laboratory computer. The flow rate of diffused methanol was recorded and used to determine methanol permeability (P) using the following Equation [14-17]:

$$C_B = \frac{AP}{V_B L} C_A (t - t_0) \qquad (3.7)$$

C_B is methanol concentration in cell B, C_A is methanol concentration in cell A, $t-t_0$ is a diffusion time, A is an effective membrane area, L is thickness of membrane and V_B is volume of distilled water in cell B.

3.3. Mechanical Properties of Membranes

3.3.1. Tensile Test

Tensile testing on nanocomposite membranes was performed at room temperature using CellScale Univert mechanical tester (Figure 3.11) to evaluate their mechanical properties. The rectangular samples with width of 30mm and length of 60mm were clamped. The testing area of samples was 5mm × 20mm. The thickness of membranes was recorded using digital vernier calliper with commercial PdNps/ Nafion® thickness of 0.141mm, 0.093mm for PdEG 11 Nafion®, 0.076mm for PdEG22/ Nafion® and 0.066mm PdEG33/Nafion®. The data collected was used to calculate tensile strength, elastic modulus, and elongation at break (elongation %) using the following equations [18]:

Tensile strength = $F/w_0 \times d_0$ (3.8)

Percentage elongation (%) = $100 (l-l_0)/l_0$ (3.9)

Where F (force) is the highest load, l_0 is the initial length and l is the final length at point of fracture.

Young modulus (Elastic modulus) was evaluated from initial linear part of slope of the stress-strain curve [8-10].

Figure 3.11: Univert Mechanical Tester.

3.4. Electrochemical Properties of Membranes

3.4.1. Electrochemical Impedance Spectroscopy (EIS) and Cyclic Voltammetry (CV)

The electrochemical cell consisting of three electrodes namely reference electrode, working electrode and counter electrode was connected to Autolab Modular Line Potentiostat/Galvanostat (Figure 3.12) to evaluate electrochemical reactions at working electrode (WE). The working electrode (glassy carbon) was prepared through mixing different concentrations of palladium nanoparticles with Nafion® solution. The resultant solution was deposited on glassy carbon and dried in the oven. The carbon glass containing palladium/Nafion® solution was used as a working electrode. All electrodes were immersed in 1M KOH. The measurements were carried out on the samples and data collected was used to plot CV and EIS.

Figure 3.12: Potentiostat/Galvanostat instrument.

3.5 References

1. Stuart, B.H. (2008). Infrared spectroscopy: fundamentals and applications. Chichester, West Sussex: John Wiley & Sons Ltd.

2. Seeram Ramakrishna S., Lim T.-K., Fujihara K., Teo W.E., and Ma, Z. (2005). An Introduction to Electrospinning and Nanofibers. Singapore, Sg World Scientific Publishing Company.

3. Sigwadi R., Nemavhola F., Dhlamini M.S., and Mokrani T. (2018). Effect of relative humidity on mechanical strength of zirconia/ Nafion® Nano-composite membrane. Journal of Computational and Applied Research in Mechanical Engineering ,7, pp.175-187.

4. Jiang, R., Kunz, H.R., and Fenton, J.M. (2006). Composite silica/Nafion® membranes prepared by tetraethylorthosilicate sol–gel reaction and solution casting for direct methanol fuel cells. Journal of Membrane Science, 272(1-2), pp.116–124.

5. Takemori, R. and Kawakami, H. (2010). Electrospun nanofibrous blend membranes for fuel cell electrolytes. Journal of Power Sources, 195(18), pp.5957–5961.

6. Yen, C.-Y., Lee, C.-H., Lin, Y.-F., Lin, H.-L., Hsiao, Y.-H., Liao, S.-H., Chuang, C.-Y. and Ma, C.-C.M. (2007). Sol–gel derived sulfonated-silica/Nafion® composite membrane for direct methanol fuel cell. Journal of Power Sources, 173(1), pp.36–44.

7. Choi J.Y., Sohn, J.-Y. and Shin, J. (2015). A Comparative Study on EB-Radiation Deterioration of Nafion Membrane in Water and Isopropanol Solvents. Energies, 8, pp. 5370-5380.

8. Das, S.K. and Berry, K.J. (2007). Two-cell theory to measure membrane resistance based on proton flow: Theory development and experimental validation. Journal of Power Sources, 173(2), pp.909–916.

9. Pourzare, K., Mansourpanah, Y. and Farhadi, S. (2016). Advanced nanocomposite membranes for fuel cell applications: a comprehensive review. Biofuel Research Journal, 3(4), pp.496–513.

10. Prasad, M., Mohanty, S. and Nayak, S.K. (2014). Polymer electrolyte membranes are based on sulfonated polysulfone and functionalized layered silicate for direct methanol fuel cell applications. High Performance Polymers, 27(6), pp.714–723.

11. Aiswarya, S.K. and Joseph, S. (2020). Synthesis of methanol blocking PVA-TiO2 cation exchange membrane for direct methanol alkaline fuel cell. Synthetic Metals, 266, p.116442.

12. Ramanujam A . S . , Kaleelkkal N.S, Kumar P.S. (2020). Preparation and characterization of proton exchange polyvinylidene fluoride membranes incorporated with sulfonated mesoporous carbon/SPEEK nanocomposite. SN Applied Sciences, 2, p. 688.

13. Marques, J.L. da S., Zanatta, A.P.S., Hattenberger, M. and Forte, M.M. de C. (2018). Nafion/sulfonated poly(indene) polyelectrolyte membranes for fuel cell application. Polímeros, 28(4), pp.293–301.

14. Goh, J.T.E., Abdul Rahim, A.R., Masdar, M.S. and Shyuan, L.K. (2021). Enhanced Performance of Polymer Electrolyte Membranes via Modification with Ionic Liquids for Fuel Cell Applications. Membranes, 11(6), p.395.

15. Martina, P., Gayathri, R., Pugalenthi, M.R., Cao, G., Liu, C., and Prabhu, M.R. (2020). Nanosulfonated silica incorporated SPEEK/SPVdF-HFP polymer blend membrane for PEM fuel cell application. Ionics, 26(7), pp.3447–3458.

16. Sigwadi R., Dhlamini M.S., Mokrani T., Nonjola P., and Nemavhola F. (2019). The impact of zirconia nano-rods on the methanol permeability and conductivity of Nafion®-ZrO2 nano-composite membrane. International Journal of Microstructure and Materials Properties, 13, pp. 381-402.

17. Iwai Y., Ikemoto S., Haramaki K., Hattori R., Yonezawa S. (2014). Influence of ligands of palladium complexes on palladium/Nafion composite membranes for direct methanol fuel cells by supercritical CO2 impregnation method. Journal of Supercritical Fluids, 94, pp. 48-58.

18. Choi, J., Kyeong M., Kim M.S., Lee S.Y., Joo S. H., Park, H.-S., Park, H.-Y., Henkensmeier, D., Lee S. Y., and Kim, H.-J. (2021). Synthesis of Sulfonated Poly (Arylene Ether Sulfone)s Containing Aliphatic Moieties for Effective Membrane Electrode Assembly Fabrication by Low-Temperature Decal Transfer Methods. Polymers, 13(11), pp.1713–1713.

Chapter 4

Preparation of Palladium Nanoparticles and Characterizations

4.1. Introduction

Palladium is one of the most transition metals that is highly investigated displaying high catalytic activity [1]. Researchers have shown interest in synthesized Pd nanoparticles due to their catalytic ability [2]. The Polyvinylpyrrolidone (PVP) is mostly used for stabilization of nanoparticle metals because of chelating agent which makes particles to be smaller. The morphology of synthesized PdNps using PVP is dependent on type of metallic precursor, temperature, and reaction time [3-10].

There are various ways to prepare Pd nanoparticles, one of the methods is sol-gel method. The sol-gel method can be prepared in two ways namely: aqueous sol gel and non-aqueous sol-gel/polyol method depends on the solvent used. The aqueous sol-gel method is when water is used as reaction medium and non-aqueous method is when organic solvent such as alcohols, ketones and aldehydes used as reaction medium [11]. The non-aqueous method (polyol) is preferred as the best method to obtain well controlled shape of metal colloids using PVP and ethylene glycol medium [4,12-14].

In this Chapter, both methods of sol-gel were utilized for production of Pd nanoparticles. The commercial palladium nanoparticles (PdNps) and synthesized Pd nanoparticles (PdEG and PdDI) were analyzed by TEM, XRD, Malvern Zetasizer Nano ZS instrument (DLS), UV-vis and FTIR.

4.2. Synthesis of Pd nanoparticles

4.2.1. Materials

The $PdCl_2$ and Na_2PdCl_4 were used as precursors. The solvent used was Ethylene Glycol and deionized water. Polyvinylpyrrolidone (PVP) with molecular weight of 13, 000 000 was used as a stabilizer. All these chemicals were purchased from Sigma Aldrich (South Africa) including ethanol, acetone, and hydrochloric acid.

4.2.2. Aqueous sol-gel method

The equipment set up for Pd nanoparticles is shown in Figure 4.1 while Figure 4.2 presents different steps of sol-gel method. 0.2M of hydrochloric acid was prepared and $PdCl_2$ was added to the solution while continuously stirring on a magnetic stirrer and mixed for 30 minutes to obtain H_2PdCl_4 solution. The resultant solution was transferred to a 2-neck flask and was refluxed for 3 hours. The solution was left for 24 hours. Drops of 1M HCl solution were added to a mixed solution of H_2PdCl_4 solution, deionized water and PVP while continuously stirring in a heating mantle. Reduction of H_2PdCl_4 was done by adding ethanol. Then, mixture was heated at the temperature of 120 °C and reduction of H_2PdCl_4 was noticed by colour change from pale-yellow to dark brown solution. Dark brown colour indicated the presence of Palladium nanoparticles and stabilized by PVP. Sigma 3K30C-Kubota centrifuge was used to centrifuge palladium nanoparticle solution at the speed of 15 000 rpm for 45 minutes. Precipitation of palladium nanoparticle was done by adding certain volume of acetone, separated by centrifuge at same previous conditions. Ethanol was added

to the solution for washing of particle by ultra-sonification processfor 1 hour [15]. The obtained nanoparticles were labelled PdDI.

4.2.3. Non-aqueous sol-gel method (Polyol method)

Na_2PdCl_4 was added to Ethylene Glycol; the mixture was refluxed for 2 hours while continuously stirring. Then, the mixture of PVP and Ethylene Glycol was prepared and stirred for 2 hours. Both mixtures were transferred to 2-neck flask containing Ethylene Glycol heated at 150 °C. The mixture was heated and stirred for 15 minutes. Then, Na_2PdCl_4 reduction was noticed by colour of solution to dark brown which is the indication of Palladium nanoparticles stabilized by PVP. Palladium nanoparticle solution was centrifuge at the speed rate of 15 000 rpm for 45 minutes. Precipitation of palladium nanoparticle was done by adding certain volume of acetone, separated by centrifuge at same previous conditions. Ethanol was added to solution for washing of nanoparticle by ultra-sonification process for 1 hour [16]. The obtained nanoparticles were labelled PdEG.

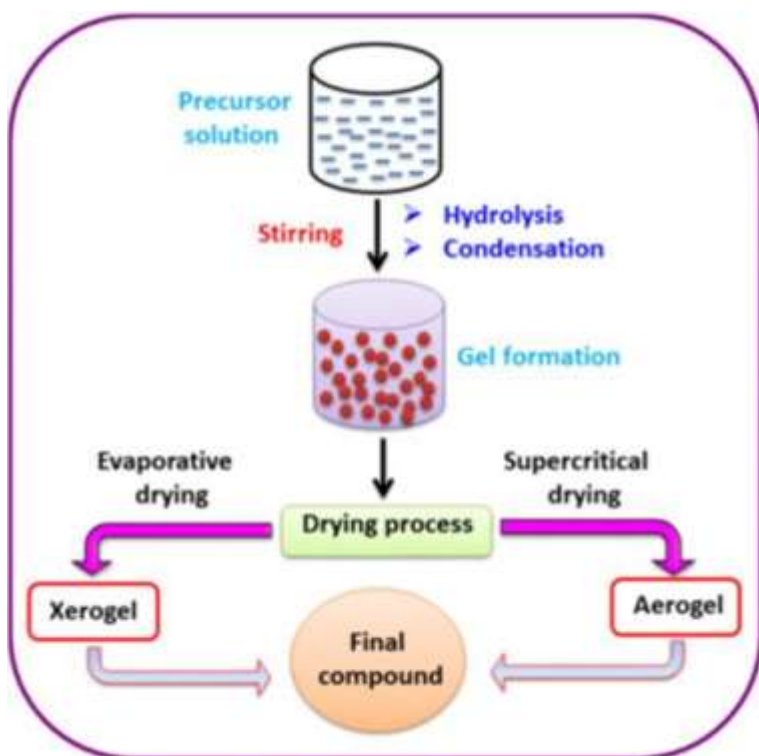Figure 4.1: Pd nanoparticle experimental set-up.

Figure 4.2: Sol-gel method to produce metal nanoparticles [1].

4.3. Results and discussion

4.3.1. HRTEM Analysis

HRTEM images of Pd nanoparticles by aqueous sol gel method (PdDI nanoparticle) in Figure 4.3 indicate the size of Pd nanoparticles between 7nm to 32nm.The average diameter in Figure 4.3 b and Figure 4.3 c was calculated to be 19 nm which correspond to size of commercial PdNps measured as <25nm. Different shapes of Pd nanoparticles were observed cubic, cuboctahedron, and spherical shapes [Figure 4.3 b & d]. The results obtained correlate to the results of Berger et.al [6] and Mallakpour et al. [17]. To perform EDX analysis, cluster of nanoparticles for both methods were chosen to obtain a better spectrum. The quantitative results of EDX also showed the

presence of Pd nanoparticles from the PdCl$_2$ solution as shown in Figure 4.4 where copper and carbon eliminate from carbon coated copper grid. Mallakpour et al. [17] carried out the similar experiment and it was reported three diffused diffraction rings of palladium nanoparticles were observed at different d- spacing of 0.221, 0.198 and 0.134 nm allocated to the (1 1 1), (2 0 0) and (2 2 0) reflections relating to FCC palladium [18-19].
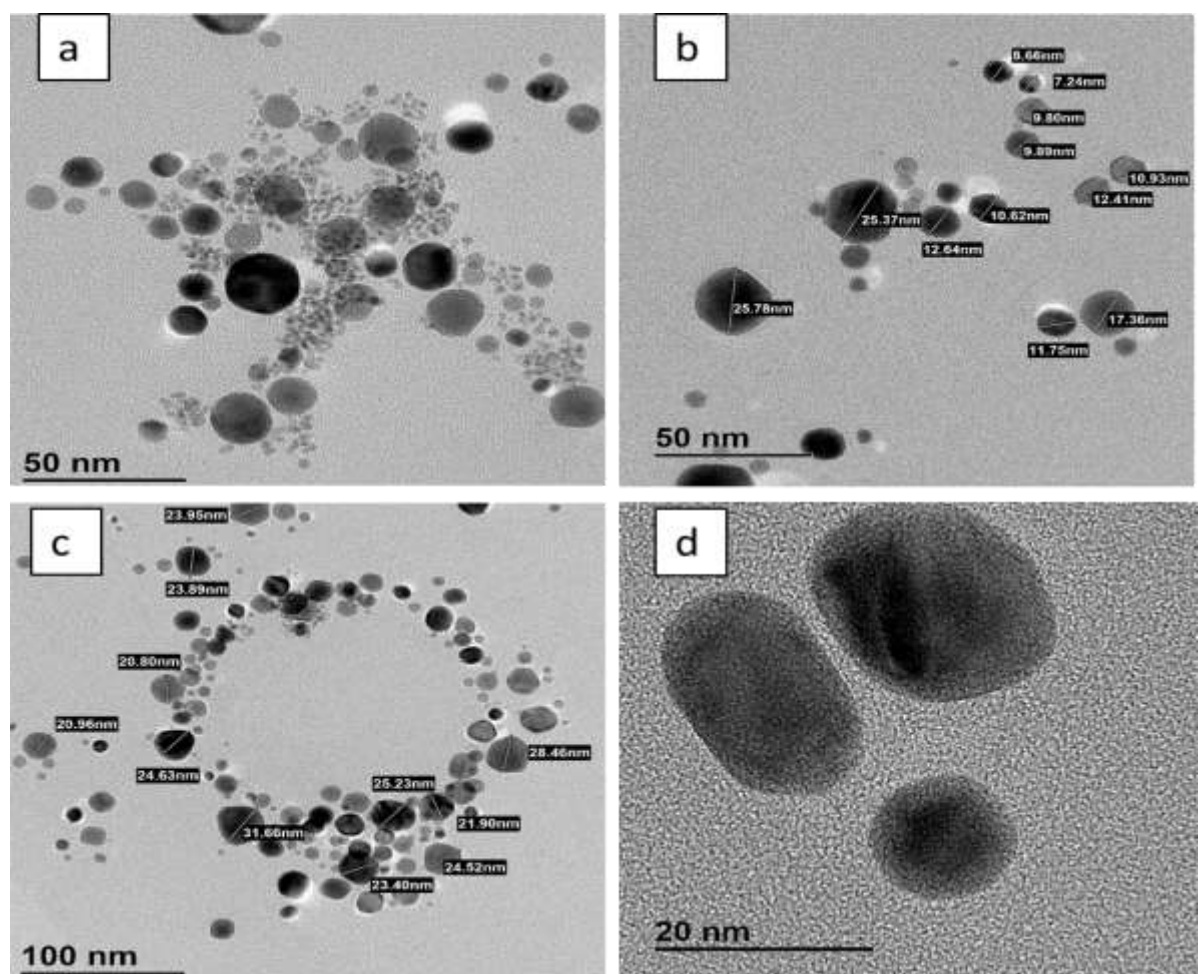

Figure 4.3: TEM images of PdDI nanoparticles (a-d).

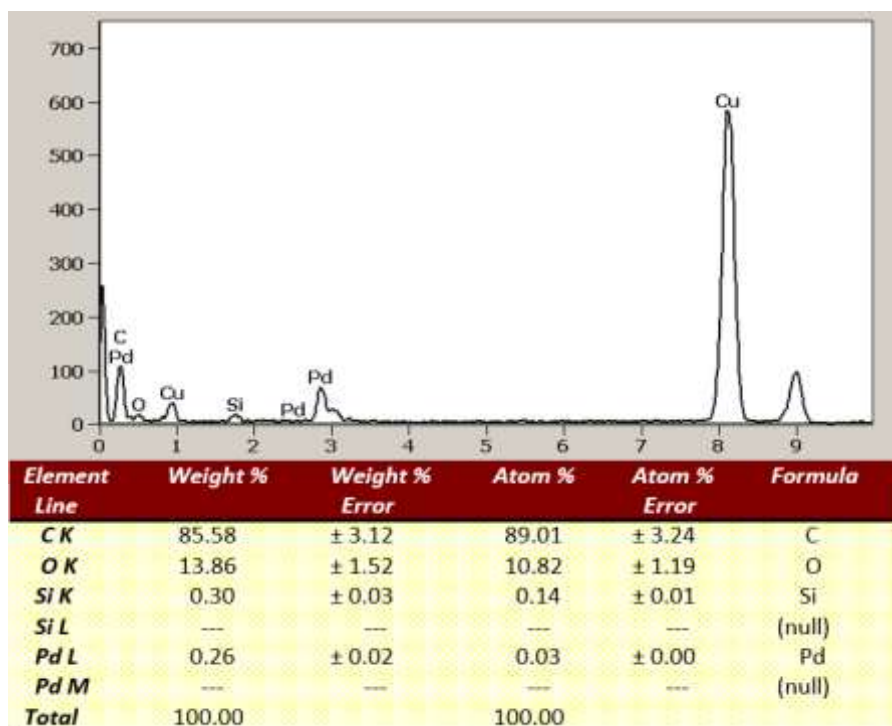| Element Line	Weight %	Weight % Error	Atom %	Atom % Error	Formula
C K	85.58	± 3.12	89.01	± 3.24	C
O K	13.86	± 1.52	10.82	± 1.19	O
Si K	0.30	± 0.03	0.14	± 0.01	Si
Si L	---	---	---	---	(null)
Pd L	0.26	± 0.02	0.03	± 0.00	Pd
Pd M	---	---	---	---	(null)
Total	100.00		100.00		

Figure 4.4: The EDX spectrum showing elemental composition of palladium (Pd) nanoparticles synthesized by sol-gel (aqueous) method.

The obtained TEM for Pd nanoparticles by non-aqueous sol-gel method (PdEG) results in Figure 4.5 shows small nanoparticles ranging between 2.44nm-8.18nm which is much better compared to aqueous sol-gel method in Figure 4.3. Other research indicated that nanoparticles synthesized using EG were smaller than the ones produced by other agents [4]. According to Yin et al. [14] and Liu et al. [20], it is very challenging to synthesize Pd nanoparticles with less 5nm size distribution but TEM results in Figure 4.5 indicated different particles sizes with particles of less than 5nm. The average diameter was calculated to be 6.05nm for Figure 4.5 b and Figure 4.5 d which is above 5nm. The PdEG nanoparticles size is less than 25nm which is the size corresponding to commercial PdNps.The size of nanoparticles produced by non-aqueous method in Figure 4.5 tend to be smaller than nanoparticles produced by aqueous method (Figure 4.3). Aram et al. [4] also stated that nanoparticles that were

produced using ethyl glycol were smaller compared to nanoparticles synthesized by other methods. Therefore, the fcc metal planes of (100) and (111) usually represent polyhedral nanoparticles with various type of shapes such as face, edge, and vertex. Figure 4.5 indicates nanoparticles in different shapes (Figure 4.5 c & d) [14, 21-23]. According to various researchers [24-27] particles in smaller diameters can enhance catalytic activity through surface effects. The size of Pd nanoparticles obtained in Figure 4.5 b & d are between 2nm to 9nm. In other literature Pd nanoparticles synthesized by polyol method were ranging from 4.5 to 7.5nm [9,24]. The quantitative results of EDX also showed the presence of Pd nanoparticles from solution (Figure 4.6) at ~1 % weight. The EDX quantitative results in Figure 4.6 indicated a higher quantity of palladium nanoparticles than the ones produced by aqueous sol-gel method. The EDX in Figure 4.6 also indicates the presence coming from the grid and carbon as results of substrate of carbon film on the TEM grid and Cu as result of carbon coated grid [17,28].

The agglomeration of particles is a big challenge when comes to synthesis of nanoparticles. TEM images can give indication if there is agglomeration of nanoparticles (secondary particles), or nanoparticles have well dispersed in the solution [29]. TEM images of Pd nanoparticles in Figure 4.3 and Figure 4.5 derived from aqueous sol-gel method and non-aqueous sol-gel method indicate low degree of agglomeration in palladium solutions. Therefore, agglomeration was not favoured in these experiments since sol-gel method is regarded as the best method to provide good homogeneous solution and nanoscale diameter [30].
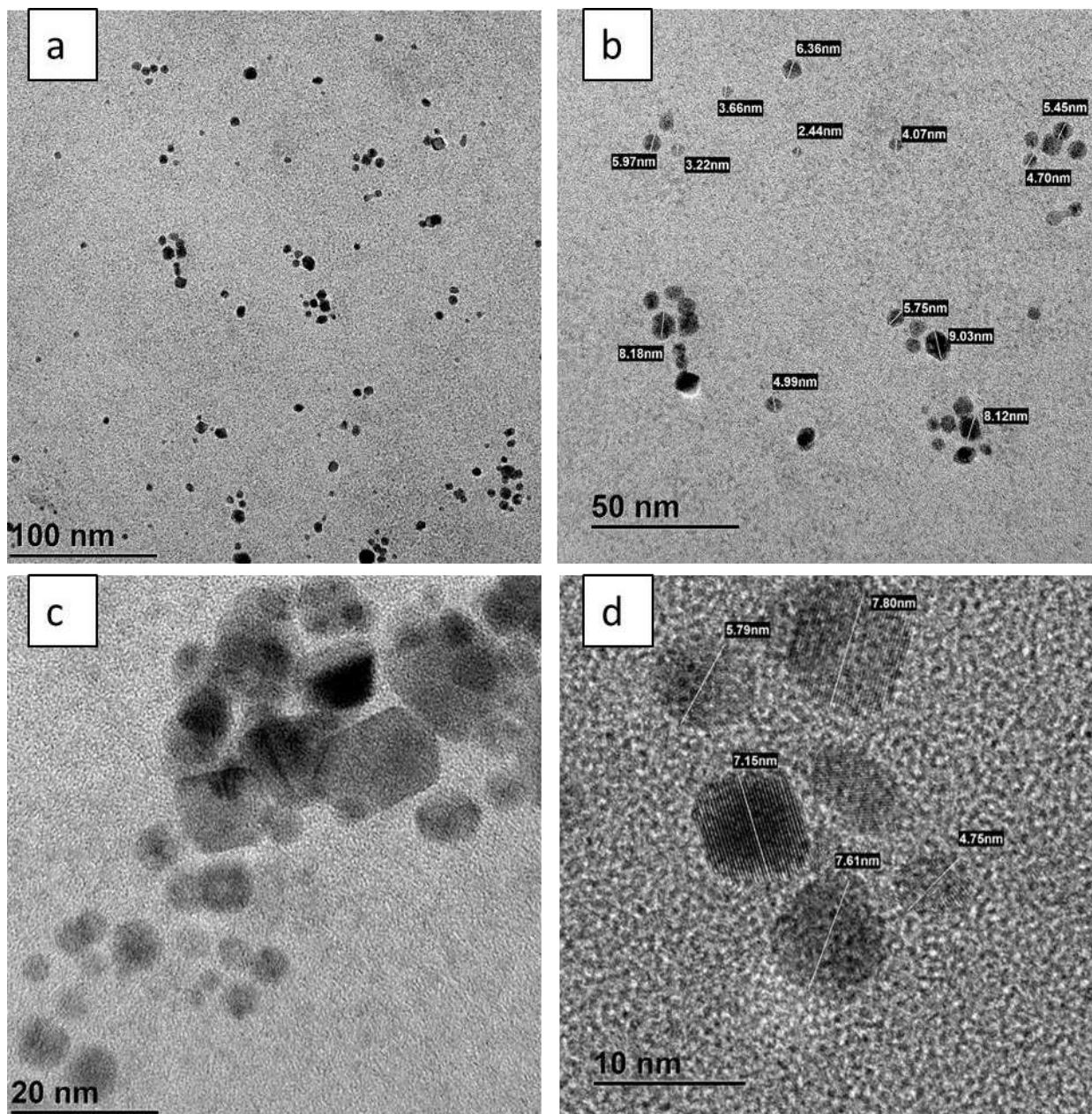
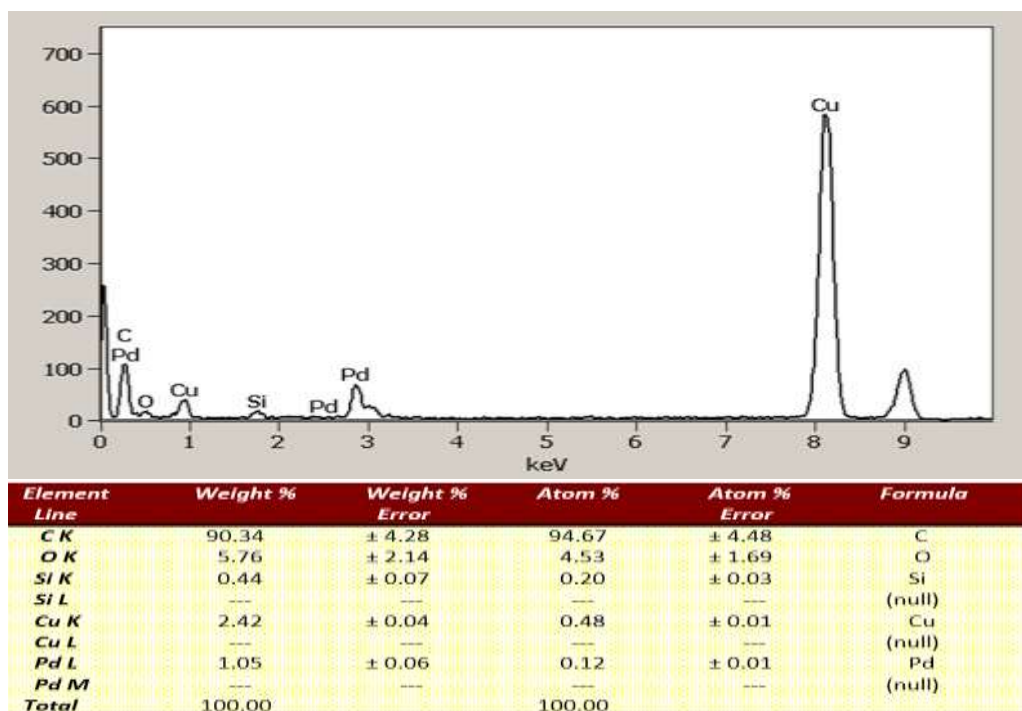Figure 4.5: TEM images of PdEG nanoparticles (a-d).

Element Line	Weight %	Weight % Error	Atom %	Atom % Error	Formula
C K	90.34	± 4.28	94.67	± 4.48	C
O K	5.76	± 2.14	4.53	± 1.69	O
Si K	0.44	± 0.07	0.20	± 0.03	Si
Si L	---	---	---	---	(null)
Cu K	2.42	± 0.04	0.48	± 0.01	Cu
Cu L	---	---	---	---	(null)
Pd L	1.05	± 0.06	0.12	± 0.01	Pd
Pd M	---	---	---	---	(null)
Total	100.00		100.00		

Figure 4.6: EDX spectrum showing elementary composition of palladium synthesized by polyol method.

4.3.2. XRD Analysis

Figure 4.7 shows the characterization diffraction peaks of palladium nanoparticles synthesized by sol-gel (PdDI Nps) and non-sol-gel (PdEG Nps) methods as well as commercial palladium nanoparticles. The XRD analysis of commercial palladium nanoparticles in Figure 4.7 (a) indicates the intense sharp five diffraction peaks at Bragg angles of 2θ = 40.49°, 46.44°, 68.40°, 82.26° and 86.72°, corresponding to the (111), (200), (220), (311) and (222) planes of the Pd metallic phase (pure Pd nanoparticles), respectively. Thus, XRD pattern confirmed the face-centered cubic lattice structure of Pd nanoparticles, which corresponds to XRD results found by various researchers [1,31-47]. Both PdEG Nps and PdDI Nps have a mixture of metallic palladium and palladium oxide nanoparticles. The PdEG Nps displayed peaks

the Bragg angle of 2θ =40.44°, 46.79°, 68.24°, 81.43° and 85.74° corresponding to (111), (200), (220), (311) and (222) planes. The PdO nanoparticles are indicated by diffraction peaks at 2θ =28.72°, 33.11°, 58.37° and 76.76° in Figure 4.7(b). The PdDI nanoparticles in Figure 4.7c exhibited Pd crystalline structure diffraction peaks at the Bragg angle of 40.09°, 46.57°, 68.09°, 82.08° and PdO peaks at 2θ=27.34°,31.64°,59.49°,66.24°,75.29°, and 83.95°. The crystallinity of Pd nanoparticles is indicated by sharp peak of XRD pattern at 2θ = 40.49° for commercial PdNps, 40.44° for PdEGNps and 40.09 PdDI Nps at (111) planes [1,24,31]. The graphs in Figure 4.7 indicate sharp peaks confirming crystal structure of metallic palladium and palladium oxide nanoparticles. Figure 4.8 (a) and (b) shows composition of synthesized palladium nanoparticles in 3D structure confirming mixture of metallic palladium and palladium oxide. Salman et al. [47] also discovered synthesized palladium nanoparticles were composed of Pd and PdO structures. PdO might be the results of the interaction of Pd salts and acid-water or alcohol during synthesis [48-53]. Thus, resulting in reduction of Pd nanoparticles into PdO nanoparticles. The existence of PdO shows pure Pd^{0} along with palladium oxide (PdO) nanoparticles [54].
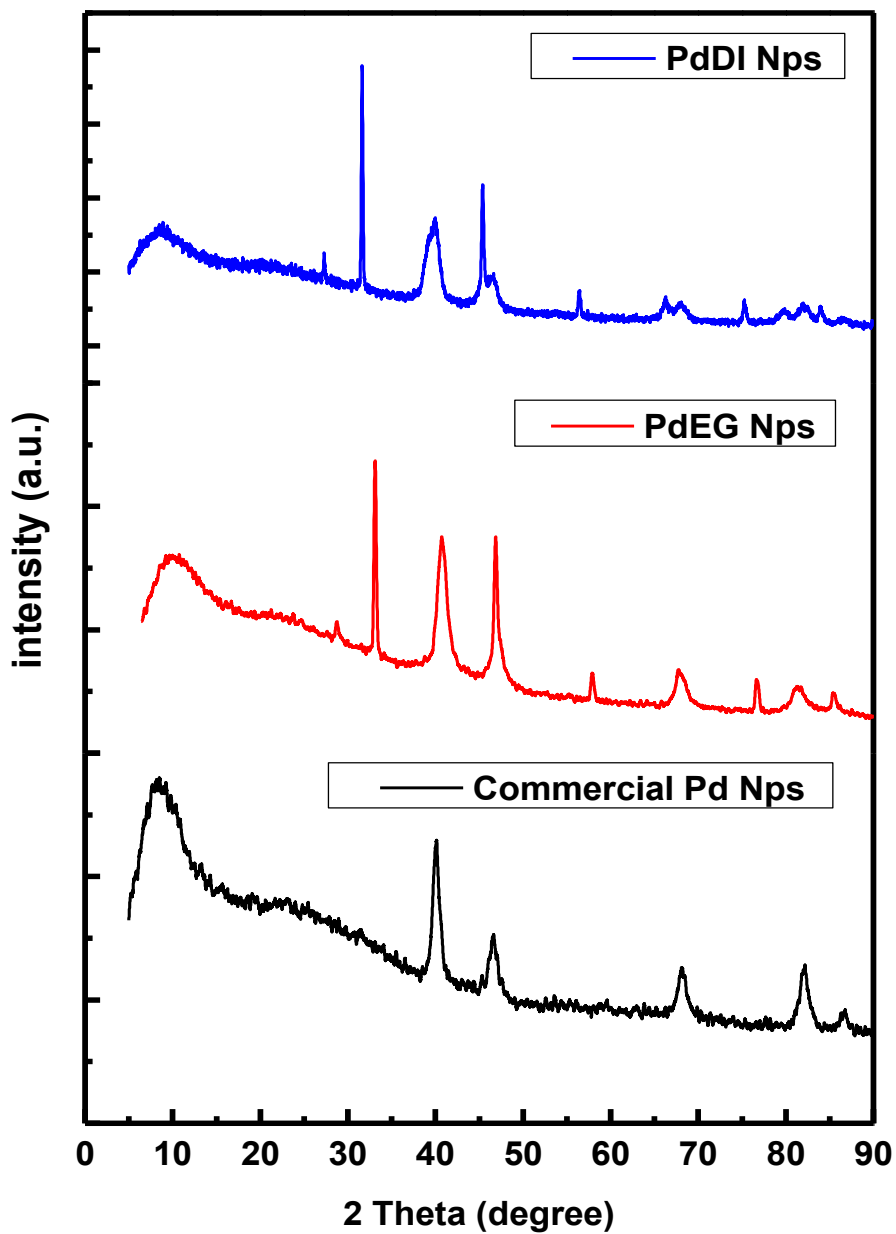
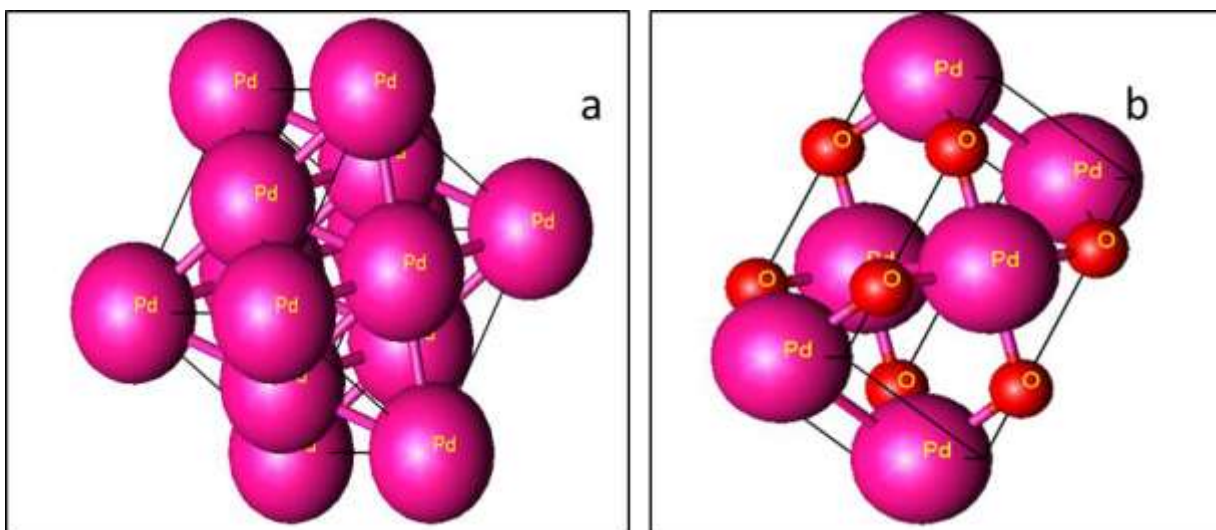Figure 4.7: XRD patterns of commercial Pd Nps, PdEG Nps and PdDI Nps.

Figure 4.8: (a) Structure of metallic palladium (b) Structure of palladium oxide.

4.3.3. UV-vis

UV–vis spectroscopy results are shown in Figure 4.9. The solutions turned from yellow to brownish colour indicating the presence of PdNps [55]. The absorption of PdEG Nps and PdDI Nps profile (Figure 4.9) was observed at 264 nm. This absorption band at 264nm is an indication of presence of $PdCl_4^{2-}$ for both PdEG Nps and PdDI Nps, commercial PdNps absorption band was noticed at 251nm. These peaks are within the range of 215nm to 284.5 nm which was observed for synthesized palladium nanoparticles using different solvents [15,54-59].

The bands of palladium nanoparticles around 300nm and 400nm were observed at 325nm and 440nm [60], 330nm and 440nm [3, 61-62], 329.94nm and 437.25nm [15]. PdEG Nps and PdDI Nps in Figure 4.9 did not exhibit absorption peaks at around 300nm and 400nm. Only absorption peak at 415nm was noticed for commercial PdNps. It is indicated that the absence of absorption peaks around 300nm and 400nm indicates that Pd^{2+} ions of Na_2PdCl_4 and $PdCl_2$ precursors were reduced to metallic palladium (Pd^0) [31]. According to Siddiqi and Husen [32], different concentrations of

PdCl$_2$ was prepared and analyzed by UV-vis. The absorption band at 400nm was noted for all solutions of PdCl$_2$. The absorption bands disappeared indicating Pd^{2+} ions were reduced to metallic palladium [32]. The same behaviour was observed when absorption peak of Pd^{2+} at 407nm became invisible indicating complete reduction of Pd^{2+} ions to metallic palladium (Pd^0) at 280nm [53].
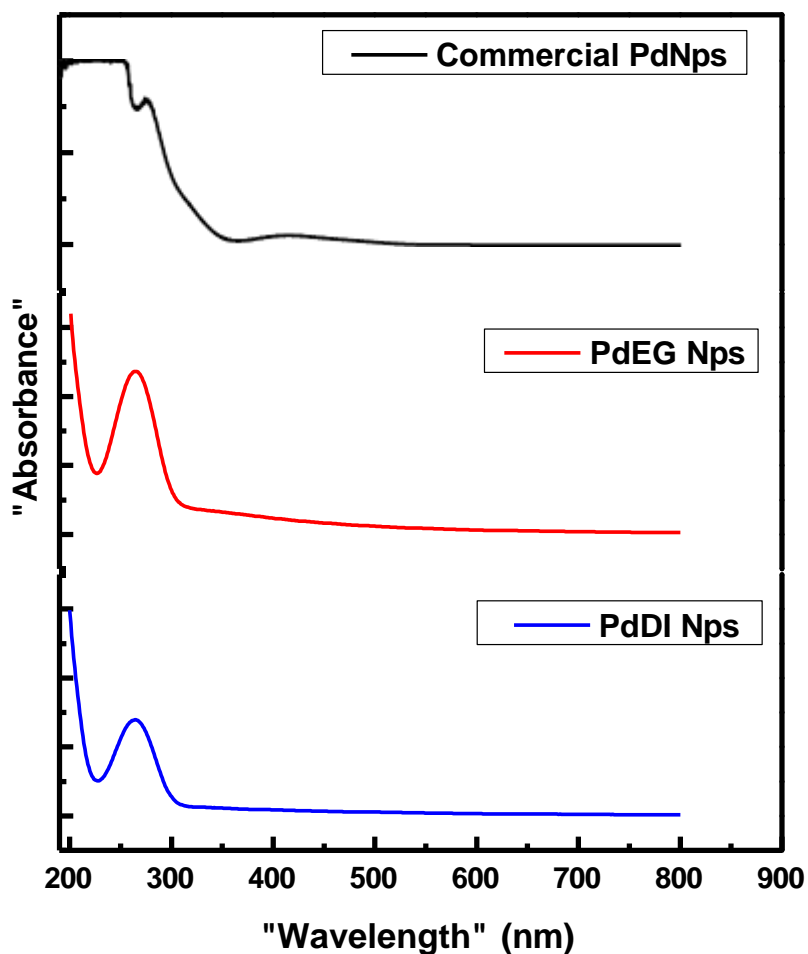

Figure 4.9: Uv-vis absorption spectrum of commercial PdNps, PdEG Nps and PdDI Nps.

4.3.4. Malvern Zetasizer (DLS)

Figure 4.10 indicates polydispersity nanoparticle solutions with z-average diameter of 14.31nm, 19.07nm and 56.5nm for PdEG nanoparticles, PdDI nanoparticles and Commercial Pd nanoparticles, respectively. The report generated for synthesized palladium nanoparticle indicates good data with an average diameter of 14.31nm for PdEG Nps and 19.07nm for PdDI Nps which is less than commercial PdNps. According to Akbari et al. [63] and Sharonova et al. [64] diameters measured by DLS method are larger than those measured by other techniques such as XRD, TEM, SEM and BET. The results from this research showed indeed DLS diameters are larger than those obtained by TEM. DLS average diameter of 14.31nm and TEM average diameter of 6.05nm were obtained for PdEG Nps while PdDI Nps indicated average diameter of 19.07nm for DLS and 19.02nm for TEM.
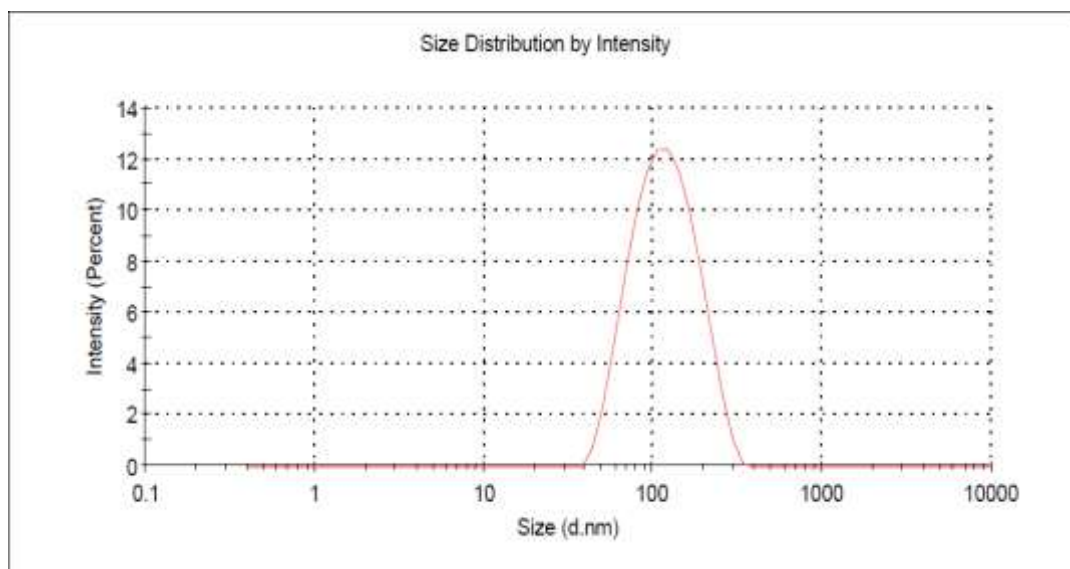
(a) PdEG Nps
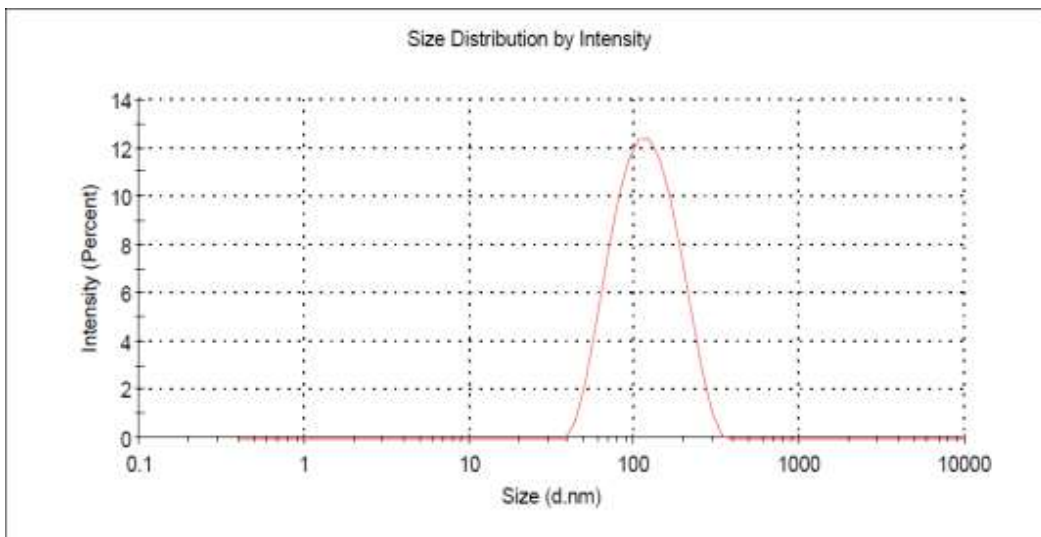
(b) PdDI Nps
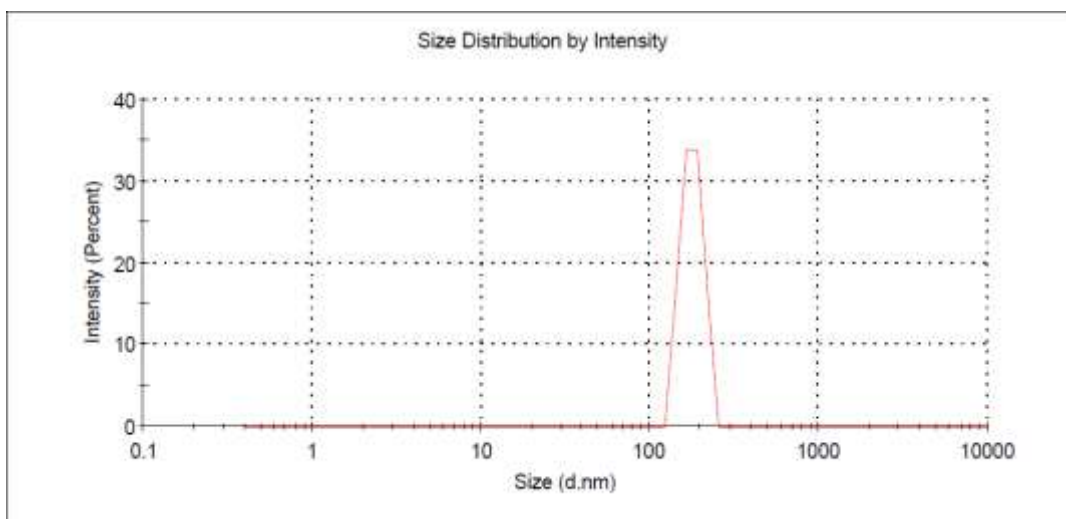
(c) Commercial PdNps

Figure 4.10: Palladium nanoparticles (a) PdEG Nps (b) PdDi NPs (c) Commercial PdNps.

4.3.5. Fourier Transform Infrared (FTIR)

The FTIR spectra of synthesized palladium nanoparticles (PdDI and PdEG) and commercial palladium nanoparticles in Figure 4.11 displayed peaks representing functional groups of palladium nanoparticles. The absorption peak at 3436.7 cm^{-1} for synthesized PdEG Nps and commercial PdNps, 3422.2 cm^{-1} for PdDI Nps are assigned to O-H vibration of alcohol groups [32,47,55,65-67]. The absorption bands at 2921.6 cm^{-1} for PdEGNps, PdDINps and commercial PdNp represent C-H stretching of polyols [48]. The absorption peaks at 1632.7 cm^{-1},1647.2 cm^{-1} and 1640.4 cm^{-1} are assigned to C=C stretching vibration of alkene [48,66] for commercial PdNps, PdEGNPs and PdDINPs respectively. The absorption peaks at 1463.2 cm^{-1} for commercial PdNps, 1426.4 cm^{-1} for PdEGNps and 1456.4 cm^{-1} for PdDI Nps represent C-H vibration of alcohols or alkene [64,66]. The absorption bands at 1293.7 cm^{-1} for both commercial PdNps and PdEG Nps, 1286.9 cm^{-1} and 1168.8 cm^{-1} for PdDI Nps are assigned to stretching of amides [68-69]. The absorption peaks at 1087.5 cm^{-1} for commercial PdNps, PdEGNps and PdDINps are assigned to C-O stretching vibrations of alcohol groups [48,66]. The vibration bands at 859.9 cm^{-1} , 844.4 cm^{-1} and 874.4 cm^{-1} for commercial PdNps, PdEGNps and PdDI Nps are assigned to C-H bend of alkenes [68].The peaks between 450 cm^{-1} and 750 cm^{-1} represent presence of palladium nanoparticles [47,55,59,70-71] with commercial PdNps peaks at 572.3 cm^{-1} and 484.2 cm^{-1}, PdEGNps peaks at 580.1 cm^{-1}, 656.1 cm^{-1} and 745.9 cm^{-1}, PdDINps peaks at 476.4 cm^{-1} and 580.05 cm^{-1}.
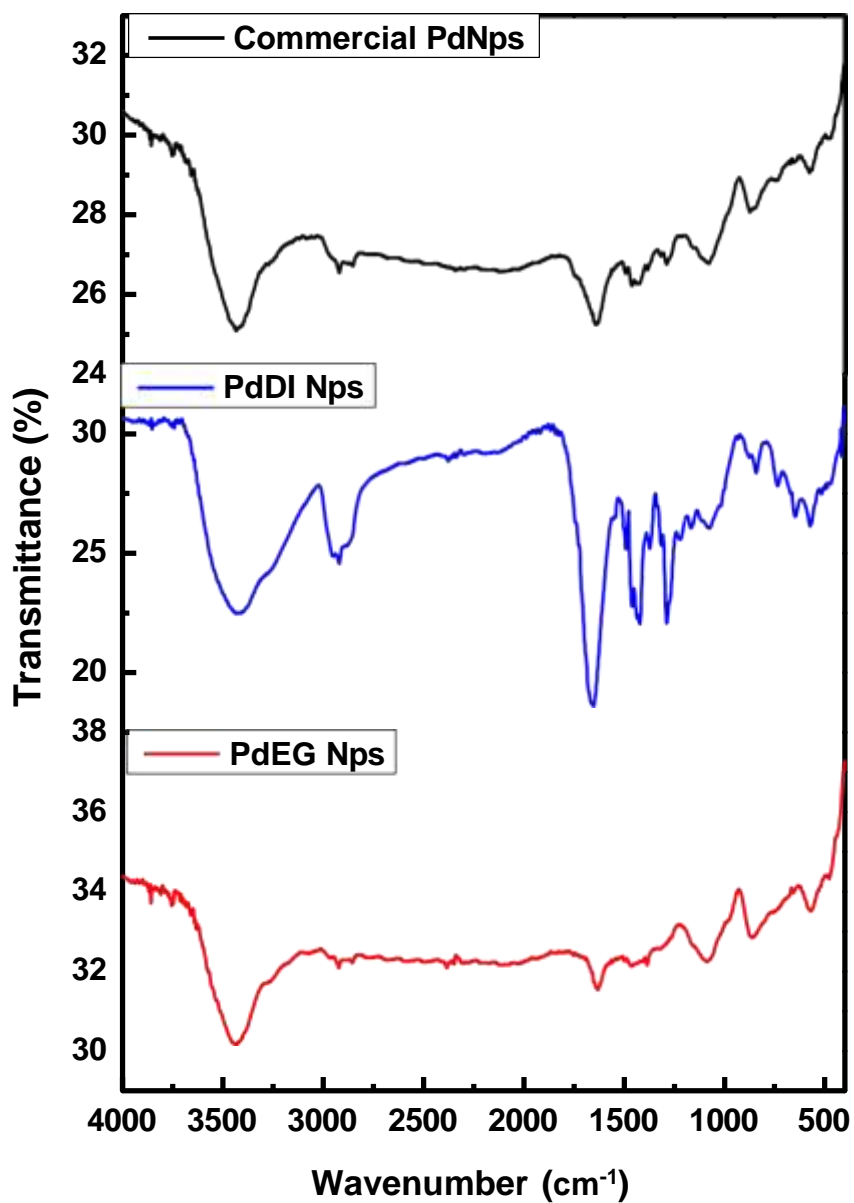
Figure 4.11: FTIR spectra of Palladium nanoparticles Commercial PdNPs, PdDI Nps and PdEG Nps.

4.4. Conclusion

In this Chapter, two methods were used to synthesize palladium nanoparticles namely aqueous method (PdDI nanoparticles) and non-aqueous method (PdEG nanoparticles). Both methods yielded mixed palladium nanoparticles containing palladium and palladium oxide nanoparticles. This can be the result of reducing agents used to support production of nanoparticles. The non-aqueous method was selected to be the best method to synthesize palladium nanoparticles (PdEG nanoparticles) based on the results of TEM, UV-vis, DLS, FTIR and XRD techniques. Therefore, palladium nanoparticles synthesized by non-aqueous method (PdEG Nps) are to be incorporated into Nafion® solution in Chapter 5 for fabrication of Palladium nanocomposite membranes.

4.5. References

1. Bharate, B. (2019). Nanocubes of Palladium, Simple, Green Approach and Catalytic Properties Under Continuous Hydrogenation System. Biomedical Journal of Scientific & Technical Research, 9(5), pp.14672-14675.

2. Hao, Y.-Z., Zhang, Y.-L., Wang, L.-H. and Ju, X.-Y. (2009). A Simple Preparation Route to Palladium Nanoparticles Catalyst from Decomposition of Supported [Pd (lysine. HCl) (Cl)2] Complex. The Open Catalysis Journal, 2(1), pp.66–70.

3. Groppo, E., Bertarione, S., Rotunno, F., Agostini, G., Scarano, D., Pellegrini, R., Leofanti, G., Adriano Zecchina and Lamberti, C. (2007). Role of the Support in Determining the Vibrational Properties of Carbonyls Formed on Pd Supported on SiO2−Al2O3, Al2O3, and MgO. The Journal of Physical Chemistry C, 111(19), pp.7021–7028.

4. Aram L. Bugaev, Vladimir A. Polyakov, Andrei A. Tereshchenko, Ashura N. Isaeva, Alina A. Skorynina, Elizaveta G. Kamyshova, Andriy P. Budnyk, Tatiana A. Lastovina, and Alexander V. Soldatov (2018). Chemical Synthesis and Characterization of Pd/SiO2: The Effect of Chemical Reagent. Metals, 8(2), p.135.

5. Schiavo, L., Aversa, L., Tatti, R., Verucchi, R. and Carotenuto, G. (2016). Structural Characterizations of Palladium Clusters Prepared by Polyol Reduction of [PdCl4]2−Ions. Journal of Analytical Methods in Chemistry, pp.1–6.

6. Berger, D., Catrina G.A., Vasile B. S., Jitaru I., Matei, C. (2010). Palladium nanoparticles synthesis with controlled morphology obtained by polyol method. UPB Scientific Bulletin, Series B 72, pp.113–120.

7. Nemamcha A., Moumeni H., Rehspringer J.L. (2009). PVP Protective mechanism of palladium nanoparticles obtained by sonochemical process. Physics Procedia, 2(3), pp.713–717.

8. Xian, J., Qing Xin Hua, Jiang, Z., Ma, Y. and Huang, W. (2012). Size-Dependent Interaction of the Poly(N-vinyl-2-pyrrolidone) Capping Ligand with Pd Nanocrystals. Langmuir, 28(17), pp.6736–6741.

9. Kumar, S.M., Herrero, J. S., Irusta, S. and Scott, K. (2010). The effect of pretreatment of Vulcan XC-72R carbon on morphology and electrochemical oxygen reduction kinetics of supported Pd nanoparticle in acidic electrolyte. Journal of Electroanalytical Chemistry, 647(2), pp.211–221.

10. Teranishi, T. and Miyake, M. (1998). Size Control of Palladium Nanoparticles and Their Crystal Structures. Chemistry of Materials, 10(2), pp.594–600.

11. Rao, B.G., Mukherjee, D., and Reddy, B.M. (2017). Novel approaches for preparation of nanoparticles. Nanostructures for Novel Therapy, pp.1–36.

12. Guo, L., Bai, J., Li, C., Meng, Q., Liang, H., Sun, W., Li, H. and Liu, H. (2013). A novel catalyst containing palladium nanoparticles supported on PVP composite nanofiber films: Synthesis, characterization, and efficient catalysis. 283, pp.107– 114.

13. Lim, B., Jiang, M., Tao, J., Camargo, P.H.C., Zhu, Y. and Xia, Y. (2009). Shape-Controlled Synthesis of Pd Nanocrystals in Aqueous Solutions. Advanced Functional Materials, 19(2), pp.189–200.

14. Yin, Z., Lin, L. and Ma, D. (2014). Construction of Pd-based nanocatalysts for fuel cells: opportunities and challenges. Catalysis Science and Technology, 4(12), pp.4116–4128.

15. Lin, C.-M., Hung, T.-L., Huang, Y.-H., Wu, K.-T., Tang, M.-T., Lee, C.-H., Chen, C.T. and Chen, Y.Y. (2007). Size-dependent lattice structure of palladium studied by x-ray absorption spectroscopy. Physical Review B, 75(12).

16. Cookson, J. (2012). The Preparation of Palladium Nanoparticles. Platinum Metals Review, 56(2), pp.83–98.

17. Mallakpour, S., Zhiani, M., Barati, A. and Rostami, H. (2013). Improving the direct methanol fuel cell performance with poly (vinyl alcohol)/titanium dioxide nanocomposites as a novel electrolyte additive. International Journal of Hydrogen Energy, 38(28), pp.12418–12426.

18. Dicks, A., and D A J Rand (2018). Fuel cell systems explained. Hoboken, Nj: John Wiley & Sons Ltd.

19. Sebastian, V., Basak, S. and Jensen, K.F. (2016). Continuous synthesis of palladium nanorods in oxidative segmented flow. AIChE Journal, 62(2), pp.373–380.

20. Liu, Q., Bauer, J.M., Schaak, R.E. and Lunsford, J.H. (2008). Supported Palladium Nanoparticles: An Efficient Catalyst for the Direct Formation of H2O2 from H2 and O2. Angewandte Chemie,47(33), pp.6221–6224.

21. Wang, Z.L. (2000). Transmission Electron Microscopy of Shape-Controlled Nanocrystals and Their Assemblies. The Journal of Physical Chemistry B, 104(6), pp.1153–1175.

22. Le Bars J., Specht, U., Bradley, J.S. and Blackmond, D.G. (1999). A Catalytic Probe of the Surface of Colloidal Palladium Particles Using Heck Coupling Reactions. Langmuir 15(22), pp.7621–7625.

23. Koper, M.T.M. (2011). Structure sensitivity and nanoscale effects in electrocatalysis. Nanoscale, 3(5), p.2054.

24. Yang, G., Wang, Y., Xu, L., Li, Y., Li, L., Sun, Y., Yuan, Z. and Tang, Y. (2020). Pd nanochains: Controlled synthesis by lysine and application in microbial fuel cells. Chemical Engineering Journal, 379, pp.122230–122230.

25. Narayanan, R. and El-Sayed, M.A. (2005). Catalysis with Transition Metal Nanoparticles in Colloidal Solution: Nanoparticle Shape Dependence and Stability. The Journal of Physical Chemistry B, 109(26), pp.12663–12676.

26. S Campbell, C.T., Parker, S.C., and Starr D.E., (2002). The Effect of Size-Dependent Nanoparticle Energetics on Catalyst Sintering. Science, 298(5594), pp.811–814.

27. Zhang, L., Sui, Q., Tang, T., Chen, Y., Zhou, Y., Tang, Y. and Lu, T. (2013). Surfactant-free palladium nanodendrite assemblies with enhanced electrocatalytic performance for formic acid oxidation. Electrochemistry Communications, 32, pp.43–46.

28. Boddu, S.R., Gutti, V.R., Ghosh, T.K., Tompson, R.V. and Loyalka, S.K. (2011). Gold, silver, and palladium nanoparticle/nano-agglomerate generation, collection, and characterization. Journal of Nanoparticle Research, 13(12), pp.6591–6601. 28.

29. Kumar, A.P., Kumar, B.P., Kumar, A.B.V.K., Huy, B.T. and Lee, Y.-I. (2013). Preparation of palladium nanoparticles on alumina surface by chemical co-precipitation method and catalytic applications. Applied Surface Science, 265, pp.500–509. 29.

30. Liu, S., Ma, C., Ma, M. and Xu, F. (2019). Magnetic Nanocomposite Adsorbents.Micro and Nano Technologies, pp.295–316.

31. Shaik, M., Ali, Z., Khan, M., Kuniyil, M., Assal, M., Alkhathlan, H., Al-Warthan, A., Siddiqui, M., Khan, M. and Adil, S. (2017). Green Synthesis and Characterization of Palladium Nanoparticles Using Origanum vulgare L. Extract and Their Catalytic Activity. Molecules, 22(1), p.165.

32. Siddiqi, K.S. and Husen, A. (2016). Green Synthesis, Characterization and Uses of Palladium/Platinum Nanoparticles. Nanoscale Research Letters, 11(1).

33. Iwai, Y., Ikemoto, S., Haramaki K., Hattori, R. and Yonezawa, S. (2014). Influence of ligands of palladium complexes on palladium/Nafion composite membranes for

direct methanol fuel cells by supercritical CO2 impregnation method. Journal of Supercritical Fluids, 94, pp.48–58.

34. Arroyo-Ramírez, L., Rubenier Montano-Serrano, Luna-Pineda, T., Román, F.R., Raptis, R.G. and Cabrera, C.R. (2013). Synthesis and Characterization of Palladium and Palladium–Cobalt Nanoparticles on Vulcan XC-72R for the Oxygen Reduction Reaction. 5(22), pp.11603–11612.

35. Nguyen, V.L., Nguyen, D.C., Hirata, H., Ohtaki, M., Hayakawa, T. and Nogami, M. (2010). Chemical synthesis and characterization of palladium nanoparticles. Advances in Natural Sciences: Nanoscience and Nanotechnology, 1(3), p.035012.

36. Roy Chowdhury, S., Sarathi Roy, P., and Bhattacharya, S.K. (2017). Green synthesis and characterization of polyvinyl alcohol stabilized palladium nanoparticles: effect of solvent on diameter and catalytic activity. Advances in Natural Sciences: Nanoscience and Nanotechnology, 8(2), p.025002.

37. Hu, G., Nitze, F., Sharifi, T., Barzegar, H.R. and Wågberg, T. (2012). Self-assembled palladium nanocrystals on helical carbon nanofibers as enhanced electrocatalysts for electro-oxidation of small molecules. Journal of Materials Chemistry, 22(17), p.8541.

38. Piermatti, O. (2021). Green Synthesis of Pd Nanoparticles for Sustainable and Environmentally Benign Processes. Catalysts, 11(11), p.1258.

39. Liang, R., Hu, A., Persic, J., and Zhou, Y.N. (2013). Palladium Nanoparticles Loaded on Carbon Modified TiO2 Nanobelts for Enhanced Methanol Electrooxidation. Nano-Micro Letters, 5(3), pp.202–212.

40. Roy, P.S., Bagchi, J., and Bhattacharya, S.K. (2009). Size-controlled synthesis and characterization of polyvinyl alcohol coated palladium nanoparticles. Transition Metal Chemistry, 34(4), pp.447–453.

41. Veisi, H., Pirhayati, M. and Kakanejadifard, A. (2017). Immobilization of palladium nanoparticles on ionic liquid-triethylammonium chloride functionalized magnetic nanoparticles: As a magnetically separable, stable, and recyclable catalyst for Suzuki-Miyaura cross-coupling reactions. Tetrahedron Letters, 58(45), pp.4269–4276.

42. Raúl Carrera Cerritos, Guerra-Balcázar, M., Rosalba Fuentes Ramírez, Ledesma-García, J. and Luis Gerardo Arriaga (2012). Morphological Effect of Pd Catalyst on Ethanol Electro-Oxidation Reaction. Materials (Basel) 5(9), pp.1686–1697.

43. Kumar Petla, R., Vivekanandhan, S., Misra, M., Kumar Mohanty, A. and Satyanarayana, N. (2012). Soybean (Glycine Max) Leaf Extract Based Green Synthesis of Palladium Nanoparticles. Journal of Biomaterials and Nanobiotechnology, 03(01), pp.14–19.

44. Brantley, W.A., Cai, Z., Foreman, D.W., Mitchell, J.C., Papazoglou, E., and Carr, A.B. (1995). X-ray diffraction studies of as-cast high-palladium alloys. Dental Materials, 11(3), pp.154–160.

45. Liao, F., Wang, Z., Guo, T., Zhang, T. and Wu, Z. (2012). Synthesis of well dispersed palladium nanoparticles-decorated poly(o-phenylenediamine) colloids with excellent performance for hydrazine oxidation. Journal of Electroanalytical Chemistry, 673, pp.38–42.

46. Heya Na, Zhang, L., Qiu, H., Wu, T., Chen, M., Yang, N., Li, L.-Z., Xing, F. and Gao, J. (2015). A two step method to synthesize palladium–copper nanoparticles on reduced graphene oxide and their extremely high electrocatalytic activity for the electrooxidation of methanol and ethanol. Journal of Power Sources 288, pp.160– 167.

47. Salman, S.H., Khashan, K.S., Hadi, A.A. (2023). Green Synthesis and Characterization of Palladium Nanoparticles by Pulsed Laser Ablation and Their Antibacterial Activity. Metals, 13, 273.

48. Arsiya, F., Sayadi, M.H. and Sobhani, S. (2017). Green synthesis of palladium nanoparticles using Chlorella vulgaris. Materials Letters, 186, pp.113–115.

49. Rajasekharreddy, P. and Rani, P.U. (2014). Biosynthesis and Characterization of Pd and Pt Nanoparticles Using Piper betle L. Plant in a Photoreduction Method. Journal of Cluster Science, 25(5), pp.1377–1388.

50. Levy-Ontman, O.; Stamker, E.; Wolfson, A (2021). The Effect of Alcohol on Palladium Nanoparticles in i-Pd (OAc)2(TPPTS)2 for Aerobic Oxidation of Benzyl Alcohol. Metals, 11, 1443.

51. Adrio, L.A., Nguyen, B.N., Guilera, G., Livingston, A.G. and Hii, K.K. (Mimi) (2012). Speciation of Pd (OAc)2in ligandless Suzuki–Miyaura reactions. Catal. Sci. Technol., 2(2), pp.316–323.

52. Huang, H., Aleksey Ruditskiy, Choi, S.-I., Zhang, L., Liu, J., Ye, Z. and Xia, Y. (2017). One-Pot Synthesis of Penta-twinned Palladium Nanowires and Their Enhanced Electrocatalytic Properties. Applied Materials and Interfaces, 9(36), pp.31203–31212.

53. Lee, S.-H., Cho, H., Yang Soo Kim, Jong Wook Hong and Lee, Y.-W. (2021). Shape- and Size-Controlled Palladium Nanocrystals and Their Electrocatalytic Properties in the Oxidation of Ethanol. Materials, 14(11), pp.2970–2970.

54. Kumar, A.P., Kumar, B.P., Kumar, A.B.V.K., Huy, B.T. and Lee, Y.-I. (2013). Preparation of palladium nanoparticles on alumina surface by chemical co-precipitation method and catalytic applications. Applied Surface Science, 265, pp.500–509.

55. Mayedwa, N., Mongwaketsi, N., Khamlich, S., Kaviyarasu, K., Matinise, N. and Maaza, M. (2018). Green synthesis of nickel oxide, palladium and palladium oxide synthesized via Aspalathus linearis natural extracts: physical properties & mechanism of formation. Applied Surface Science, 446, pp.266–272.

56. Pestryakov, A.N.; Lunin, V.V.; Fuentes, S.; Bogdanchikova, N.; Barrera, A. (2003). Influence of modifying additives on the electronic state of supported palladium. Chemical Physics Letters, 367, 102–108.

57. Kravchuk, L.S.; Stel'mak, E.I.; Ivashchenko, N.I.; Valieva, S.V.; Molod'yanova, V.S. (1992). Formation and physicochemical properties of the system palladium oxide (PdO)/ZrO2. Kinetika i Kataliz, 33, 672–677.

58. Vinodhini, S., Vithiya, B.S.M. and Prasad, T.A.A. (2022). Green synthesis of palladium nanoparticles using aqueous plant extracts and its biomedical applications. Journal of King Saud University - Science, 34(4), p.102017.

59. Muniz-Miranda, M., Zoppi, A., Muniz-Miranda, F. and Calisi, N. (2020). Palladium Oxide Nanoparticles: Preparation, Characterization and Catalytic Activity Evaluation. Coatings, 10(3), p.207.

60. Tew, M.W., Miller, J.T. and van Bokhoven, J.A. (2009). Particle Size Effect of Hydride Formation and Surface Hydrogen Adsorption of Nanosized Palladium Catalysts: L3 Edge vs K Edge X-ray Absorption Spectroscopy. The Journal of Physical Chemistry C, 113(34), pp.15140–15147.

61. Evangelisti, C., Nicoletta Panziera, Alessio D'Alessio, Luca Bertinetti, Botavina, M. and Vitulli, G. (2010). New monodispersed palladium nanoparticles stabilized by poly-(N-vinyl-2-pyrrolidone): Preparation, structural study, and catalytic properties. Journal of Catalysis, 272(2), pp.246–252.

62. Fernand Fiévet, Lagier Jp, Blin B, Beaudoin, B., and M. Figlarz (1989). Homogeneous and heterogeneous nucleations in the polyol process for

thepreparation of micron and submicron size metal particles. Solid State Ionics 32-33, pp.198–205.

63. Akbari, B., Tavandashti, M.P., and Zandrahimi M. (2011). Particle size characterization of nanoparticles – A practical approach. Iranian Journal of Materials Science and Engineering, 8(2), pp. 48-54.

64. Sharonova, A.A., Loza, K., Surmenev, R.A., Prymak, O. and Epple, M. (2016). Synthesis of positively and negatively charged silver nanoparticles and their deposition on the surface of titanium. Materials Science and Engineering, 116, pp.012009–012009.

65. Fahmy, S.A., Fawzy, I.M., Saleh, B.M., Issa, M.Y., Bakowsky, U. and Azzazy, H.M.E.-S. (2021). Green Synthesis of Platinum and Palladium Nanoparticles Using Peganum harmala L. Seed Alkaloids: Biological and Computational Studies. Nanomaterials, 11(4), p.965.

66. Viswadevarayalu A., Ramana P. V., J. Sumalatha J., Reddy S. A. (2016) Biocompatible synthesis of palladium nanoparticles and their impact on fungal species. Journal of Nanoscience and Technology 2(3), pp. 169–172.

67. Abbas, G., Kumar, N., Kumar, D. and Pandey, G. (2019). Effect of Reaction Temperature on Shape Evolution of Palladium Nanoparticles and Their Cytotoxicity against A-549 Lung Cancer Cells. American Chemical Society Omega, 4(26), pp.21839–21847.

68. Malathi R. and Ganesan, V. (2015). Biological synthesis of palladium nanoparticles using leaf extract of Sebastiania chamaelea (L.) Muell. Arg. International Journal of Chemtech Research, 7(2), pp.734–739.

69. Suryawanshi A.D., Padampalle A.S. and Suryawanshi D.D. (2018). Green synthesis of Palladium nanoparticles by Soybean (Glycin Max.) leaf extract, Int. Res. Journal of Science & Engineering, Issue A5, pp. 26-30.

70. Moamen S. Refat*, Hosam A Saad, Adil A. Gobouri, Mohammed Alsawat, Kaouther Belgacem, Refat M.S., Saad H.A, Gobouri A.A., Alsawat M., Belgacem K., Majrashi B.M. and Adam A.M.A. (2021). Synthesis, characterization, and photocatalytic efficiency of a new smart PdO Oxide Nanomaterials for using in the recycling and sustainable wastewater treatment. Bulletin of the Chemical Society of Ethiopia, 35(1), pp. 107-118.

71. Manjunatha Kempasiddaiah, Vishal Kandathil, Dateer, R.B., Sasidhar, B.S., Patil, S.A. and Patil, S.A. (2020). Immobilizing biogenically synthesized palladium nanoparticles on cellulose support as a green and sustainable dip catalyst for cross-coupling reaction. Cellulose, 27(6), pp.3335–3357.

Chapter 5

Preparation and Characterization of nano-composite membranes

5.1. Introduction

Composite membranes have been fabricated to improve performance of fuel cell technology in various types of fuel cells [1-6]. Recently, research has been focusing on developing polymer materials that are cost efficient to improve properties such as chemical stability, mechanical strength as well as proton conductivity [7-8]. It has been stated that methanol crossover from anode to cathode side in DMFCs has negative effect on its performance and tends to make catalysts inactive [1,9-10]. The modification of DMFC polymer electrolyte membrane is required to reduce methanol permeation by maintaining high ion conductivity [11]. Hence, various researchers have focused on discovering better ways of improving the performance of fuel cells. One of the approaches is to incorporate inorganic filler such as palladium nanoparticles [1]. Pd as catalyst has shown very promising catalytic behaviour in terms of oxygen reduction reaction (ORR) to improve performance of fuel cell [1]. Palladium membranes can improve performance of DMFCs since methanol cannot crossover and protons can be penetrated in the palladium membranes [12]. Palladium was selected as filler in this research due to excellent characteristics such as proton conductor and capability of having low methanol permeability [12].

5.2. Preparation of composite membranes

A recast method was used to prepare Pd/Nafion® nanocomposite membrane. N, N-dimethylformamide (DMF) was mixed with 5 % Nafion® 117 solution. Different palladium nanoparticles solution (volume percentage of 11 %, 22% and 33%) were incorporated in the resultant solution to create PdEG11/Nafion®, PdEG22/Nafion® and PdEG33/Nafion® recast membranes. To create commercial PdNps/Nafion® recast membrane, 4.5mg of commercial PdNps were added to the solution. The solution was stirred for 45 minutes at room temperature and placed in ultrasonic bath for 30 minutes. The solution was transferred to the glass beaker and put in the oven at 80 °C for 24 hours to remove solvent. The membrane was heated at 160 °C for 1 hour and added deionized water so that it can be peeled off from glass beaker. Then the membranes were dried in the oven at 60 °C for 1 hour.

5.3. Results and Discussion

5.3.1. XRD Analysis

Nafion® recast membrane and nanocomposite membranes were characterized by X-ray diffraction to investigate the structural changes. The broad peak indicates amorphous region of a polymer while sharp peak points out a crystalline region of the material and their intensities turn to be high [13-14]. The XRD patterns of Nafion® and nanocomposite Nafion® membranes are shown in Figure 5.1. The peak at Brag angle of $2\theta = 17.8°$ indicates hexagonal crystalline structure corresponding to plane of (100) made of Nafion® PFSA backbone [4,14-18]. The broad peak at 38.9° [19] was

noticed for pristine Nafion[®], PdEG 11/Nafion[®] and PdEG 22/Nafion[®] recast membranes, which indicates amorphous region of Nafion[®] polymer. The peak becomes sharper as indication of increased degree of crystallinity of polymer membrane [20]. The crystallinity of Nafion[®] membrane was expected to increase for all Pd nanocomposite membranes. The peaks besides peaks at Brag angle of 2θ = 17.8° and 38.9° were noticed for only commercial PdNps/Nafion[®] and PdEG33/ Nafion[®] recast membranes. This could be due to the low amount of palladium nanoparticles in the PdEG11/Nafion[®] and PdEG22/Nafion[®] recast membrane or XRD scattering beam did not reach the region where there is PdNps. It also reported that there are challenges for nano- composite materials not having homogeneous surface because of poor dispersion of nanomaterials causing agglomeration and ununiform distribution in the polymer matrix [21]. The small sharp and broad peaks were noticed for commercial PdNps/Nafion[®] recast membrane as result of increased crystallinity of membranes. The peaks for commercial PdNps/Nafion[®] recast membrane appeared at different Brag angles of 2θ = 40.177°, 46.553° ,68.089° and 81.897° corresponding to planes (111), (200), (220) and (311) of metallic palladium whereas PdEG33/Nafion[®] recast membranes membrane indicated small peaks at Brag angles of 2θ = 40.177° and 46.553° representing (111) and (200) planes.
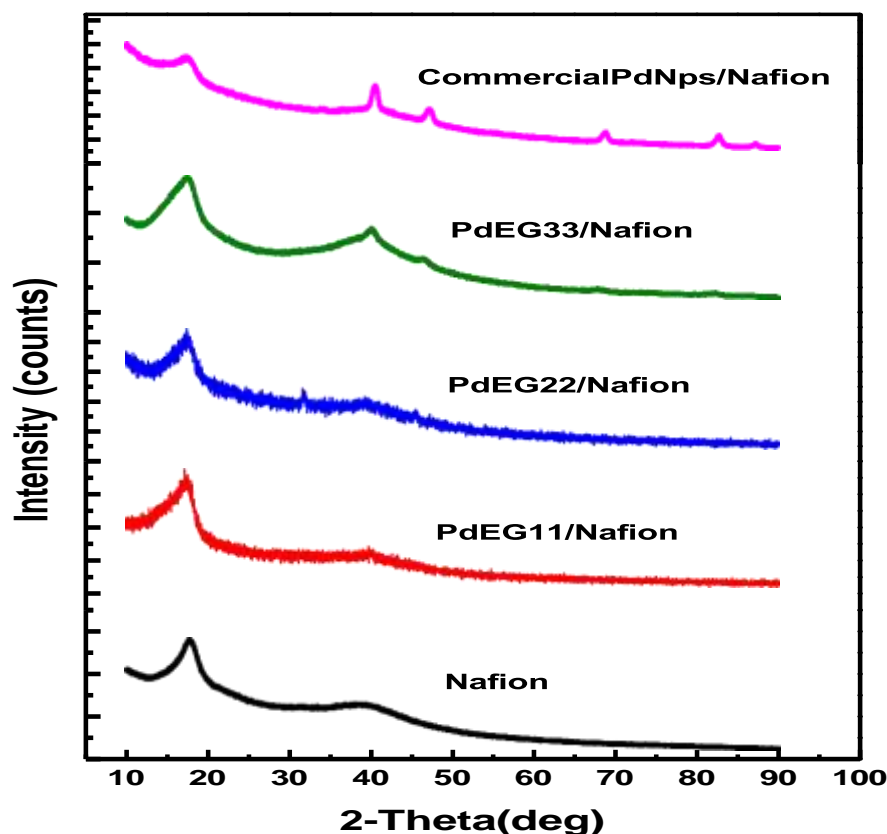
Figure 5.1: XRD patterns of Nafion®, commercial PdNps/Nafion®, PdEG11/Nafion®, PdEG22/Nafion® and PdEG33/Nafion®.

5.3.2. XRF Analysis

The nanocomposite membranes analysed by XRD were further analysed using Shimadzu 1800 XRF analyser to obtain the amount of palladium nanoparticles present in the recast membranes. XRF technique is different from other techniques such as XRD whereby the entire surface area of membrane samples is exposed to beam. Therefore, the results obtained from this technique represent approximately the amount of palladium nanoparticles embedded in Nafion® matrix. Table 5.1 indicates the X R F results o f commercial P d N p s /Nafion® membrane and Pd/Nafion®

nanocomposite membranes. The composition of palladium in weight percent was found to be 4% for commercial PdNps/Nafion®, 8% for PdEG 11/Nafion®, 16% for PdEG 22/Nafion® and 26% for PdEG 33/Nafion® in Table 5.1.

Table 5.1: XRF analysis of Nafion®, commercial PdNps/Nafion®, PdEG11/Nafion®, PdEG22/Nafion® and PdEG33/Nafion®

	Ni (%)	Cu (%)	Fe (%)	Cr (%)	Mn (%)	Zn (%)	Sn (%)	Br (%)	Pd (%)
Nafion®	57.97	26.48	14.44	1.03	0.063	0.02			
Commercial PdNps/Nafion®	65.70	17.20	11.84	1.09					4.17
PdEG 11/Nafion®	55.09	16.59	19.42	0.77	0.08				8.05
PdEG 22/Nafion®	43.48	22.25	17.28	0.47			0.11		16.41
PdEG 33/Nafion®	43.83	15.54	14.13		0.05			0.05	26.03

5.3.3. FESEM Analysis

The SEM images of commercial PdNps/Nafion® membrane and Pd/Nafion® nanocomposite membranes are shown in Figure 5.2. Figure 5.3 and Figure 5.4 show the membranes morphology were uniform without any cracks. The SEM images of PdEG11/Nafion® in Figure 5.3 and PdEG22/Nafion® in Figure 5.4 indicate the presence of palladium with black spherical particles supported by EDS analysis. EDS analysis in Figure 5.3 and Figure 5.4 also indicated the presence of residue element of sodium and chloride, which might be results of precursor Na_2PdCl_4 used for

synthesis of PdEG nanoparticles while C-peaks were the result of carbon–coating during sample preparation. The sulphur element might originate from sulphonated Nafion® membrane.

SEM image of PdEG 33/Nafion® membrane in Figure 5.5 was completely different from the first two membranes. The palladium nanotubes/nanowires were obtained, and this might be the fact that the membrane was left over in the conventional oven at temperature of 160^0C for 48 hrs instead of 30minutes as stipulated in the experimental procedure. Study on nanotubes/nanowires by various researchers were performed at temperatures between 95 to 200 ^{0}C [22-26]. Therefore, the results indicate that morphological structure of PdEG33/Nafion® changes dramatically due to the effect of temperature and time. Therefore, palladium nanorods/nanowires obtained in this research were the results of allowance of high temperature at pro-long hours.

Figure 5.2: Recast membranes (a) Commercial PdNps/Nafion® (b) PdEG11/Nafion® (c) PdEG22/Nafion® and (d) PdEG33/Nafion®.
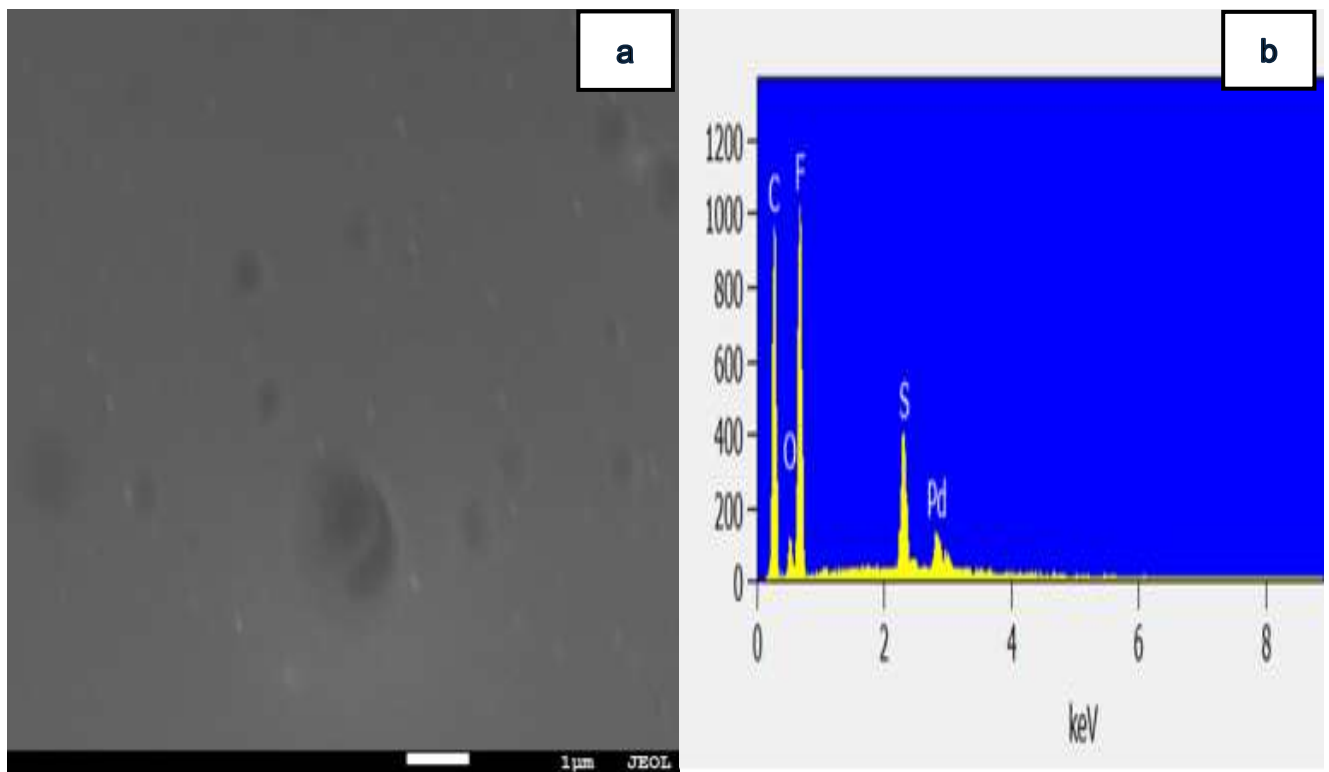
Figure 5.3: PdEG11/Nafion®: (a) SEM image (b) EDS elementary spectrum.

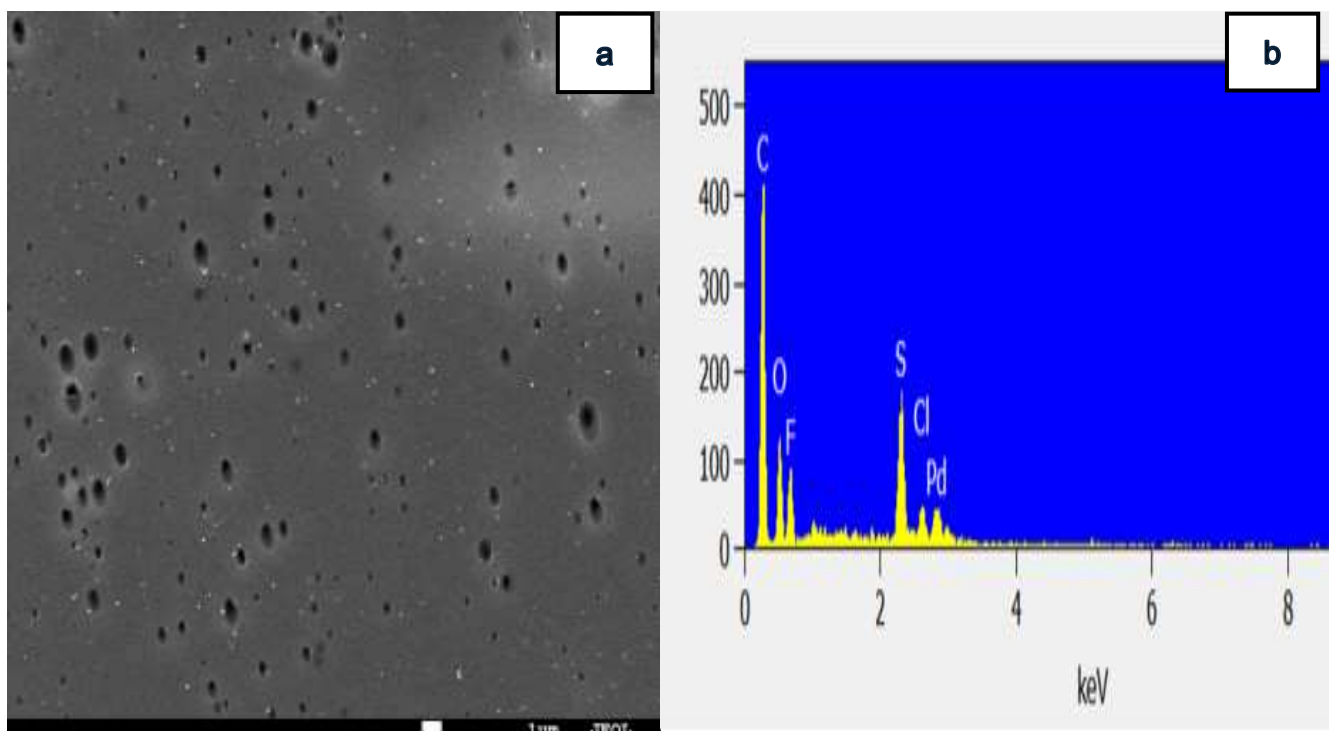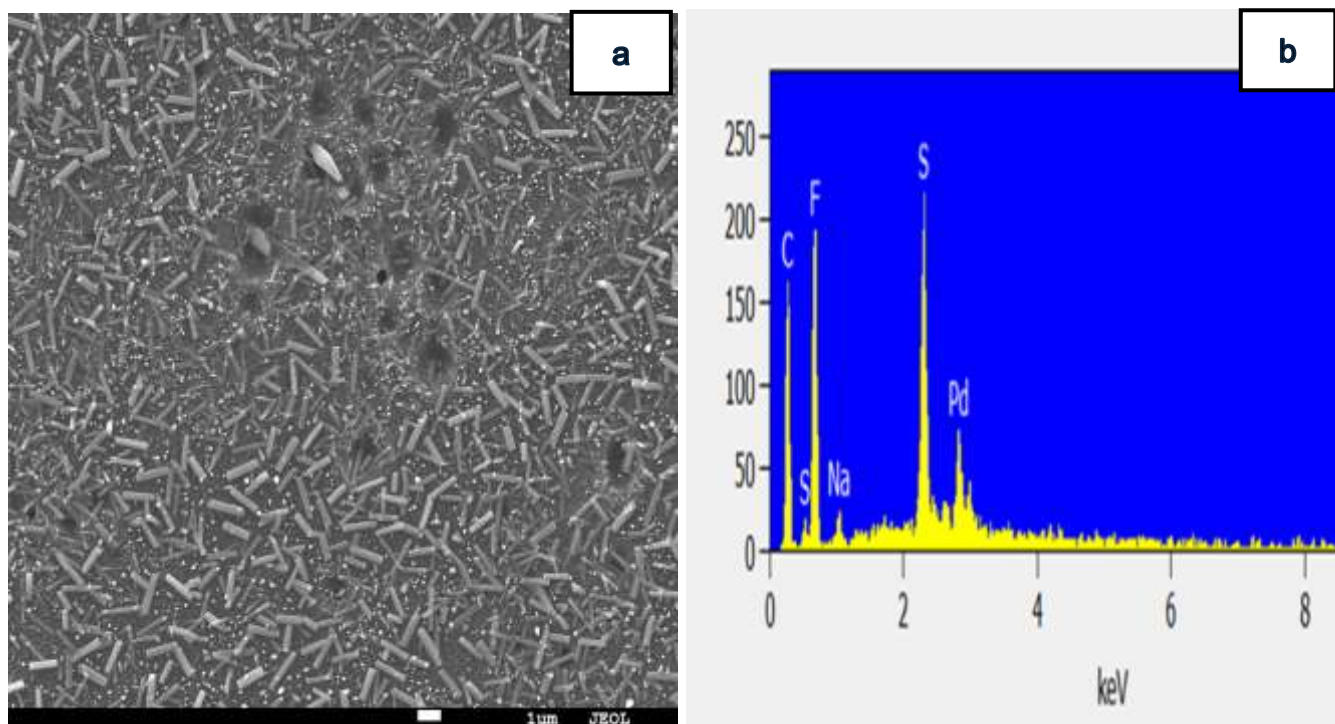Figure 5.4: PdEG22/Nafion®: (a) SEM image (b) EDS elementary spectrum.

Figure 5.5: PdEG33/Nafion®: (a) SEM image (b) EDS elementary spectrum.

5.3.4. Water Contact Angle Analysis

The study of wettability of solid by liquid is evaluated by performing contact angle measurements [27-28]. The technique of contact angle analysis is regarded as an economical, simple, and fast method to evaluate wetting properties of a solid by a liquid [29]. The hydrophobic group of PTFE backbone membrane surface such as Nafion® have impact on contact angle by holding back water drop from advancing. The sulfonic acid group (hydrophilic region) absorbs water, resulting in water flooding in Nafion® membrane [30-31].

To evaluate wettability of pristine Nafion®, PdEG11/Nafion®, PdEG22/Nafion®, PdEG33/Nafion® and commercial PdNps/Nafion® recast membrane, sessile drop measurement (Figure 5.6) was utilized to measure contact angle of each membrane.

The water contact angle of different membranes was plotted in Figure 5.7. Figure 5.7 showed an increase in contact angle of Nafion® nanocomposite membranes when compared to Nafion®. According to Ramanujam et al. [32], higher contact angle means low wettability which could be the result of surface being smooth and non-existence of polar groups. The PdEG 11/Nafion® and PdEG33/Nafion® membranes showed hydrophobic properties with contact angles greater than 90° [33-34], average 94.5°, 93.9° respectively corresponding to low wettability. The pristine Nafion®, PdEG22/Nafion® and commercial PdNps/ Nafion® with low contact angle less than 90° indicating degree of wetting is favoured [33]. The lowest contact angle recorded was Nafion® at 83.06° followed by PdEG22/Nafion® at 83.8° and commercial PdNps/ Nafion® at 86.06°.
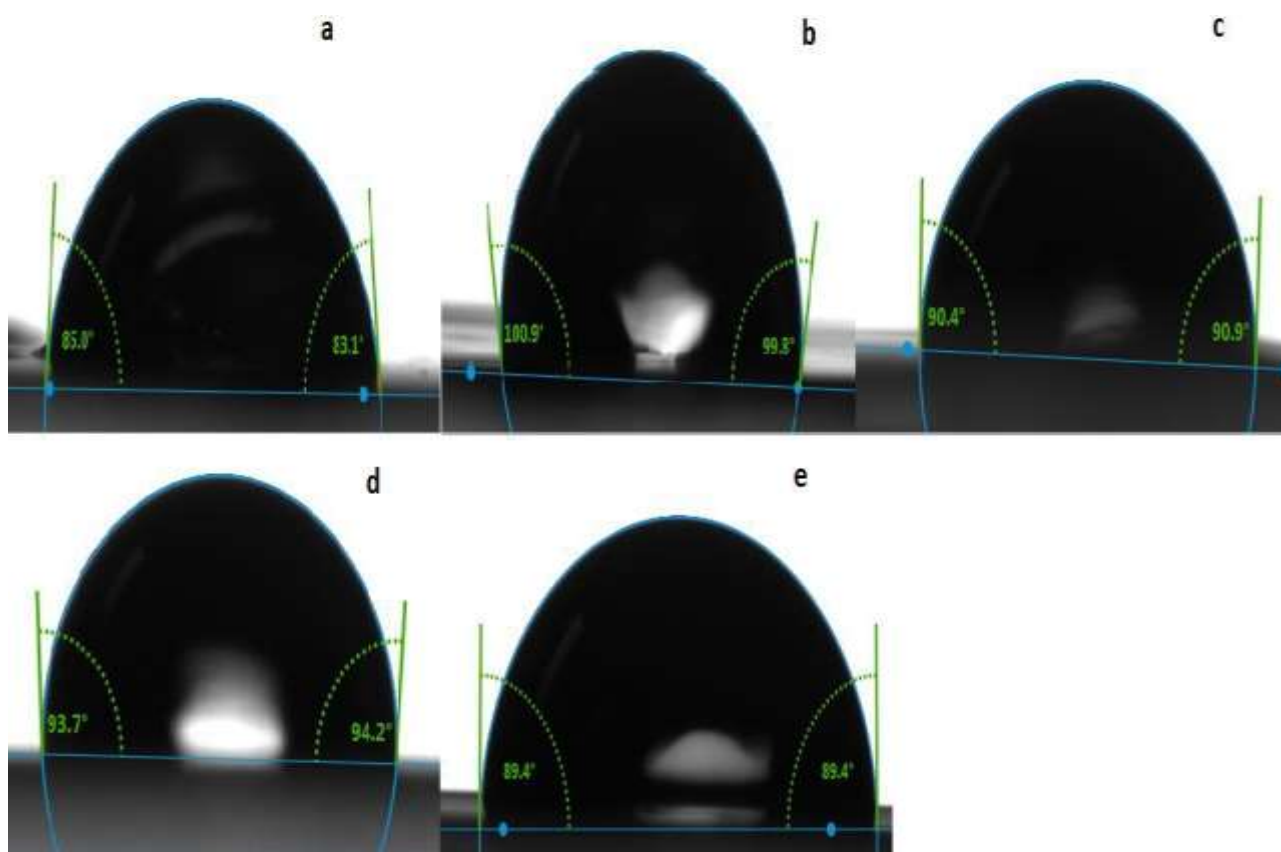
Figure 5.6: Sessile drop images on the surfaces of recast membranes (a)Nafion®(b) PdEG11/Nafion®(c)PdEG22/Nafion®(d)PdEG33/Nafion®(e)commercialPdNps/Nafion®
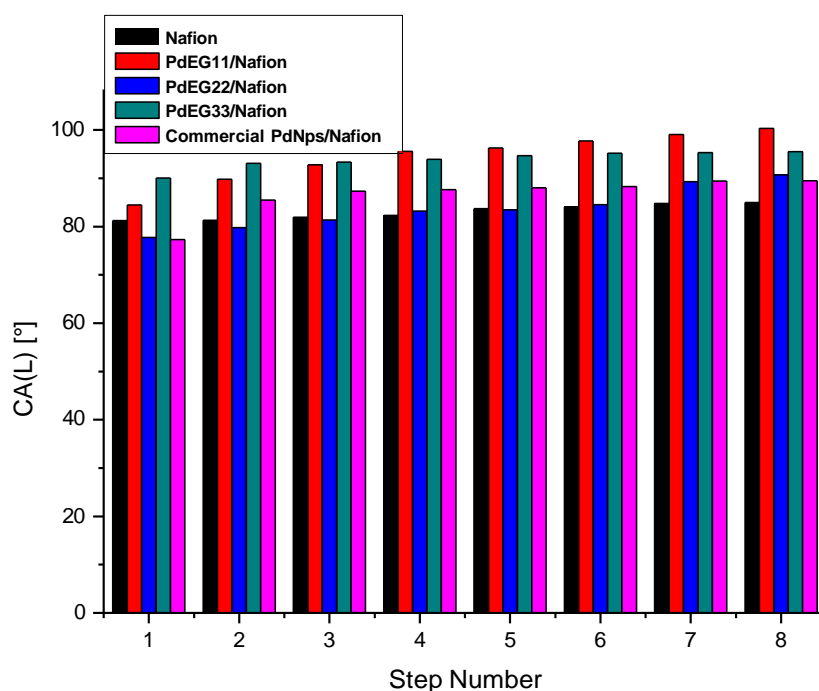
Figure 5.7: Water Contact Angle of Nafion®, commercial PdNps/Nafion®, PdEG11/Nafion®, PdEG22/Nafion® and PdEG33/Nafion®.

5.3.5. Thermal Gravimetric Analysis (TGA)

In this study nano-composite membranes of PdEG 11/Nafion®, PdEG 22/Nafion® and PdEG33/Nafion® were analysed and compared to Nafion® and commercial PdNps/Nafion® recast membrane (Figure 5.8). Figure 5.8 shows that weight loss was experienced at three stages for all membranes. The first stage was dehydration of membranes. The second stage is the result of decomposition of the sulfonic acid group and the third stage is the complete decomposition sulfonic acid group of Nafion® polymer backbone [35-36]. The degradation temperature increases due to incorporation of inorganic metal fillers into polymer solution since they are temperature tolerant [37-38]. The membranes in Figure 5.8 kept their weight at more than 90% at

temperature of 330 °C for recast nanocomposite membranes and Nafion® at temperature of 323 °C before they undergo decomposition stage. The first stage of degradation of PdEG11/Nafion®, PdEG22/Nafion®, PdEG33/Nafion®, commercial PdNps/Nafion® at 330 °C and Nafion® at 323 °C due to evaporation of water molecules [29,39-41]. All membranes in Figure 5.8 undergone second stage and lost their weight at temperature above 400 ⁰C due to sulfonic group degradation [29,39-40,42-43]. Nafion® undergone second decomposition stage at temperature of 450 °C and PdEG11/Nafion®, PdEG22/Nafion®, PdEG33/Nafion®, commercial PdNps/Nafion® membranes at 480 °C.

The final decomposition started with PdEG11/Nafion® at 660°C followed by Nafion® at 770°C. The final decomposition recast membranes of commercial PdNps/Nafion®, PdEG22/Nafion® and PdEG33/Nafion® recast membranes was at 900°C. According to Figure 5.8, the thermal stability of Nafion® membrane was enhanced whereby commercial PdNps/Nafion®, PdEG22/Nafion® and PdEG33/Nafion® indicated highest thermal stability with remaining palladium residue mass of 0.309%, 0.418 % and 1.440 % respectively at a temperature of 900⁰C.
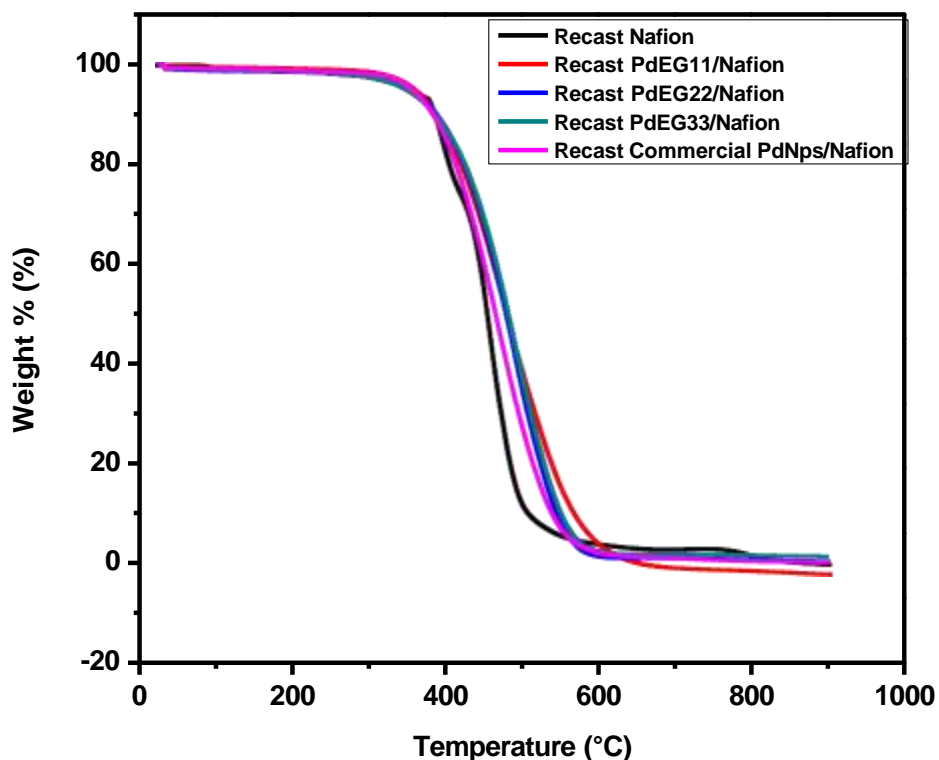
Figure 5.8: Thermal stability of Nafion®, commercial PdNps/Nafion®, PdEG11/Nafion®, PdEG22/Nafion® and PdEG33/Nafion® membranes.

5.3.6. Dynamic Scanning Calorimeter (DSC)

The endothermic peak below 200°C indicates water content and affinity of water molecules [44-45]. The bigger area of the peak denotes elevated affinity of water or hydrophilicity [44,46]. The study of glass transition of Nafion® 117 in hydrated and dehydrate state was performed by Jung and Jung [44]. It was reported that the glass transition temperature of Nafion® 117 membrane was drastically increased when its water content was reduced by hot-press method. The glass transition of Nafion® 117 membrane can be reduced by water which can act as plasticizer [44-47]. The glass transition of Nafion® at 24% of water content was 108°C and it gradually reduced to 132°C at complete dehydration state [44]. In Figure 5.9, the glass transition

temperature was only observed for PdEG22/Nafion® membrane at 120 °C. Commercial PdNps/Nafion®, PdEG11/Nafion® and PdEG33/Nafion® did not exhibit the glass transition temperature.

According to Wang et al. [47] the shape of the graph with two peaks symbolizes a sample with a eutectic impurity representing a crystallization phase. Polymeric or impure materials are identified by exhibiting longer tails and concave side shapes. Amorphous samples will show wide peaks owing to size distribution within structure of the components [48]. Modification of products by introducing impurities in polymer and semiconductor processing has indicated a vital role throughout crystallization stages. Two or more phases are formed from liquid phase through eutectic crystallization [49].

All membranes in Figure 5.9 indicated exothermic behaviour due to decomposition of material [50] representing eutectic crystallization with two peaks. The peaks of PdEG22/Nafion® membrane are broader compared to other membranes indicating crosslinking behaviour. The first crystalline peaks are at 386 °C,397 °C,390 °C,391 °C for recast membranes of Commercial PdNps/Nafion®, PdEG11/Nafion®, PdEG22/Nafion® and PdEG33/Nafion® respectively. The second crystalline peaks temperatures are at 455 °C, 466 °C, 460 °C, 467 °C for recast membranes of commercial PdNps/Nafion®, PdEG11/Nafion®, PdEG22/Nafion® and PdEG33/Nafion®, respectively. The endothermic peaks in DSC graph can be used to estimate the amount of freezing bound water as well as freezing free water in the nanocomposite membranes indicating hydrophilic behaviour of material [51]. Figure 5.9 did not exhibit the endothermic peaks for commercial PdNps/Nafion®, PdEG11/Nafion®, and PdEG33/Nafion® indicating hydrophobic behaviour. Therefore,

the results shown in Figure 5.9 correspond to the results of membranes water uptake
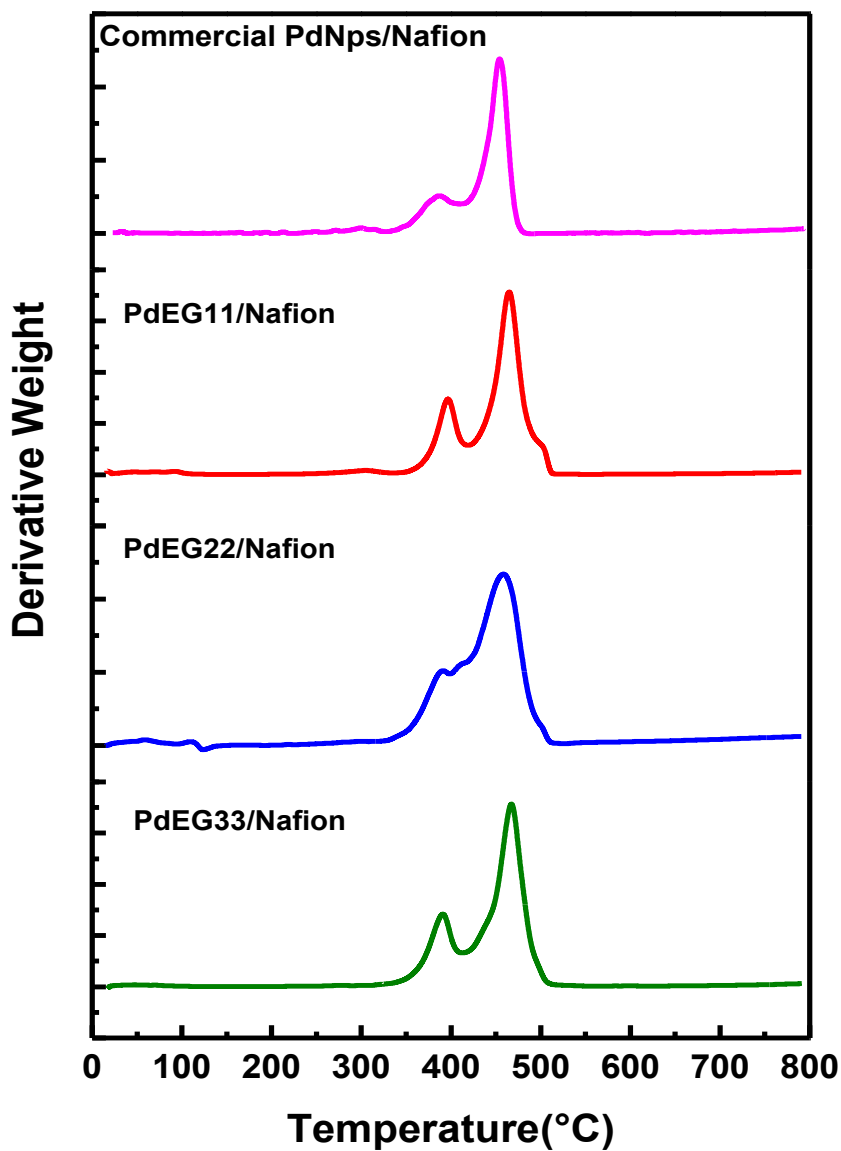and water contact angle which exhibited hydrophobic behaviour.

Figure 5.9: DSC analysis of commercial PdNps/Nafion®, PdEG11/Nafion®,
PdEG22/Nafion® and PdEG33/Nafion®.

5.3.7. Fourier Transform Infrared (FTIR).

Figure 5.10 shows the FTIR results of recast Nafion® membrane and commercial
PdNps/Nafion®, PdEG11/Nafion®, PdEG22/Nafion® and PdEG33/Nafion®

nanocomposite membranes. The broad absorption peak of Nafion® membrane at 3475 cm^{-1} is assigned to stretching vibration of -OH groups [52-53]. C-F bands are found between 1400 cm^{-1} and 1100 cm^{-1} [54-55] with strong absorption band of Nafion® at 1141 cm^{-1} assigned to CF2 asymmetric stretching [52,56]. Nafion® absorption band appears at 1212 cm^{-1} due to SO^{-3} asymmetric stretching of C-F vibrational modes mixing with the symmetric stretching mode [55]. Other C-F bands are found in the range 1000 cm^{-1} to 500 cm^{-1} representing the band of C-F stretching group (CF2- CF(CF3)) [56,30] at 982 cm^{-1} for Nafion®. The absorption spectra in the region of 1000 cm^{-1} to 1350 cm^{-1} represent sulfonic groups with Nafion® absorption band at 1055 cm^{-1} assigned to S-O stretching of SO^{-3} asymmetric stretching [52,55-57].

Structural properties of Nafion® are changed when organic materials (fillers) are added to Nafion® membrane. The nanocomposite membranes namely, commercial PdNps/Nafion®, PdEG11/Nafion®, PdEG22/Nafion® and PdEG33/Nafion® structure composes of new peaks due to addition of PdNps. Thus, the original peaks of Nafion® were shifted in all nanocomposite membranes. The Nafion® peak at 982 cm^{-1} is shifted to 969 cm^{-1} for PdEG11/Nafion® and PdEG33/Nafion® and 979 cm^{-1} for PdEG22/Nafion® due C-O-C symmetric stretching [22,55]. The characteristic band at 1055 cm^{-1} was shifted to 1049 cm^{-1} for PdEG22/Nafion®, 1043 cm^{-1} for PdEG11/Nafion® and PdEG33/Nafion®, 1035 cm^{-1} for commercial PdNps/Nafion® representing C-O peak due to stretching of alcohols adsorbed on palladium surface [58].

The adsorption band of SO^{-3} asymmetric stretching of C-F vibrational modes mixing with the symmetric stretching mode at 1212 cm^{-1} [55] remain the same for all nanocomposite membranes. The characteristic peak at 1141 cm^{-1} representing CF2

asymmetric stretching [52,56] shifted to 1127 cm^{-1} for commercial PdNps/Nafion$^®$ and remain the same for PdEG11/Nafion$^®$, PdEG22/Nafion$^®$ and PdEG33/Nafion$^®$. The adsorption band of 1644 cm^{-1} due to C-H stretching of polyols [58] remain the same for PdEG11/Nafion$^®$ and shifted to 1649 cm^{-1} for PdEG 22/Nafion$^®$ and commercial PdNps/Nafion$^®$, 1657 cm^{-1} for PdEG 33/Nafion$^®$.

New emerging absorption bands were noticed for all PdEG/Nafion$^®$ membranes and commercial PdNps/Nafion$^®$ membrane. The new absorption peaks at 3851 cm^{-1},3739 cm^{-1}, 3618 cm^{-1}, 2355 cm^{-1}, 1692 cm^{-1}, 1522 cm^{-1}, 1466 cm^{-1}, 767 cm^{-1}, 676 cm^{-1}, 577 cm^{-1}, 498 cm^{-1} for commercial PdNps/Nafion$^®$: 2357 cm^{-1},725 cm^{-1},626 cm^{-1},515 cm^{-1} for PdEG33/Nafion$^®$: 3731 cm^{-1}, 2355 cm^{-1}, 1466 cm^{-1}, 633 cm^{-1}, 513 cm^{-1} for PdEG22/Nafion$^®$ and 2358 cm^{-1},626 cm^{-1},515 cm^{-1} for PdEG11/Nafion$^®$. The new absorption bands in Figure 5.10 might be due to the addition of PdNps to Nafion$^®$ matrix which are close to values obtained by other research publications on synthesis of palladium nanoparticles [59-65].
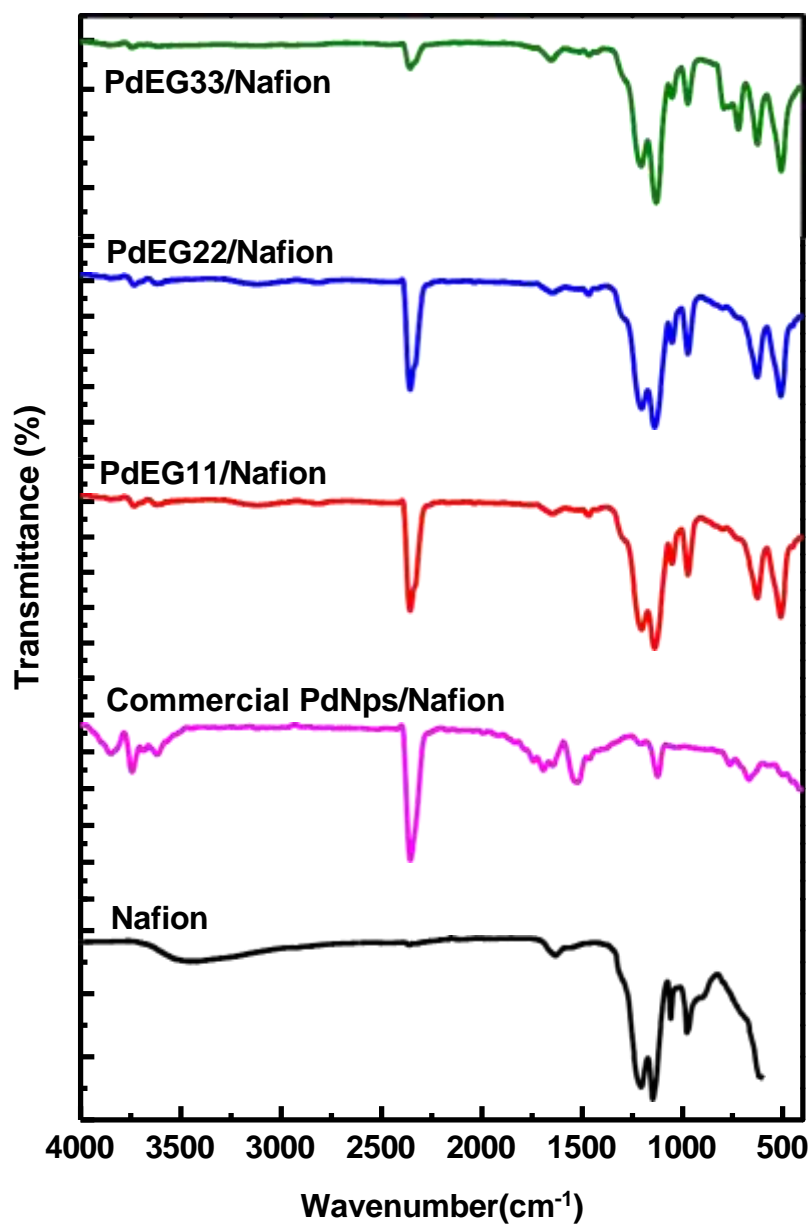
Figure 5.10: FTIR spectra of Nafion®, commercial PdNps/Nafion®, PdEG11/Nafion®, PdEG22/Nafion® and PdEG33/Nafion®.

5.3.8. Water Uptake (WU)

Generally, the membrane with high water content normally indicates outstanding proton conductivity. However, in application of DMFC high water content can affect performance of fuel cell by increasing methanol permeability, reducing dimensional stability and mechanical strength [66-67]. Various research indicated that increasing filler content improves water uptake up to certain level, thus at highest filler loading water uptake is reduced that may be caused by agglomeration [68-77]. The commercial Nafion® membrane has a low water uptake (approximately 22) compared to recast Nafion® membranes [78-81]. This indicates that properties of Nafion® membrane may be improved by recast method which is a different method from the one used to produce commercial Nafion® membrane (Extrusion method).

The water uptake increases with increase in temperature for acid Nafion® membranes [79-80]. At high temperature micro pores and ion clusters formation tend to increase causing higher water uptake in membrane [80,82]. The data obtained from other literatures indicate water uptake becomes high when temperature increases at specific relative humidity [80]. Water uptake and swelling properties are affected by surface of hydrophobic membranes [29].

The nanocomposite membranes in Figure 5.11 indicated lower water uptake with commercial PdNps/Nafion® experience a lowest water uptake indicating hydrophobic behaviour. The water uptake was very low for commercial PdNps/Nafion®, PdEG11/Nafion®, PdEG22/Nafion® and PdEG33/Nafion® at temperatures of 30 °C and 60 °C when compared to Nafion®. The water uptake of commercial PdNps/Nafion®, PdEG11/Nafion®, PdEG22/Nafion® and PdEG33/Nafion® improved at elevated temperatures of 80 °C and 100 °C with PdEG33/Nafion® having highest

water uptake comparable to Nafion®. It is stated that the layer of cathode catalyst must be hydrophobic to avoid flooding and loss of catalyst activity [32]. According to Figure 5.11, PdEG33/Nafion® is more hydrophobic compared to other nanocomposite membranes.
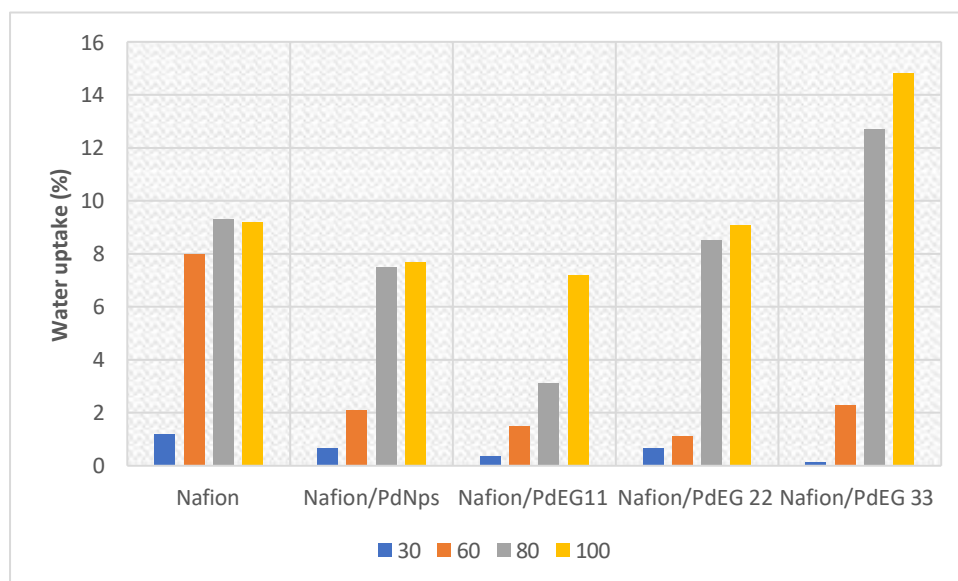
Figure 5.11: Water uptake of Nafion®, commercial PdNps/Nafion®, PdEG11/Nafion®, PdEG22/Nafion® and PdEG33/Nafion®.

5.3.10. Ion Exchange Capacity (IEC)

Ion exchange capacity (IEC) of Nafion®, commercial PdNps/Nafion®, PdEG11/Nafion®, PdEG22/Nafion® and PdEG33/Nafion® recast membranes in Figure 5.12 was higher than the Nafion® recast membrane. Ion exchange capacity acts as a proton conductivity indicator in direct methanol fuel cell. Higher IEC was obtained due to an increase loading of filler content thus resulting in increasing proton conductivity [73]. At higher filler loading, IEC was reduced with increase in water uptake [78]. This is evidence from the results of water uptake in Figure 5.1 showing PdEG33/Nafion®

has highest water uptake and lower IEC (Figure 5.12). The same trend was noticed by Thiam et al. [8] where IEC value was reduced due to higher filler loading.

The ion exchange capacity value of Nafion® was recorded from various research as 0.91mmol/g [83], 0.93 mmol/g [22], 0.79 mmol/g [78], 0.7778 mmol/g [84], 0.86 mmol/g [81,85]. For this research, the ion exchange capacity of Nafion® in Figure 5.12 was recorded as 0.81 mm/g in which the value falls between the values obtained in the above literature. According to Awang et al. [51], low water uptake was experienced with improved IEC and proton conductivity. The lowest water uptake recorded was PdEG11/Nafion® with the highest IEC compared to PdEG22/Nafion® and PdEG33/Nafion®. Nanocomposite membranes in Figure 5.12 indicated improved results with highest IEC values compared to Nafion® recast membrane due to palladium nanoparticles being good proton conductors [12].
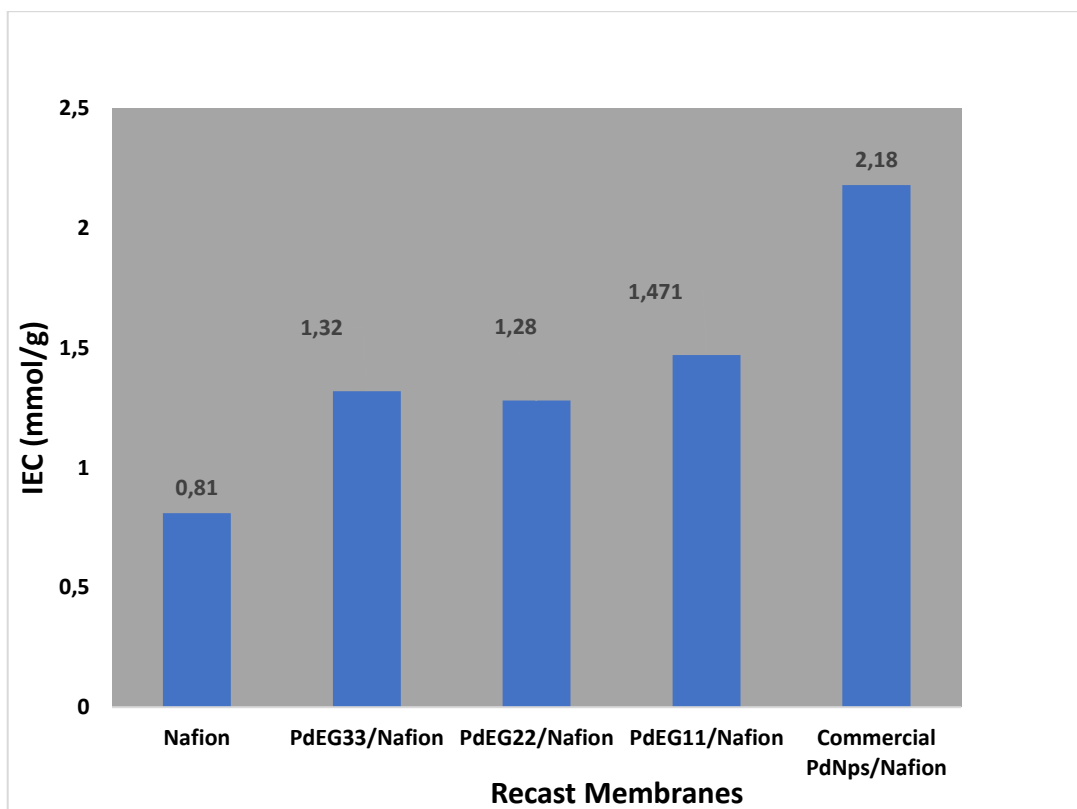
Figure 5.12: Ion Exchange Capacity of Nafion®, commercial PdNps/Nafion®, PdEG11/Nafion®, PdEG22/Nafion® and PdEG33/Nafion®.

5.3.11. Proton Conductivity

The characteristics requirement of membrane is high proton conductivity and should be capable of preventing methanol from crossing over to cathode side [73]. The other property that may affect proton conductivity is membrane thickness. Higher resistance is experienced with thicker membranes which affect proton conductivity. The preferred membrane thickness for DMFC applications is between $30 < \mu m < 100$ compared to commercial Nafion® membrane ($>100 \mu m$ or $0.1mm$) [4]. The thickness of nanocomposite membranes in Table 5.2 is within recommended range of 30-100 μm. Table 5.2 indicates the proton conductivity of recast Nafion®, Nafion® 117,

PdEG11/Nafion®, PdEG22/Nafion®, PdEG33/Nafion® and commercial PdNPs/Nafion®. The nanocomposite membranes in Table 5.2 displayed high values of proton conductivity compared to recast Nafion® and Nafion® 117. The nanocomposite membranes showed higher conductivity with the highest value of 0.6 S cm^{-1} for PdEG11/Nafion®, 0.41 S cm^{-1} for PdEG22/Nafion® ,0.28 S cm^{-1} for PdEG33/Nafion®, 0.26 S cm^{-1} for commercial PdNPs/Nafion® in comparison with 0.25 S cm^{-1} for recast Nafion® and 0.022 S cm^{-1} for Nafion® 117. Table 5.2 results show proton conductivity of nanocomposite membranes is reduced as palladium nanoparticles content is increased in Nafion® matrix. Therefore, the results in Table 5.2 indicates high proton conductivity compared to recast Nafion® membrane and Nafion® 117 membrane which correspond to IEC results in Figure 5.12.

Table 5.2: Proton Conductivity of Nafion® and Pd/Nafion® nanocomposite membranes

Recast Membrane	Thickness(mm)	Proton Conductivity (Scm^{-1})	Reference
PdEG11/Nafion®	0.0093	0.60	Current work
PdEG 22/Nafion®	0.0076	0.41	Current work
PdEG 33/Nafion®	0.0066	0.28	Current work
Commercial PdNps/Nafion®	0.0141	0.26	Current work
Recast Nafion®	-	0.25	Current work
Nafion® 117	-	0.022	[85-87]

5.3.10 Methanol Permeability and membrane selectivity

Membranes used in DMFC such as Nafion® should be conductive with low methanol permeability [66,88]. The material at cathode of DMFCs should be resistance to methanol and show ability towards oxygen reduction reaction [1]. Methanol oxygen reaction at the cathode lowers efficiency of DMFC due to methanol crossover from anode to cathode via polymer electrolyte membrane [89]. Hence, the methanol

crossover affects current density of DMFC thus reducing fuel efficiency and cathode activity [32].

Addition of inorganic filler resulted in reducing the methanol permeability, but it also increased with increase in temperature [8,10]. Methanol permeability increases at higher temperatures due to changes in membrane structure. Increase in temperature causes vibration of chains and molecules of membrane resulting in increase of free volume which decrease prevention of methanol crossover [4].

The methanol permeability in Figure 5.13 was improved at higher Pd loadings. The same trend was observed by Altaf et al. [74]. The results from various literatures demonstrate that there was bonding and networking of nanoparticles and polymer matrix which prevented methanol crossover [51-52,74,90]. The results from this research indicated low methanol permeability with low water uptake for the recast Pd nanocomposite membranes (Figure 5.13 & Figure 5.12). According to Awang et al. [51] it is normal that membranes which have low water uptake experience less methanol permeability and the membranes produced from their research work displayed similar results. It also stated that more dense composite membranes experience low degree of swelling which result in improved methanol transport resistance [91].

In DMFC, methanol blocking effect can be affected by swelling of PEMs in temperature ranging from 60°C to 120°C hence it needs to be hindered [4]. All recast membranes in Figure 5.13 showed improved methanol permeability results at individual temperature with ultra-low methanol permeability at 25°C and 40°C. The highest methanol permeability of recast membranes in Figure 5.13 was recorded at 60°C and 80°C when compared to Nafion$^{®}$ methanol permeability values from other research

literatures 8.91×10^{-7} cm^{2}s^{-1} [82] and 12.8×10^{-7} cm^{2}s^{-1} [92-93]. Nanocomposite membranes in Figure 5.13 indicated 0% of methanol permeability at temperature of 25°C. The methanol permeability of nanocomposite membranes increased from 40°C to 80°C. PdEG22/Nafion® displayed low methanol permeability compared to other nanocomposite membranes followed by PdEG33/Nafion®, commercial PdNps/Nafion®. PdEG11/Nafion® has the highest methanol permeability comparable to other nanocomposite membranes. Therefore, the results from this research indicated that blending Pd nanoparticles with Nafion® can be an effective method for suppressing crossing of methanol from anode to cathode.

The selectivity (ratio of proton conductivity and methanol permeability) is important since it is used as indicator to evaluate suitability of membrane to be applied as PEM in DMFC [11]. The selectivity of membranes was determined at temperatures of 60°C and 80°C (Table 5.3). The selectivity of palladium nanocomposite membranes is high compared to pristine Nafion® membrane. Therefore, the results in Table 5.3 suggest that palladium nanocomposite membranes may be suitable to be used as PEM in DMFC.

Table 5.3: The selectivity of Nafion® and Pd/Nafion® nanocomposite membranes

Membrane	Selectivity at 60°C (Sc cm^{-3})	Selectivity at 80°C (Sc cm^{-3})
PdEG11/Nafion®	2.9×10^6	1.33×10^6
PdEG22/Nafion®	6.4×10^6	1.14×10^6
PdEG33/Nafion®	7.6×10^6	7.4×10^5
CommercialPdNps/Nafion®	3.9×10^6	7.4×10^5
Nafion®	5.3×10^5	2.7×10^5
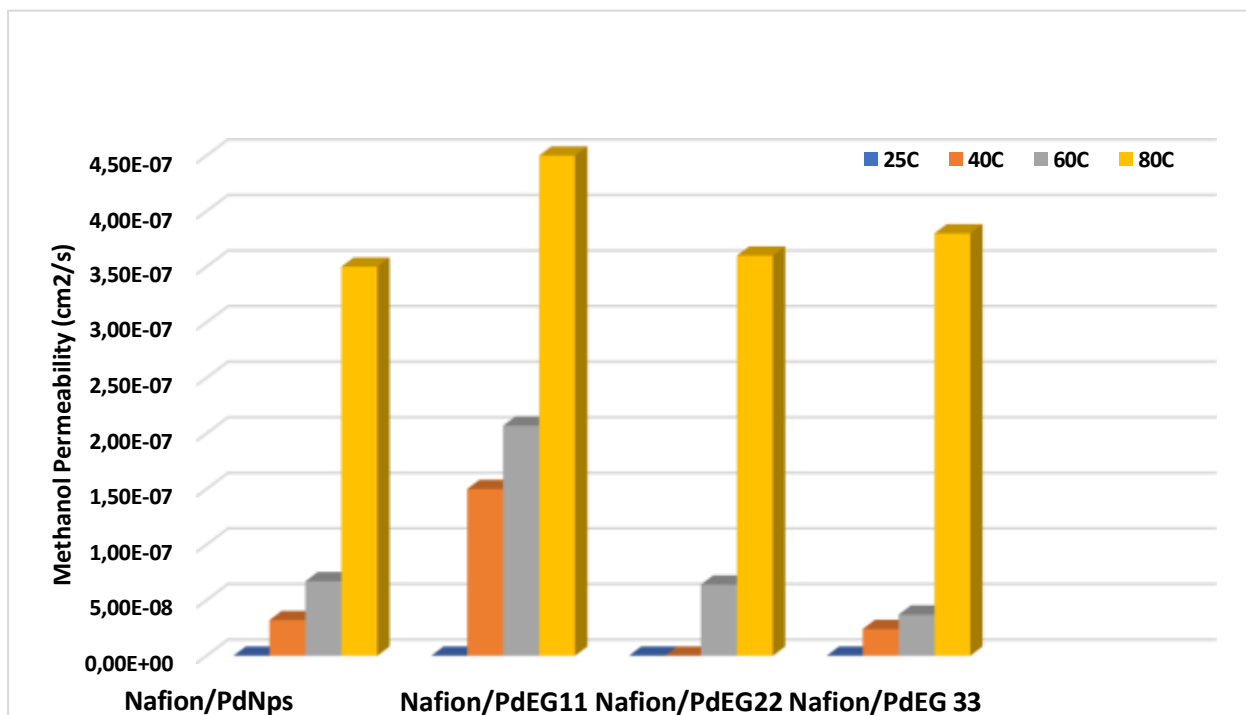
Figure 5.13: Methanol permeability of Nafion®, commercial PdNps/Nafion®, PdEG11/Nafion®, PdEG22/Nafion® and PdEG33/Nafion®.

5.3.12. Electrochemical Characterization

5.3.12.1 Cyclic Voltammetry

Cyclic Voltammetry (CV) was used to study the electro-catalytic behaviour of Nafion® and its nano-composite membranes in the presence of 1 M KOH. The potential range between -0.9V and 1V was used to perform cyclic voltammetry studies at scan rate of 10mVs for all membranes. Research studies of cyclic voltammetry [94-96] revealed that there were five distinguished peaks of Pd nano-catalyst visible: I. hydrogen oxidation peak, II. oxidative desorption of hydrogen and adsorption of hydroxide peak, III. oxidation of Pd peak IV. reduction of Palladium oxide and V. reductive adsorption/absorption of hydrogen.

The peak of PdO at potential of -0.25 V was identified by Liang et al. [95] which is like those obtained in Figure 5.14. The results in Figure 5.14 indicated three characteristics peaks in the anodic area and two characteristics peaks in the cathodic area. According to Liang et al. [95], Awasthia and Singh [96], an increase in anodic current can be assigned to conversion of Pd (II) into Pd (II) oxide (PdO) layer on the membrane surface [97].

The shape of palladium nanocomposite membrane CV cycles is identical to the ones published by Liang et al. [95]. In the cathode, the maximum oxidation current is 0.45V for both Commercial PdNps/Nafion® and PdEG11/Nafion® whereas PdEG22/Nafion® and PdEG33/Nafion® potential was 0.43V and 0.41V respectively comparable to Nafion® with 0.4V. The anodic reduction current of nanocomposite was improved when compared to Nafion® membrane.

It was concluded that nanocomposite membranes may be used for anode and cathode sides of fuel cell stack [94]. Raseruthe et al. [94] reported that onset potential in the lower oxidation area together with the elevated current density peak indicated improved catalyst activity. PdEG11/Nafion®, PdEG22/Nafion®, PdEG33/Nafion® and commercial PdNps/Nafion® nano-composite membranes in Figure 5.14 exhibited five peaks, the results are supported by other research studies [95-97]. Therefore, it can be concluded that nano- composite membranes can be used on both anodic and cathodic side of fuel cell stack.
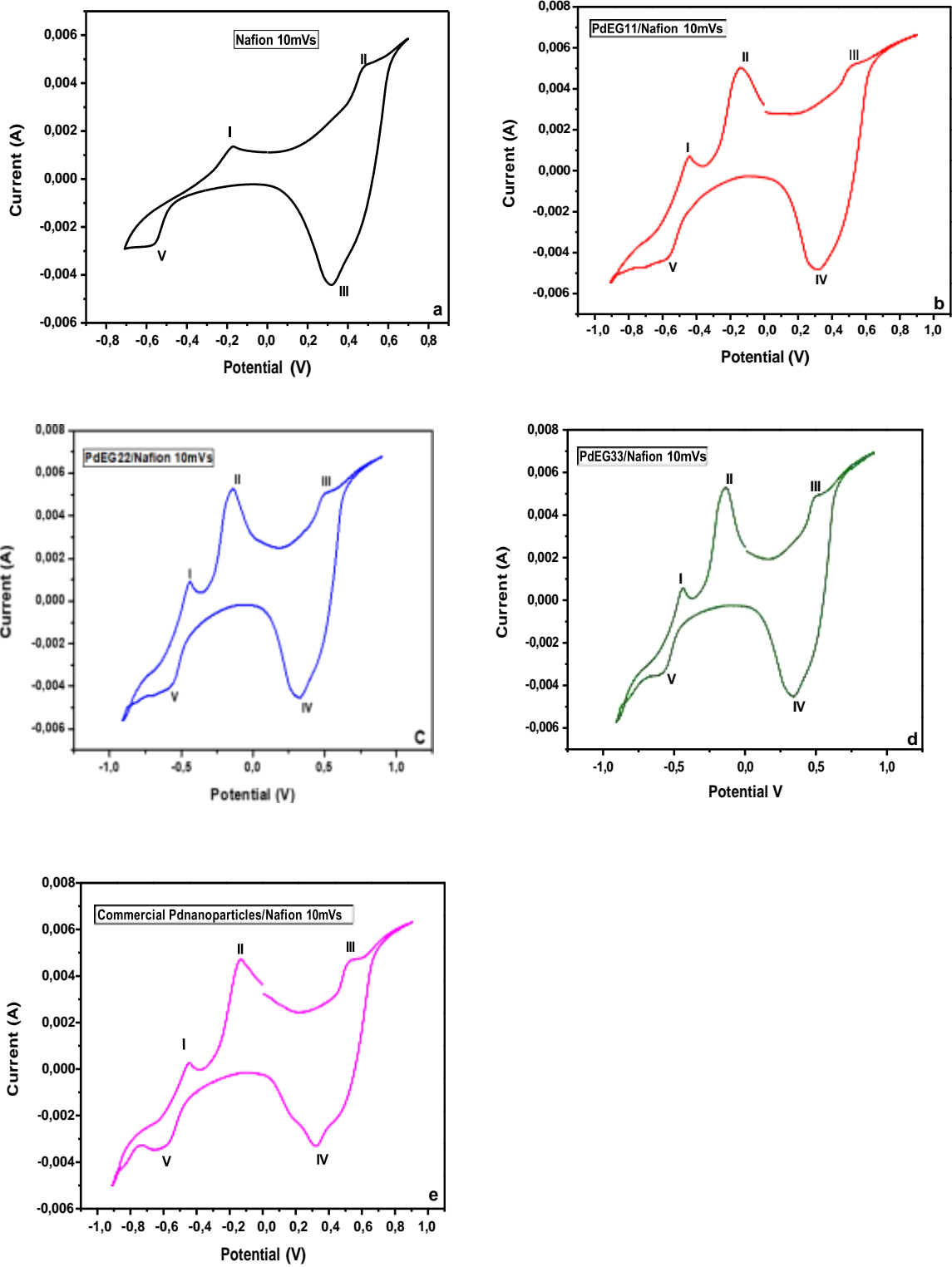
Figure 5.14: Cyclic voltammetry study of (a) Nafion® (b) PdEG11/Nafion®, (c) PdEG22/Nafion® (d) PdEG/Nafion® (e) Commercial PdNps/Nafion®.

5.3.12.2. Electrochemical Impedance Spectroscopy

The Nyquist plot is generated by plotting Z_{real} on the X-axis and Z_{imag} on the Y-axis. According to Magar et al. [98], the impedance on the right at the X-axis of the Nyquist plot is conducted with low frequency and the left side of impedance represents higher frequency. The pattern of Nyquist plot depends on how the working electrode was prepared (composition of working electrode). Hence, there are various Nyquist plots formed based on different materials used to prepare working electrode [98]. The Nyquist plot in Figure 5.15 indicates high frequency range for Nafion®, PdEG11/Nafion®, PdEG22/Nafion®, PdEG33/Nafion® and commercial PdNps/Nafion® membranes. The vertical slope for Nafion® suggests that the membrane is capable of the highest charge storage and semicircle shape for commercial PdNps/Nafion® membrane indicating the most maximum charge transfer resistance (Rct) [99]. The semicircle shape for nanocomposite membranes in Figure 5.15 is seen in low frequency region indicating high ionic resistance [99] with commercial PdNPs/Nafion® and PdEG33/Nafion® experiencing the highest ionic resistance. The results in Figure 5.15 corresponds to the results in Table 5.3 indicating high ionic resistance for commercial PdNPs/Nafion® and PdEG33/Nafion® and low ionic resistance for PdEG11/Nafion® and PdEG22/Nafion®.
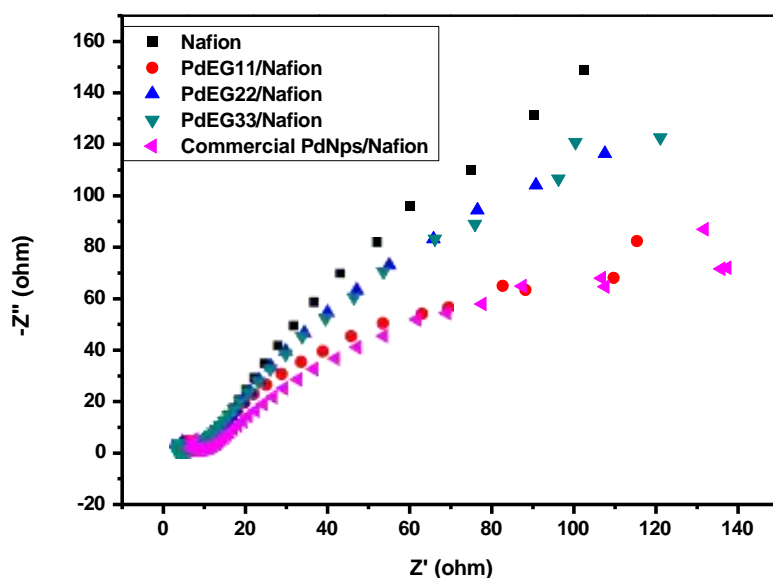
Figure 5.15: Electrochemical Impedance Spectroscopy of Nafion®, PdEG11/Nafion®, PdEG22/Nafion®, PdEG33/Nafion® and commercial PdNps/Nafion®.

5.10.13. Mechanical Properties

The reinforcement such as fibre, particles or platelets are added to improve mechanical properties [100-101]. Increasing filler content tends to decrease tensile strength and young modulus while increasing elongation at break [102-103]. Tensile strength and young modulus of Nafion® composite membranes were enhanced but elongation at break was reduced [104]. Mushtag et al. [105] performed mechanical strength test on different polymer blend membranes whereby the first experiment tensile strength and young modulus decreased as filler content increases and elongation at break increases. The second experiment tensile strength, young modulus and elongation at break increased with increase in filler content. Therefore, this is an indication that mechanical properties of materials depend on nature, or characteristics of material used.

The results from this research work are illustrated in Figure 5.16 and Table 5.4. In Figure 5.16 (a&b) PdNps/Nafion$^®$ membrane indicated highest tensile strength comparable with PdEG11/Nafion$^®$, PdEG22/Nafion$^®$ and PdEG33/Nafion$^®$. PdEG33/Nafion$^®$ has the highest tensile strength and elastic modulus at both test speeds followed by PdEG11/Nafion$^®$ and PdEG22/Nafion$^®$. Elastic modulus was determined by linear slope of the stress-strain curve. Elastic modulus and tensile strength were increased with an increase in palladium content. Figure 5.16 shows that there is no significant difference in the values of elastic modulus at various test speed rates. The tensile strength of all membranes was reduced at high-speed test rate. According to Table 5.4 all Pd nanocomposite membranes for both test speed of 5mm/s and 10mm/s were subjected to the same change in length of 11.999mm which represents 60% elongation before fracture.
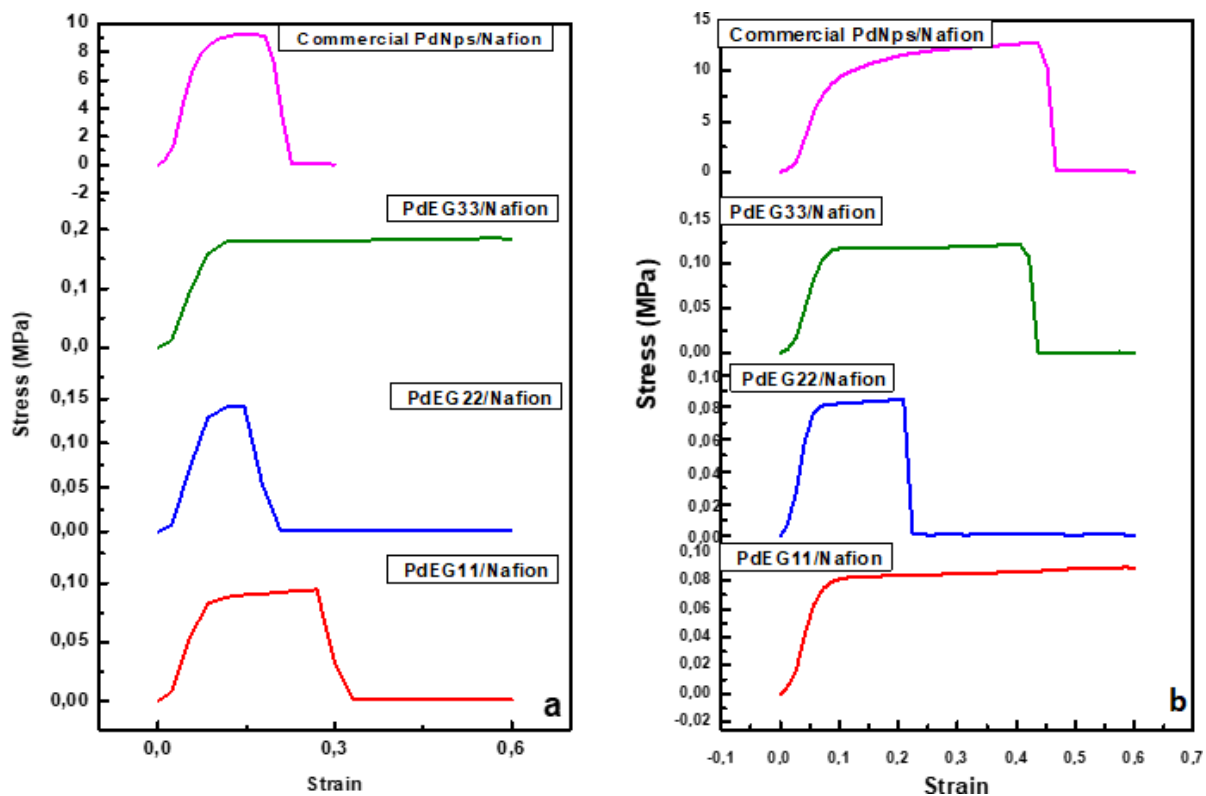
Figure 5.16: Stress-strain curves of palladium nanocomposite membranes at (a) 10mm/s (b) 5mm/s.

Table 5.4: Tensile strength, elastic modulus, and elongation at break of Pd nanocomposite membranes.

Tensile Test at 10mm/s				
Samples	Tensile Strength (MPa)	Elastic Modulus (MPa)	Elongation (mm)	Elongation at break (%)
PdEG11/Nafion[®]	0.094	1.66	11.999	60
PdEG22/Nafion[®]	0.141	1.99	11.999	60
PdEG33/Nafion[®]	0.186	2.46	11.999	60
Commercial PdNps/Nafion[®]	9.254	113.5	11.999	60

Tensile Test at 5mm/s				
PdEG11/Nafion®	0.089	1.84	11.999	60
PdEG22/Nafion®	0.095	2.01	11.999	60
PdEG33/Nafion®	0.122	2.3	11.999	60
Commercial PdNps/Nafion®	12.75	165.9	11.999	60

5.4. Conclusion

The main purpose of incorporating palladium into Nafion® is to improve its properties. The palladium nanoparticles synthesized by non-sol gel method, PdEGNps were successfully incorporated in Nafion® to create Pd/Nafion® nanocomposite. The presence of palladium nanoparticles was visible in most characterization analysis used to determine structural and thermal properties of membranes. The techniques such FTIR, XRD, XRF, TGA, SEM confirmed that indeed the nanoparticles were present in the nanocomposite membranes except XRD analysis of PdEG11/Nafion® and PdEG22/Nafion® did not show structural change.

The fuel cell membrane properties were analysed by water uptake, contact angle, ion exchange capacity, methanol permeability, and proton conductivity. The nanocomposite membranes showed hydrophobic properties based on water contact angle and water uptake results. Methanol permeability of nanocomposite membranes was low compared to pristine Nafion® membrane, which is one of requirement of fuel cell to have low methanol permeation through membrane. The nanocomposite membranes indicated a blocking effect for methanol crossover. The selectivity of palladium nanocomposite membranes showed they may be suitable to be used as PEM in DMFC.

The proton conductivity and IEC indicated that palladium nanocomposite membranes are more conductive than pristine Nafion® membrane. These results were supported by EIS analysis. The cyclic voltammetry study indicated that there is improvement of electrocatalytic activity of palladium membranes.

The mechanical stability of polymer membrane should be improved due to incorporation of a filler and increase its crystallinity. Furthermore, the mechanical strength of membrane is enhanced when crystallinity is increased.

The tensile strength and elastic modulus of nanocomposite membranes were improved when palladium content is increased while elongation at break remain the same. PdEG33/Nafion® membrane was selected as the best nanocomposite membrane and displayed best results based on characterization analysis as well as membrane properties. It is recommended that PdEG33/Nafion® can be used at cathode side of fuel cell due to its hydrophobic and conductivity properties.

5.5. References

1. Sanij, F.D., Leung P. B., Shah A., Su H., Xu Q. (2021). Advanced Pd-based nanomaterials for electrocatalytic oxygen reduction in fuel cells: A review. International Journal of Hydrogen Energy, 46 (27), pp. 14596-14627.

2. Dal Pont, K., Serghei, A. and Espuche, E. (2021). Multifunctional Pd-Based Nanocomposites with Designed Structure from In Situ Growth of Pd Nanoparticles and Polyether Block Amide Copolymer. Polymers, 13(9), p.1477.

3. Kamal Kumar Arora, Srivastava, S., Solanki, P.R. and Puri, N. (2019). Electrochemical Hydrogen Gas Sensing Employing Palladium Oxide/Reduced Graphene Oxide (PdO-rGO) Nanocomposites. IEEE Sensors Journal, 19(18), pp.8262–8271.

4. Junoh, H., Jaafar, J., Nordin, N., Ismail, A., Othman, M., Rahman, M., Aziz, F. and Yusof, N. (2020). Performance of Polymer Electrolyte Membrane for Direct Methanol Fuel Cell Application: Perspective on Morphological Structure. Membranes, 10(3), p.34.

5. Yang, G., Wang, Y., Xu, L., Li, Y., Li, L., Sun, Y., Yuan, Z. and Tang, Y. (2020). Pd nanochains: Controlled synthesis by lysine and application in microbial fuel cells. Chemical Engineering Journal 379, p.122230.

6. Cozzi, D., de Bonis C., Epifanio D.', Mecheri A., Ana B., and Licoccia, S. (2014). Organically functionalized titanium oxide/Nafion composite proton exchange membranes for fuel cells applications. Journal of Power Sources 248, pp.1127–1132.

7. Martina, P., Gayathri, R., Pugalenthi, M.R., Cao, G., Liu, C., and Prabhu, M.R. (2020). Nanosulfonated silica incorporated SPEEK/SPVdF-HFP polymer blend membrane for PEM fuel cell application. Ionics, 26(7), pp.3447–3458.

8. Thiam H.S, Chia M.Y., Cheah Q.R., Hoon Koo C. C., Lai S.O., and Chong C.K (2017). Proton Conductivity and Methanol Permeability of NafionSiO2/SiWA Composite Membranes. AIP Conference Proceedings 1828, 020007.

9. Hosseinpour, M., Sahoo, M., Perez-Page, M., Baylis, S.R., Patel, F., and Holmes, S.M. (2019). Improving the performance of direct methanol fuel cells by implementing multilayer membranes blended with cellulose nanocrystals. International Journal of Hydrogen Energy, 44(57), pp.30409–30419.

10. Prapainainar P., Du, Z., Theampetch A., Prapainainar C., Kongkachuichay P., and Holmes, S.M. (2020). Properties and DMFC performance of Nafion/mordenite composite membrane fabricated by solution-casting method with different solvent ratio. Energy, 190, p.116451.

11. Msomi, P.F., Nonjola P.T., Ndungu P.G., Ramontja J. (2020). Poly (2,6-dimethyl 1,4phenylene)/polysulfone anion exchange membrane blended with TiO2 with improved water uptake for alkaline fuel cell application. International Journal of Hydrogen Energy 45 (53), pp. 29465-29476.

12. Iwai, Y., Ikemoto, S., Haramaki K., Hattori, R. and Yonezawa, S. (2014). Influence of ligands of palladium complexes on palladium/Nafion composite membranes for direct methanol fuel cells by supercritical CO2 impregnation method. Journal of Supercritical Fluids 94, pp.48–58.

13. Dutta, K., Das, S., and Patit Paban Kundu (2014). Low methanol permeable and highly selective membranes composed of pure and/or partially sulfonated PVdF-co-HFP and polyaniline. Journal of Membrane Science 468, pp.42–51.

14. Cui, Y., Baker, A.P., Xu, X., Xiang, Y., Wang, L., Lavorgna, M. and Wu, J. (2015). Enhancement of Nafion based membranes for direct methanol fuel cell applications through the inclusion of ammonium-X zeolite fillers. Journal of Power Sources 294, pp.369–376.

15. Wang, Y.-J., Colby, R.H. and Kim, D. (2011). Proton conducting $9P_2O_5$–$6TiO_2$–$85SiO_2$ glass-filled Nafion® composite membranes. Journal of Membrane Science, 366(1-2), pp.421–426.

16. Li, T. and Yang, Y. (2009). A novel inorganic/organic composite membrane tailored by various organic silane coupling agents for use in direct methanol fuel cells. Journal Power Sources, 187(2), pp.332–340.

17. Wu, B., Zhao, M., Shi, W.-Y., Liu, W., Liu, J., Xing, D., Yao, Y., Hou, Z., Ming, P., Gu, J. and Zou, Z. (2014). The degradation study of Nafion/PTFE composite membrane in PEM fuel cell under accelerated stress tests. International Journal of Hydrogen Energy 39(26), pp.14381–14390.

18. Lin, H.-L. and Wang, S.-H. (2014). Nafion/poly (vinyl alcohol) nano-fiber composite and Nafion/poly (vinyl alcohol) blend membranes for direct methanol fuel cells. Journal of Membrane Science, 452, pp.253–262.

19. Wei, Y.-S., Shen, L., Wang, F., Yang, W.-D., Zhu, H., Wang, Z. and Han, K. (2011). Synthesis and characterization of novel nanocomposite membrane of sodium titanate/Nafion®. Material Letters, 65, pp. 1684-1687.

20. Mamta; Kumari, R., Yadav, C., Kumar, R.; Maurya, K.K., Singh, V.N. (2023). Thermally Deposited Sb_2Se_3/CdS-Based Solar Cell: Experimental and Theoretical Analysis. Nanomaterials, 13, p. 1135.

21. Al Aani, S., Wright, C.J., Atieh, M.A. and Hilal, N. (2017). Engineering nanocomposite membranes: Addressing current challenges and future opportunities. Desalination, 401, pp.1–15.

22. Huang, H., Aleksey Ruditskiy, Choi, S.-I., Zhang, L., Liu, J., Ye, Z. and Xia, Y. (2017). One-Pot Synthesis of Penta-twinned Palladium Nanowires and Their Enhanced Electrocatalytic Properties. Applied Materials and Interfaces, 9(36), pp.31203–31212.

23. Zhu, H., Zhang, H., Liang, J., Rao, G., Li, J., Liu, G., Du, Z., Fan, H. and Luo, J. (2011). Controlled Synthesis of Tellurium Nanostructures from Nanotubes to Nanorods and Nanowires and Their Template Applications. The Journal of Physical Chemistry C, 115(14), pp.6375–6380.

24. Wang, Z., Wang, L. and Wang, H. (2008). PEG-Mediated Hydrothermal Growth of Single-Crystal Tellurium Nanotubes. Crystal Growth & Design, 8(12), pp.4415–4419.

25. Gacem, A., Modi, S., Yadav, V.K., Islam, S., Patel, A., Dawane, V., Jameel, M., Inwati, G.K., Piplode, S., Solanki, V.S. and Basnet, A. (2022). Recent Advances in Methods for Synthesis of Carbon Nanotubes and Carbon Nanocomposite and their Emerging Applications: A Descriptive Review. Journal of Nanomaterials, p.e7238602.

26. Adeniran, B. and Mokaya, R. (2015). Low temperature synthesized carbon nanotube superstructures with superior CO_2 and hydrogen storage capacity. Journal of Materials Chemistry A, 3(9), pp.5148–5161.

27. Vielstich W., Lamm A., and Gasteiger H. A (2003). Handbook of Fuel Cells: Fundamentals technology and Application. Volume 3 Fuel Cell Technology and Application: Part 1. John Wiley and Sons Ltd.

28. Larminie L.J, and Dicks A.L (2003). Fuel Cell Systems Explained: Second Edition. John Wiley and Sons Ltd.

29. Goh, J.T.E., Abdul Rahim, A.R., Masdar, M.S. and Shyuan, L.K. (2021). Enhanced Performance of Polymer Electrolyte Membranes via Modification with Ionic Liquids for Fuel Cell Applications. Membranes, 11(6), p.395.

30. Huang F., Wei Q., Cai Y (2012). Surface functionalization of polymer nanofibers. Woodhead Publishing Limited, Chapter 6.

31. Ketpang K., Shanmugam, S., Suwanboon C., Chanunpanich N., and Lee, D. (2015). Efficient water management of composite membranes operated in polymer electrolyte membrane fuel cells under low relative humidity. Journal of Membrane Science, 493, pp.285–298.

32. Ramanujam, A.S., Kaleekkal, N.J. and Kumar, P.S. (2020). Preparation and characterization of proton exchange polyvinylidene fluoride membranes incorporated with sulfonated mesoporous carbon/SPEEK nanocomposite. SN Applied Sciences, 2(4), pp.688.

33. Mollà S., and Compań V. Nano-composite SPEEK-based membranes for Direct Methanol Fuel Cells at intermediate temperatures. Journal of Membrane Science 492, pp. 123-136.

34. Kumar, A.P., Kumar, B.P., Kumar, A.B.V.K., Huy, B.T. and Lee, Y.-I. (2013). Preparation of palladium nanoparticles on alumina surface by chemical co-precipitation method and catalytic applications. Applied Surface Science, 265, pp.500–509.

35. Lage L. G., Delgado P. G., and Kawano Y. (2004). Thermal stability and decomposition of nafion® membranes with different cations. Journal of Thermal Analysis and Calorimetry 75(2), pp.521–530.

36. Petreanu, I., Ebrasu, D., Sisu, C. and Mihai Varlam (2012). Thermal analysis of sulfonated polymers tested as polymer electrolyte membrane for PEM fuel cells. Journal of Thermal Analysis and Calorimetry, 110(1), pp.335–339.

37. Mokhtaruddin, S.R., Mohamad, A.B., Loh, K.S. and Hasan Kadhum, A.A. (2016). Thermal Properties and Conductivity of Nafion-Zirconia Composite Membrane. Malaysian Journal of Analytical Science, 20(3), pp.670–677.

38. Shao, Z.-G., Joghee, P. and Hsing, I-Ming. (2004). Preparation and characterization of hybrid Nafion–silica membrane doped with phosphotungstic acid for high temperature operation of proton exchange membrane fuel cells. Journal of Membrane Science, 229(1-2), pp.43–51.

39. Sigwadi, R., Dhlamini, M.S., Mokrani, T., Ṇemavhola, F., Nonjola, P.F. and Msomi, P.F. (2019). The proton conductivity and mechanical properties of Nafion®/ ZrP nanocomposite membrane. Heliyon, 5(8), p.e02240.

40. Park, S.; Abate, S.Y.; Lee, H.K.; Kim, H.-K (2020). On the quantification of degrees of reaction and hydration of sodium silicate-activated slag cements. Materials and Structures, 53, p 65.

41. Smitha, B., Devi, D.A. and Sridhar, S. (2008). Proton-conducting composite membranes of chitosan and sulfonated polysulfone for fuel cell application. International Journal of Hydrogen Energy, 33(15), pp.4138–4146.

42. Ketpang K., Shanmugam, S., Suwanboon C., Chanunpanich N., and Lee, D. (2015). Efficient water management of composite membranes operated in polymer electrolyte membrane fuel cells under low relative humidity. Journal of Membrane Science, 493, pp.285–298.

43. Kyu, T., Hashiyama M., and Eisenberg, A. (1983). Dynamic mechanical studies of partially ionized and neutralized Nafion polymers. Canadian Journal of Chemistry 61(4), pp.680–687.

44. Jung, H.-Y. and Jung W. K. (2012). Role of the glass transition temperature of Nafion 117 membrane in the preparation of the membrane electrode assembly in a direct methanol fuel cell (DMFC). International Journal of Hydrogen Energy, 37(17), pp.12580–12585.

45. Kim Y. S., Dong, L., Hickner, M.A., Glass, T.A., Webb, V., and McGrath, J.E. (2003). State of Water in Disulfonated Poly (arylene ether sulfone) Copolymers and a Perfluorosulfonic Acid Copolymer (Nafion) and Its Effect on Physical and Electrochemical Properties. Macromolecules, 36(17), pp.6281–6285.

46. Harrison, W.L., Hickner, M.A., Kim, Y.S. and McGrath, J.E. (2005). Poly (Arylene Ether Sulfone) Copolymers and Related Systems from Disulfonated Monomer Building Blocks: Synthesis, Characterization, and Performance - A Topical Review. Fuel Cells, 5(2), pp.201–212.

47. Wang, F., Hickner, M., Kim, Y.S., Zawodzinski, T.A. and McGrath, J.E. (2002). Direct polymerization of sulfonated poly (arylene ether sulfone) random (statistical) copolymers: candidates for new proton exchange membranes. Journal of Membrane Science, 197(1-2), pp.231–242.

48. Sickler B. Interpreting DSC Data. Tempo Labs, Materials Research Laboratory UCSB. Available at: https://www.mrl.ucsb.edu/sites/default/files/mrl_docs/instruments/Interpreting%20 DSC%20Data%20v1A.pdf. Accessed date: 22-10-2022.

49. Moniri S., Xiao X., and Shahani A.J. (2019). The mechanism of eutectic modifcation by trace impurities. Scientific Reports, 9, pp. 3381-3393.

50. Gómez R., E.E., Mina Hernández, J.H. and Diosa Astaiza, J.E. (2020). Development of a Chitosan/PVA/TiO2 Nanocomposite for Application as a Solid Polymeric Electrolyte in Fuel Cells. Polymers, 12(8), p.1691.

51. Awang, N., Jaafar, J. and Ismail, A.F. (2018). Thermal Stability and Water Content Study of Void-Free Electrospun SPEEK/Cloisite Membrane for Direct Methanol Fuel Cell Application. Polymers, 10(2), p.194.

52. Thiam H.S., Daud W.R.W., Kamarudin S.K., Mohamad A.B., Kadhum A.A.H., Loh K.S., Majlan E.H. (2013). Nafion/PdeSiO2 nanofiber composite membranes for direct methanol fuel cell applications. International Journal of Hydrogen Energy, 38 (22), pp.9474-9483.

53. Pongpiachan, S. (2014). FTIR Spectra of Organic Functional Group Compositions in PM2.5 Collected at Chiang-Mai City, Thailand during the Haze Episode in March 2012. Journal of Applied Sciences, [online] 14(22), pp.2967–2977.

54. Zhang, F., Tu, Z., Yu, J., Li, H., Huang, C. and Zhang, H. (2013). Impregnation of imidazole functionalized polyhedral oligomeric silsesquioxane in polymer electrolyte membrane for elevated temperature fuel cells. Royal Society of Chemistry Advances, 3(16), p.5438-5446.

55. Singh, R.P., Keiji Kunimatsu, Miyatake, K. and Takao Tsuneda (2016). Experimental and Theoretical Infrared Spectroscopic Study on Hydrated Nafion Membrane. Macromolecules, 49(17), pp.6621–6629.

56. Kayarkatte, M.K., Delikaya, Ö. and Roth, C. (2018). Polyacrylic acid-Nafion composites as stable catalyst support in PEM fuel cell electrodes. Materials Today Communications, 16, pp.8–13.

57. Laporta M., Pegoraroa M., and Zanderighi L. (1999). Perfluorosulfonated membrane (NaÐon): FT-IR study of the state of water with increasing humidity. Physics Chemistry Chemistry Physics, 1, pp. 4619-4628.

58. Viswadevarayalu A., Venkata R.P., Sumalatha J., Reddy S.A. (2016). Biocompatible Synthesis of Palladium Nanoparticles and Their Impact on Fungal Species. Journal of Nanoscience and Technology, 2 (3), pp. 169-172.

59. Sahin, M. and Gubbuk, I.H. (2022). Green synthesis of palladium nanoparticles and investigation of their catalytic activity for methylene blue, methyl orange and rhodamine B degradation by sodium borohydride. Reaction Kinetics, Mechanisms and Catalysis, 135(2), pp.999–1010.

60. Manjunatha Kempasiddaiah, Vishal Kandathil, Dateer, R.B., Sasidhar, B.S., Patil, S.A. and Patil, S.A. (2020). Immobilizing biogenically synthesized palladium nanoparticles on cellulose support as a green and sustainable dip catalyst for cross-coupling reaction. Cellulose, 27(6), pp.3335–3357.

61. Arsiya, F., Sayadi, M.H. and Sobhani, S. (2017). Green synthesis of palladium nanoparticles using Chlorella vulgaris. Materials Letters, 186, pp.113–115.

62. Vinodhini, S., Vithiya, B.S.M. and Prasad, T.A.A. (2022). Green synthesis of palladium nanoparticles using aqueous plant extracts and its biomedical applications. Journal of King Saud University - Science, 34(4), p.102017.

63. Refat M.S., Saad H.A., Gobouri A.A., Alsawat M., Belgacem K., Majrashi B.M. and Adam A.M.A. (2021). Synthesis, characterization, and photocatalytic efficiency of a new smart PdO Oxide Nanomaterials for using in the recycling and

sustainable wastewater treatment. Bulletin of the Chemical Society of Ethiopia, 35(1), pp. 107- 118.

64. Salman, S.H.; Khashan, K.S.; Hadi, A.A. (2023). Green Synthesis and Characterization of Palladium Nanoparticles by Pulsed Laser Ablation and Their Antibacterial Activity. Metals, 13, p. 273.

65. Mayedwa, N., Mongwaketsi, N., Khamlich, S., Kaviyarasu, K., Matinise, N. and Maaza, M. (2018). Green synthesis of nickel oxide, palladium and palladium oxide synthesized via Aspalathus linearis natural extracts: physical properties & mechanism of formation. Applied Surface Science, 446, pp.266–272.

66. Pourzare, K., Mansourpanah, Y. and Farhadi, S. (2016). Advanced nanocomposite membranes for fuel cell applications: a comprehensive review. Biofuel Research Journal, 3(4), pp.496–513.

67. Kim, J.-Y., Mulmi S., Lee, C., Park H.S., Chung Y. W., and Lee Y. H. (2006). Preparation of organic–inorganic nanocomposite membrane using a reactive polymeric dispersant and compatibilizer: Proton and methanol transport with respect to nanophase separated structure. Journal of Membrane Science, 283(1-2), pp.172–181.

68. Pu, L., Zhang, H., Yuan, T., Zou, Z., Zou, L., Li, X. and Yang, H. (2015). High performance platinum nanorod assemblies based double-layered cathode for passive direct methanol fuel cells. Journal of Power Sources, 276, pp.95–101.

69. Zhong, S., Cui, X., Gao, Y., Liu, W. and Dou, S. (2014). Fabrication and properties of poly (vinyl alcohol)-based polymer electrolyte membranes for direct methanol

fuel cell applications. International Journal of Hydrogen Energy, 39(31), pp.17857–17864.

70. Liang, X., Pan, G., Xu, L. and Wang, J. (2015). A modified decal method for preparing the membrane electrode assembly of proton exchange membrane fuel cells. Fuel, 139, pp.393–400.

71. Rambabu G. and Bhat, S.D. (2014). Simultaneous tuning of methanol crossover and ionic conductivity of sPEEK membrane electrolyte by incorporation of PSSA functionalized MWCNTs: A comparative study in DMFCs. Chemical Engineering Journal, 243, pp.517–525.

72. Di, Z., Xie, Q., Li, H., Mao, D., Li, M., Zhou, D. and Li, L. (2015). Novel composite proton-exchange membrane based on proton-conductive glass powders and sulfonated poly (ether ether ketone). Journal of Power Sources, 273, pp.688–696.

73. Shaari, N., Kamarudin, S.K., Basri, S., Shyuan, L.K., Masdar, M.S. and Nordin, D. (2018). Enhanced Proton Conductivity and Methanol Permeability Reduction via Sodium Alginate Electrolyte-Sulfonated Graphene Oxide Bio-membrane. Nanoscale Research Letters, 13(1), p.82.

74. Altaf, F., Batool, R., Gill, R., Rehman, Z.U., Majeed, H., Ahmad, A., Shafiq, M., Dastan, D., Abbas, G. and Jacob, K. (2021). Synthesis and electrochemical investigations of ABPBI grafted montmorillonite-based polymer electrolyte membranes for PEMFC applications. Renewable Energy, 164, pp.709–728.

75. Maiti J., Kakati N., Lee, S.-H., Jee S.W., Viswanathan, B., and Yoon Y. S. (2012). Where do poly (vinyl alcohol) based membranes stand in relation to Nafion® for direct methanol fuel cell applications? Journal of Power Sources, 216, pp.48–66.

76. Boroglu M.S., Çavuş S., Amorim, I. and Ata, A. (2011). Synthesis and characterization of poly (vinyl alcohol) proton exchange membranes modified with

4,4-diaminodiphenylether-2,2-disulfonic acid. Express Polymers Letters, 5(5), pp.470–478.

77. Pereira, F., Vallé, K., Belleville, P., Morin, A., Lambert, S. and Sanchez, C. (2008). Advanced Mesostructured Hybrid Silica−Nafion Membranes for High-Performance PEM Fuel Cell. Chemistry of Materials, 20(5), pp.1710–1718.

78. Li, Y., Zhao, T. and Yang, W. (2010). Measurements of water uptake and transport properties in anion-exchange membranes. International Journal of Hydrogen Energy 35(11), pp.5656–5665.

79. Zawodzinski, T.A., Springer, T.E., Davey, J., Jestel, R., Lopez, C., Valerio, J. and Gottesfeld, S. (1993). A Comparative Study of Water Uptake By and Transport Through Ionomeric Fuel Cell Membranes. Journal of The Electrochemical Society, 140(7), pp.1981–1985.

80. Zawodzinski, T.A. (1993). Water Uptake by and Transport Through Nafion® 117 Membranes. Journal of The Electrochemical Society, 140(4), p.1041.

81. Hinatsu, J.T., Mizuhata, M. and Takenaka, H. (1994). Water Uptake of Perfluorosulfonic Acid Membranes from Liquid Water and Water Vapor. Journal of The Electrochemical Society, 141(6), pp.1493–1498.

82. Ahmad, H., Kamarudin, S.K., Hasran, U.A. and Daud, W.R.W. (2011). A novel hybrid Nafion-PBI-ZP membrane for direct methanol fuel cells. International Journal of Hydrogen Energy, 36(22), pp.14668–14677.

83. Ilbeygi H., Ghasemi, M., Daryoush Emadzadeh, Ahmad Fauzi Ismail, Zaidi, A., Aljlil, S.A., Mohd, Martin, D.J. and Samaneh Keshani (2015). Power generation and wastewater treatment using a novel SPEEK nanocomposite membrane in a dual chamber microbial fuel cell. International Journal of Hydrogen Energy, 40(1), pp.477–487.

84. Zhou, L., Dong Hyun Yang, Yu, W., Zhang, J. and Li, C. (2015). An efficient polymer solar cell using graphene oxide interface assembled via layer-by-layer deposition. Organic Electronics, 23, pp.110–115.

85. Silva, V.S., B. Ruffmann, Vetter, S., Mendes, A., Madeira, L.M. and Suzana Pereira Nunes (2005). Characterization and application of composite membranes in DMFC. Catalysis Today, 104(2-4), pp.205–212.

86. Wang, Y., He, Q., Ding, K., Wei, H., Guo, J., Wang, Q., O'Connor, R., Huang, X., Luo, Z., Shen, T., Wei, S. and Guo, Z. (2015). Multiwalled Carbon Nanotubes Composited with Palladium Nanocatalysts for Highly Efficient Ethanol Oxidation. Journal of The Electrochemical Society, 162(7), pp. F755–F763.

87. Ren, S., Sun, G., Li, C., Liang, Z., Wu, Z., Jin, W., Qin, X. and Yang, X. (2006). Organic silica/Nafion® composite membrane for direct methanol fuel cells. Fuel Cells Bulletin, 12, pp.12–16.

88. Yang, T. (2009). Composite membrane of sulfonated poly (ether ether ketone) and sulfated poly (vinyl alcohol) for use in direct methanol fuel cells. Journal of Membrane Science, 342(1-2), pp.221–226.

89. Zakil F. A., Kamarudin S.K., Basri S. (2016). Modified Nafion membranes for direct alcohol fuel cells: An overview. Renewable and Sustainable Energy Reviews 65, pp.841–852.

90. Yan, H., Yang, H., Li, A. and Cheng, R. (2016). pH-tunable surface charge of chitosan/graphene oxide composite adsorbent for efficient removal of multiple pollutants from water. Chemical Engineering Journal, 284, pp.1397–1405.

91. Smith, T.A., Santamaria, A.D., Jae Yong Park and Yamazaki, K. (2014). Alloy Selection and Die Design for Stamped Proton Exchange Membrane Fuel Cell (PEMFC) Bipolar Plates. Procedia CIRP 14, pp.275–280.

92. Pandey, J., Seepana, M.M. and Shukla, A. (2015). Zirconium phosphate-based proton conducting membrane for DMFC application. International Journal of Hydrogen Energy, 40(30), pp.9410–9421.

93. Ahmad, H., Kamarudin, S.K., Hasran, U.A. and Daud, W.R.W. (2010). Overview of hybrid membranes for direct-methanol fuel-cell applications. International Journal of Hydrogen Energy, 35(5), pp.2160–2175.

94. Raseruthe, K.E., Matthews, T., Gwebu, S.S., Pillay, K. and Maxakato, N.W. (2021). Investigating the effect of carbon support on palladium-based catalyst towards electro-oxidation of ethylene glycol. Materials Research Express, 8(1), p.015017.

95. Liang, Z., Zhao, T., Xu, J. and Zhu, L. (2009). Mechanism study of the ethanol oxidation reaction on palladium in alkaline media. Electrochimica Acta, 54(8), pp.2203–2208.

96. Awasthi, R. and Singh, R.N. (2012). Synthesis and structural characterization of a ternary palladium–ruthenium–tin nanoalloy supported on graphene nanosheets for methanol electrooxidation in alkaline medium. Catalysis Science & Technology, 2(12), p.2428.

97. Bhavani K.S., Anusha T., Stuparu, M.C. and Brahman P.K. (2021). Synthesis and characterization of palladium nanoparticles-corannulene nanocomposite: An anode electrocatalyst for direct oxidation of methanol in alkaline medium. Journal of Electroanalytical Chemistry, 900, pp.115654–115654.

98. Magar, H.S., Hassan, R.Y.A. and Mulchandani, A. (2021). Electrochemical Impedance Spectroscopy (EIS): Principles, Construction, and Biosensing Applications. Sensors (Basel, Switzerland), 21(19), p.6578.

99. Ahmed, T., Ya, H.H., Khan, R., Lubis H.S. A.M. and Mahadzir, S. (2020). Pseudo-Ductility, Morphology and Fractography Resulting from the Synergistic Effect of

CaCO3 and Bentonite in HDPE Polymer Nano Composite. Materials, 13(15), p.3333.

100. Tüfekci, M., Durak, S.G., Pir, İ., Acar, T.O., Demirkol, G.T. and Tüfekci, N. (2020). Manufacturing, Characterisation and Mechanical Analysis of Polyacrylonitrile Membranes. Polymers, 12(10), p.2378.

101. Seo, D.C., Jeon, I., Jeong, E.S. and Jho, J.Y. (2020). Mechanical Properties and Chemical Durability of Nafion/Sulfonated Graphene Oxide/Cerium Oxide Composite Membranes for Fuel-Cell Applications. Polymers, 12(6), p.1375.

102. Thiam, H.S., Daud, W.R.W., Kamarudin, S.K., Mohammad, A.B., Kadhum, A.A.H., Loh, K.S. and Majlan, E.H. (2011). Overview on nanostructured membrane in fuel cell applications. International Journal of Hydrogen Energy, 36(4), pp.3187–3205.

103. Sudiarti T., Wahyuningrum, D., Bundjali B., and Arcana I. (2017). Mechanical strength and ionic conductivity of polymer electrolyte membranes prepared from cellulose acetate-lithium perchlorate. Materials Science and Engineering, 223, pp.012052–012052.

104. Guillen, G.R., Pan, Y., Li, M., and Hoek, E.M.V. (2011). Preparation and Characterization of Membranes Formed by Nonsolvent Induced Phase Separation: A Review. Industrial & Engineering Chemistry Research, 50(7), pp.3798–3817.

105. Mushtaq A., Mukhtar H., Shariff A. Effect of Mechanical Properties in Enhanced Polymeric Blend Membranes (2021). Pakistan Journal of Scientific and Industrial Research Series A: Physical Sciences, 64, pp, 97-102.

Chapter 6

Conclusions and Recommendations

6.1 Conclusion

Palladium nanoparticles were successfully synthesized using two different methods. The Polyol method was chosen to be the best method to synthesize Pd nanoparticles based on TEM results. The Palladium nanoparticles synthesized by non-aqueous polyol method were used to fabricate nano-composite membranes since the method yielded better size (6.05nm) compared to aqueous method (19nm). The results of XRD confirmed the face-centered cubic lattice structure of Pd nanoparticles. The different nano-composite membranes were characterized by XRD, FESEM, XRF, FTIR and Water contact angle measurement. Membrane properties such as IEC, Water uptake, methanol permeability, proton conductivity and selectivity were performed to investigate if the Pd nanocomposite membranes will be suitable for fuel cell applications.

Reduction of Pd^{2+} to Pd^0 was indicated by Uv-vis spectroscopy and XRD pattern also indicated Pd^0 ffc structure of palladium nanoparticles. The peak of Palladium oxide was also identified from cyclic voltammetry plots for nanocomposite membranes.

It is evident from the work performed that size distribution differs according to technique used. The size distribution of Uv-vis, TEM and DLS indicated different size dimeters of palladium nanoparticles. Research literature also indicated that the size of nanoparticles was different for each technique used.

Therefore, it was suggested that PdEG33/Nafion® be selected as the best membrane to be used in DMFC since it exhibited the best results of mechanical properties in terms of tensile strength, percentage elongation and elastic modulus.

The membrane in DMFCs should be resistance to methanol and show the ability towards oxygen reduction reaction. The nanocomposite membranes were successfully prepared by recast method and characterized. It is indicated that the size of palladium particles has an effect on proton conductivity of the membrane. The nanocomposite membranes showed improved methanol permeability and proton conductivity compared to pristine Nafion® membrane due to nanoparticles that were incorporated in Nafion® membrane. The membrane selectivity of palladium nanocomposite membranes showed they are suitable to be used as PEM in DMFC based on their high selectivity values and their ability to reduce methanol crossover.

Various research indicates that higher filler loading increases water uptake, but it turns out to be reduced with highest amount of filler content. The results from this research work agree with research studies, for the highest palladium nanoparticles loading water uptake was reduced. Based on study of literature review, it is evident that the type of filler (Palladium, Silica, Titanium and Montmorillonite) has effect on the fuel cell membrane since characteristics of filler is different based on its nature. Hence, incorporation of filler into polymer matrix yields different results in terms of water uptake, ion exchange capacity, proton conductivity and methanol permeability.

Although higher water uptake is needed to facilitate proton transportation in fuel cell which affects IEC, proton conductivity and methanol permeability, the results from this research indicated low water uptake with improved IEC and proton conductivity with low methanol permeability compared to pristine Nafion®. This might be due to

properties of palladium nanoparticles that enhanced the structure of membrane acting as proton conductor and blocking effect thus reducing water uptake and methanol permeability. It is stated that the layer of cathode catalyst must be hydrophobic to avoid flooding and loss of catalyst activity. Therefore, it is recommended that palladium nanocomposite membranes fabricated from this research study be used to restrict methanol crossover since nanocomposite membranes exhibited hydrophobic property (based on water uptake and water contact angle) with low methanol permeability and be used as ORR cathodic catalyst.

6.2. Recommendations

The next research work, palladium nanocomposite fabricated in this research work will be further analysed for fuel cell application such as single cell performance. The PdO (Pd^{2+}) nanoparticles will be reduced to metallic palladium (Pd^0) by H_2/N_2 followed by O_2/N_2 using Micromeritics AutoChemII instrument. A technique such as BET will be used to investigate surface area and pore size of palladium nanoparticles. Furthermore, palladium can be used for Oxygen Reduction Reaction (ORR) since alloyed material of palladium are considered as the best approaches to reduce cost of electrocatalyst.